NIWA
Taihoro Nukurangi

Relationships between interannual climate modes and rainfall in the Wellington region

Updated December 2024

Prepared for Greater Wellington Regional Council

December 2024

Climate, Freshwater & Ocean Science

Prepared by:
Nicolas Fauchereau
Gregor Macara

For any information regarding this report please contact:
Gregor Macara
Climate Scientist
Climate Data and Applications
+64 4 386 0509
gregor.macara@niwa.co.nz

National Institute of Water & Atmospheric Research Ltd
Private Bag 14901
Kilbirnie
Wellington 6241

Phone +64 4 386 0300

NIWA CLIENT REPORT No: 2024362WN
Report date: December 2024
NIWA Project: WRC23307

Revision	Description	Date
Version 1.0	Final version sent to client	13 December 2024

Quality Assurance Statement		
	Reviewed by:	Andrew Tait, Chief Scientist – Climate, Atmosphere and Hazards
	Formatting checked by:	Jess Moffat
	Approved for release by:	Alison MacDiarmid

© All rights reserved. This publication may not be reproduced or copied in any form without the permission of the copyright owner(s). Such permission is only to be given in accordance with the terms of the client's contract with NIWA. This copyright extends to all forms of copying and any storage of material in any kind of information retrieval system.

Whilst NIWA has used all reasonable endeavours to ensure that the information contained in this document is accurate, NIWA does not give any express or implied warranty as to the completeness of the information contained herein, or that it will be suitable for any purpose(s) other than those specifically contemplated during the project or agreed by NIWA and the client.

Contents

Executive summary **7**

1 Introduction **8**

2 Methods **9**

2.1 Datasets 9

2.2 Definition of climate modes 9

2.3 Parameters 10

2.4 Composites 10

2.5 Caveats 13

2.6 Observed rainfall trends 15

3 Total Rainfall **18**

3.1 ENSO – positive phase (El Niño) 18

3.2 ENSO – negative phase (La Niña) 21

3.3 IOD – positive phase 24

3.4 IOD – negative phase 26

3.5 SAM – positive phase 28

3.6 SAM – negative phase 30

3.7 SPSD – positive phase 33

3.8 SPSD – negative phase 35

4 Rain days **37**

4.1 ENSO – positive phase (El Niño) 37

4.2 ENSO – negative phase (La Niña) 40

4.3 IOD – positive phase 43

4.4 IOD – negative phase 45

4.5 SAM – positive phase 47

4.6 SAM – negative phase 49

4.7 SPSD – positive phase 51

4.8 SPSD – negative phase 53

5 Heavy rain days **55**

5.1 ENSO – positive phase (El Niño) 55

5.2 ENSO – negative phase (La Niña) 58

5.3 IOD – positive phase 61
5.4 IOD – negative phase 63
5.5 SAM – positive phase 65
5.6 SAM – negative phase 67
5.7 SPSD – positive phase 69
5.8 SPSD – negative phase 71

6 Dry days 73
6.1 ENSO – positive phase (El Niño) 73
6.2 ENSO – negative phase (La Niña) 76
6.3 IOD – positive phase 79
6.4 IOD – negative phase 81
6.5 SAM – positive phase 83
6.6 SAM – negative phase 85
6.7 SPSD – positive phase 87
6.8 SPSD – negative phase 89

7 Subregional analyses and relationships with large-scale sea surface temperatures 91

8 Summary 97
8.1 Recommendations 97

9 Glossary of abbreviations and terms 99

10 References 100

Figures

Figure 2-1: Monthly evolution of the Niño 3.4 (ENSO) index for select events. 12
Figure 2-2: Monthly evolution of the IOD for select events. 12
Figure 2-3: Correlation coefficient between Niño 3.4 and IOD (left) and SPSD (right). 13
Figure 2-4: Seasonal time-series of the SAM index. 14
Figure 2-5: Trends in seasonal rainfall accumulation. 15
Figure 2-6: Trends in seasonal number of dry days. 16
Figure 2-7: Trends in seasonal number of very wet days. 16
Figure 2-8: Sub-regional trend in winter (JJA) rainfall. 17
Figure 3-1: Rainfall anomalies (operational VCSN) during El Niño. 18
Figure 3-2: Rainfall anomalies (augmented VCSN) during El Niño. 19
Figure 3-3: Rainfall anomalies (MSWEP) during El Niño. 20
Figure 3-4: Rainfall anomalies (operational VCSN) during La Niña. 21
Figure 3-5: Rainfall anomalies (augmented VCSN) during La Niña. 22

Figure 3-6: Rainfall anomalies (MSWEP) during La Niña. 23
Figure 3-7: Rainfall anomalies (operational VCSN) during the positive phase of IOD. 24
Figure 3-8: Rainfall anomalies (MSWEP) during the positive phase of IOD. 25
Figure 3-9: Rainfall anomalies (operational VCSN) during the negative phase of IOD. 26
Figure 3-10: Rainfall anomalies (MSWEP) during the negative phase of IOD. 27
Figure 3-11: Rainfall anomalies (operational VCSN) during the positive phase of SAM. 28
Figure 3-12: Rainfall anomalies (MSWEP) during the positive phase of SAM. 29
Figure 3-13: Rainfall anomalies (operational VCSN) during the negative phase of SAM. 31
Figure 3-14: Rainfall anomalies (MSWEP) during the negative phase of SAM. 32
Figure 3-15: Rainfall anomalies (operational VCSN) during the positive phase of SPSD. 33
Figure 3-16: Rainfall anomalies (MSWEP) during the positive phase of SPSD. 34
Figure 3-17: Rainfall anomalies (operational VCSN) during the negative phase of SPSD. 35
Figure 3-18: Rainfall anomalies (MSWEP) during the negative phase of SPSD. 36
Figure 4-1: Rain day anomalies (operational VCSN) during El Niño. 37
Figure 4-2: Rain day anomalies (augmented VCSN) during El Niño. 38
Figure 4-3: Rain day anomalies (MSWEP) during El Niño. 39
Figure 4-4: Rain day anomalies (operational VCSN) during La Niña. 40
Figure 4-5: Rain day anomalies (augmented VCSN) during La Niña. 41
Figure 4-6: Rain day anomalies (MSWEP) during La Niña. 42
Figure 4-7: Rain day anomalies (operational VCSN) during the positive phase of IOD. 43
Figure 4-8: Rain day anomalies (MSWEP) during the positive phase of IOD. 44
Figure 4-9: Rain day anomalies (operational VCSN) during the negative phase of IOD. 45
Figure 4-10: Rain day anomalies (MSWEP) during the negative phase of IOD. 46
Figure 4-11: Rain day anomalies (operational VCSN) during the positive phase of SAM. 47
Figure 4-12: Rain day anomalies (MSWEP) during the positive phase of SAM. 48
Figure 4-13: Rain day anomalies (operational VCSN) during the negative phase of SAM. 49
Figure 4-14: Rain day anomalies (MSWEP) during the negative phase of SAM. 50
Figure 4-15: Rain day anomalies (operational VCSN) during the positive phase of SPSD. 51
Figure 4-16: Rain day anomalies (MSWEP) during the positive phase of SPSD. 52
Figure 4-17: Rain day anomalies (operational VCSN) during the negative phase of SPSD. 53
Figure 4-18: Rain day anomalies (MSWEP) during the negative phase of SPSD. 54
Figure 5-1: Heavy rain day anomalies (operational VCSN) during El Niño. 55
Figure 5-2: Heavy rain day anomalies (augmented VCSN) during El Niño. 56
Figure 5-3: Heavy rain day anomalies (MSWEP) during El Niño. 57
Figure 5-4: Heavy rain day anomalies (operational VCSN) during La Niña. 58
Figure 5-5: Heavy rain day anomalies (augmented VCSN) during La Niña. 59
Figure 5-6: Heavy rain day anomalies (MSWEP) during La Niña. 60
Figure 5-7: Heavy rain day anomalies (operational VCSN) during the positive phase of IOD. 61
Figure 5-8: Heavy rain day anomalies (MSWEP) during the positive phase of IOD. 62
Figure 5-9: Heavy rain day anomalies (operational VCSN) during the negative phase of IOD. 63
Figure 5-10: Heavy rain day anomalies (MSWEP) during the negative phase of IOD. 64

Figure 5-11: Heavy rain day anomalies (operational VCSN) during the positive phase of SAM. 65
Figure 5-12: Heavy rain day anomalies (MSWEP) during the positive phase of SAM. 66
Figure 5-13: Heavy rain day anomalies (operational VCSN) during the negative phase of SAM. 67
Figure 5-14: Heavy rain day anomalies (MSWEP) during the negative phase of SAM. 68
Figure 5-15: Heavy rain day anomalies (operational VCSN) during the positive phase of SPSD. 69
Figure 5-16: Heavy rain day anomalies (MSWEP) during the positive phase of SPSD. 70
Figure 5-17: Heavy rain day anomalies (operational VCSN) during the negative phase of SPSD. 71
Figure 5-18: Heavy rain day anomalies (MSWEP) during the negative phase of SPSD. 72
Figure 6-1: Dry day anomalies (operational VCSN) during El Niño. 73
Figure 6-2: Dry day anomalies (augmented VCSN) during El Niño. 74
Figure 6-3: Dry day anomalies (MSWEP) during El Niño. 75
Figure 6-4: Dry day anomalies (operational VCSN) during La Niña. 76
Figure 6-5: Dry day anomalies (augmented VCSN) during La Niña. 77
Figure 6-6: Dry day anomalies (MSWEP) during La Niña. 78
Figure 6-7: Dry day anomalies (operational VCSN) during the positive phase of IOD. 79
Figure 6-8: Dry day anomalies (MSWEP) during the positive phase of IOD. 80
Figure 6-9: Dry day anomalies (operational VCSN) during the negative phase of IOD. 81
Figure 6-10: Dry day anomalies (MSWEP) during the negative phase of IOD. 82
Figure 6-11: Dry day anomalies (operational VCSN) during the positive phase of SAM. 83
Figure 6-12: Dry day anomalies (MSWEP) during the positive phase of SAM. 84
Figure 6-13: Dry day anomalies (operational VCSN) during the negative phase of SAM. 85
Figure 6-14: Dry day anomalies (MSWEP) during the negative phase of SAM. 86
Figure 6-15: Dry day anomalies (operational VCSN) during the positive phase of SPSD. 87
Figure 6-16: Dry day anomalies (MSWEP) during the positive phase of SPSD. 88
Figure 6-17: Dry day anomalies (operational VCSN) during the negative phase of SPSD. 89
Figure 6-18: Dry day anomalies (MSWEP) during the negative phase of SPSD. 90
Figure 7-1: Definition of GWRC rainfall regions on the VCSN grid (left) and corresponding mean seasonal cycle (3 month rainfall accumulations). 91
Figure 7-2: Time series of seasonal (3-month sliding windows, i.e., NDJ, DJF, etc.) rainfall anomalies for the four Wellington subregions. 92
Figure 7-3: Seasonal rainfall anomaly correlations between the four Greater Wellington subregions, over the period 1961-2024. 93
Figure 7-4: First two EOF on rainfall seasonal anomalies (from VCSN) for the period 1961-2024. Standard EOF. 94
Figure 7-5: Correlation between GWRC Region A seasonal rainfall anomalies and SST anomalies. 95
Figure 7-6: Correlation between GWRC Region B seasonal rainfall anomalies and SST anomalies. 95
Figure 7-7: Correlation between GWRC Region C seasonal rainfall anomalies and SST anomalies. 96
Figure 7-8: Correlation between GWRC Region D seasonal rainfall anomalies and SST anomalies. 96

Executive summary

This study investigates the relationships between inter-annual climate modes and different indices of rainfall in the Wellington region. It represents an update to a similar study undertaken by NIWA for the Greater Wellington Regional Council in 2018, and includes additional analyses focused on the characteristics of rainfall variability and trends over the Greater Wellington region.

The climate modes considered were the El Niño Southern Oscillation (ENSO), the Southern Annular Mode (SAM), the Indian Ocean Dipole (IOD), and the South Pacific Subtropical Dipole (SPSD). Rainfall indices considered were total rainfall, rain days, heavy rain days, and dry days.

A composite analysis approach, which is suited to uncover the potential non-linear impacts of the above climate modes over the regional climate of the Wellington, revealed that the signals associated with these inter-annual climate modes are, broadly speaking, neither strong nor statistically significant. However, some statistically significant and relatively robust signals were identified for the Greater Wellington region, including:

- Reduced spring (SON) rainfall and fewer heavy rain days during positive phases of ENSO (El Niño) over the whole region.
- Reduced summer (DJF) rainfall for northern parts of the region during positive phases of the IOD.
- Increased winter (JJA) rainfall and more rain days for many parts of the region during negative phases of SAM.
- Increased summer (DJF) rainfall for the Wairarapa during positive phases of the SPSD.

In addition, supplementary analyses focused on the characteristics of rainfall variability and trends over the Greater Wellington region revealed the following:

- Some negative trends in seasonal rainfall accumulations in some areas are discernible and super-imposed on large interannual (year to year) variability, in some limited areas this trend is statistically significant.
- The primary mode (extracted via Empirical Orthogonal Functions) of year to year variability is homogeneous over the region, and explains about 76% of the total variance, a secondary mode, explaining about 12% of the total rainfall variance, is characterised by rainfall anomalies of opposite sign either side of the Tararua ranges.

For future work, NIWA suggests the findings of this study could be leveraged to improve the relevance – and possibly the accuracy – of tailored seasonal climate outlooks for the Greater Wellington region. Further work would also be needed to better understand how the state of the different climate modes investigated in this study modulate the accuracy of probabilistic forecasts for the region derived from the initialised ensemble seasonal forecasting prediction system (the C3S Multi-Model-Ensemble) that NIWA utilises to underpin its Seasonal Climate Outlook (SCO).

1 Introduction

In 2018, NIWA produced a report which examined the relationships between climate modes and different climate variables in the Greater Wellington region (Fauchereau et al., 2018). This report is an updated and extended version of that 2018 work, focusing on rainfall. The present report utilises the intervening years of available data, leverages additional sources of rainfall data, and provides supplementary analyses.

The report focuses on the relationship between seasonally aggregated rainfall parameters and interannual climate modes (Sections 3 to 5), with the information primarily presented as maps. Descriptive text corresponding to the maps is included, but is limited to the dominant patterns only. The rainfall parameters selected are total rainfall, the number of rain days, the number of days exceeding the climatological 90th percentile of daily rainfall (referred to as 'heavy rainfall'), and the number of dry days. The climate modes considered are the El Niño Southern Oscillation (ENSO), the Southern Annular Mode (SAM), the Indian Ocean Dipole (IOD) and the South Pacific Subtropical Dipole (SPSD).

In addition, statistical analyses have been conducted to shed light on rainfall trends and rainfall variability in the Greater Wellington region and the latter's relationship with large-scale sea surface temperature (SST) anomalies (Section 7).

2 Methods

2.1 Datasets

Rainfall

The focus of this report is on rainfall. Three datasets have been used to document rainfall variability over the Greater Wellington region:

- The 'Operational' Virtual Climate Station Network (VCSN) at 5 km resolution. This version of VCSN comprises daily rainfall accumulations from January 1961 to present. These data are actively maintained and updated by NIWA (NIWA, 2024), and have been recently utilised as the source dataset for the statistical bias-correction of the updated downscaled climate change projections for New Zealand that NIWA has produced.
- The 'Augmented' VCSN at 500 m resolution. This version of the VCSN incorporates rainfall data from regional councils (including Greater Wellington Regional Council). It comprises daily rainfall accumulations from January 1972 – October 2021. These data are non-operational, with no bias-correction, and have demonstrated ring-like artefacts around relatively high elevation terrain (Macara et al., 2024). These data are not actively updated by NIWA. Due to these limitations, the 'Augmented' VCSN data are only used for comparison with ENSO.
- The MSWEP 2.8.0 (Multi-Scale Weighted Ensemble Precipitation) dataset: MSWEP is a global, merged (i.e., integrating satellite, in-situ, and reanalysis data) dataset produced by the glo2ho initiative (Beck et al., 2019). MSWEP comprises daily rainfall accumulations from January 1979 to present. This dataset has been shown to compare favourably with VCSN as well as other precipitation products (see Vishwanathan et al., 2023).

Sea surface temperatures

Sea Surface Temperature (SST) anomalies are used to define ENSO (via the Niño 3.4 index domain), the IOD, and the SPSD. SST are also considered in Section 7 (regional analyses and relationships with large-scale sea surface temperatures). In all cases, the SST anomalies were calculated from the gridded Extended Reconstructed Sea Surface Temperature (ERSST) v5 dataset (Huang et al., 2017) and the climatological period is 1991-2020.

Geopotential height

The SAM index is derived from an Empirical Orthogonal Function analysis (EOF, also known as Principal Component Analysis) applied to atmospheric monthly geopotential height anomalies at 850 hPa (see Section 2.2 below). The dataset used is the National Centers for Environmental Prediction (NCEP) / National Center for Atmospheric Research (NCAR) reanalysis system (Kalnay et al., 1996).

2.2 Definition of climate modes

For all indices:

- The climatological period for calculation of the anomalies is 1991-2020 (formerly 1981-2010 in the 2018 version of this report).

- No detrending was applied. This methodological choice is expected to be relevant mostly in the case of the SAM, for which is more detailed comment is provided in Section 2.5 (*caveats*).
- Seasonal (summer: DJF, autumn: MAM, winter: JJA, spring: SON) anomalies are calculated as the average of the corresponding monthly anomalies for each index.

For individual indices, readers are referred to Fauchereau et al. (2018) for detailed definitions. Brief definitions are included below:

- ENSO – average SST anomalies in the central / eastern equatorial Pacific (5N-5S, 190-240); represented by the Niño 3.4 index domain.
- SAM – first PC associated with first EOF of monthly Z850 anomalies from NCEP / NCAR (NCEP 1) reanalysis, Southern Hemisphere (south of 20°S) weighted by cos(latitude), 1950-2024. Note:
  - The SAM index shows a (well-known) positive trend.
  - This positive trend depends on the period of analysis.
  - Composite seasons selection (based on 7 top / bottom values for each season) are sensitive to dataset, method of calculation, and period of analysis.
- IOD – standardised (1991-2020) difference between monthly SST anomalies in the Eastern and Western Tropical Indian Ocean.
- SPSD – standardised (1991-2020) difference between monthly SST anomalies northeast/southwest of New Zealand.

2.3 Parameters

The rainfall-related parameters included in this report are described below:

- Seasonal rainfall total anomalies, in percentage of normal (1991-2020), for seasons summer (DJF), autumn (MAM), winter (JJA) and spring (SON).
- Total rain days (≥ 0.5 mm/day). Seasonal, anomalies (in number of days).
- Dry days (counterpart of total rain days, i.e., days with rainfall < 0.5 mm), seasonal, anomalies (in number of days).
- Heavy rain days: days with rainfall exceeding the climatological 90th-percentile of rain days. The percentiles are calculated using all days falling within the target season (e.g., for summer (DJF), the 90th-percentile is calculated using all days from 1 December of year -1 to 28(29) February of year +1). Anomalies expressed in number of days.

2.4 Composites

Composite samples of the positive and negative phase of each climate mode have been utilised for this report:

- Composite samples of each climate mode index are based on the seven highest/lowest index values (see below for further refinements).

- Climate modes impacts are non-linear over New Zealand (and the Greater Wellington region). The varying response of rainfall parameters to climate modes were tested for significance using multiple t-tests, derived using the method described in Benjamini and Hochberg (1995).
- All calculations and mapping used the Python programming language and the scientific python ecosystem.

Further notes on the climate mode composites:

ENSO, and to a lesser extent the SPSD, tend to peak during the Southern Hemisphere summer (DJF), while the IOD tends to peak during the Southern Hemisphere spring (SON).

For these indices that are strongly 'phase-locked' onto the mean seasonal cycle, the definition of the seasonal composite samples can either anchored *relative* to the mode's seasonal peak (summer (DJF) for ENSO or the SPSD, spring (SON) for the IOD), or based on the seven most extreme (e.g., highest for El Niño, lowest for La Niña) values recorded *independently* for each season.

For the relative definition, typical evolution of ENSO values before and after the summer (DJF) peak would lead to selecting the winter (JJA) and spring (SON) seasons before the peak, i.e., winter (JJA) (year – 1) and spring (SON) (year – 1) and the autumn (MAM) season immediately following the peak, i.e., autumn (MAM) (year 0).

Discussions between NIWA and Dr. Alex Pezza (Senior Climate Scientist, GWRC) compared the results for the two options, and canvased considerations regarding the interpretability and the intended use for this report. Following these discussions, it was agreed to use the 'independent seasons' definitions, i.e., the composite years are defined *independently* for each season, based upon the seven highest/lowest values recorded for each index over the period 1961-2024 (operational VCSN) and 1979-2024 (MSWEP). Similarly, the highest/lowest three values of ENSO were selected for the 'augmented' VCSN assessments.

For reference, Figure 2-1 presents the evolution of the ENSO index from six months before the summer (DJF) peak to six months after, based upon the highest/lowest seven values over the 1 March 1961 – 29 February 2024 period. Similarly, Figure 2-2 shows that the IOD tends to peak during the Southern Hemisphere spring (SON).

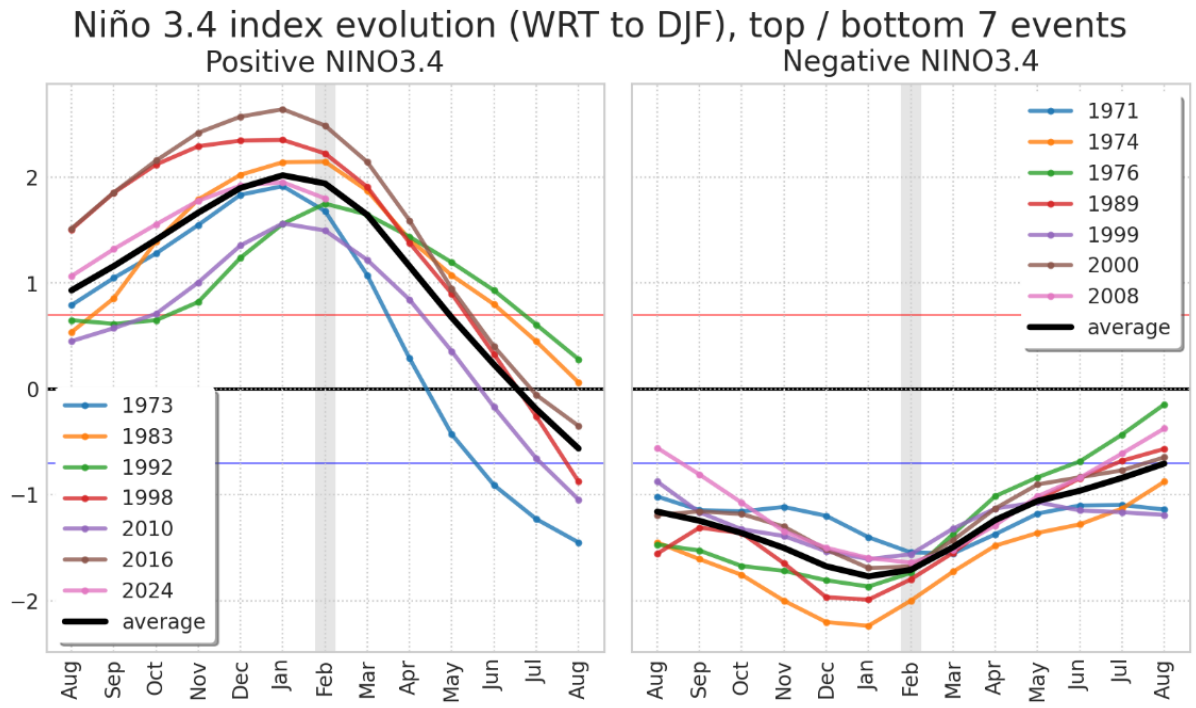

Figure 2-1: Monthly evolution of the Niño 3.4 (ENSO) index for select events.

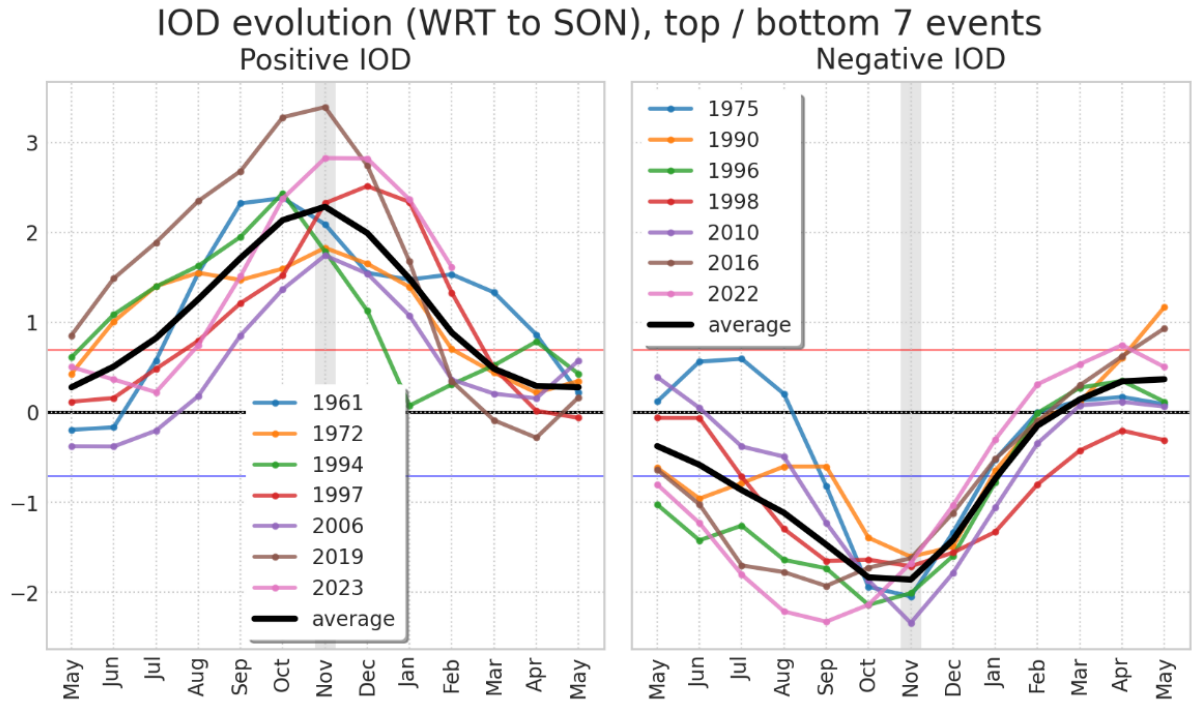

Figure 2-2: Monthly evolution of the IOD for select events.

2.5 Caveats

The climate modes are not strictly independent, and several studies have highlighted the relationships between, for example, the IOD and ENSO (Zhang et al., 2021), and ENSO and the SPSD (Guan et al., 2014; Zheng and Wang, 2021).

Positive IOD events (with warmer than normal SSTs in the western Indian Ocean and cooler than normal SST in the eastern Indian Ocean) tend to *precede* the peak of El Niño events, although this relationship is not robustly linear.

Similarly, positive ENSO events (El Niño) tend to be associated with negative SPSD events, with cooler than normal SSTs around New Zealand, and warmer than normal SSTs to the southeast of New Zealand. La Niña are associated largely with an opposite pattern, which is consistent with the tendency for Marine Heat Waves (MHWs) to occur during La Niña events. To a large extent, the SPSD can be considered a regional manifestation of ENSO and part of the causal chain (or 'teleconnection') linking the distant coupled ocean – atmosphere anomalies taking place in the tropical Pacific during ENSO events, and the associated temperature and rainfall anomalies observed in New Zealand.

Figure 2-3 presents the correlation coefficients between the time-series of ENSO, and the IOD and the SPSD, respectively. The results are stratified by season. Correlations significant at the 99% level are shown, with a False Discovery Rate correction applied (Benjamini and Hochberg, 1995).

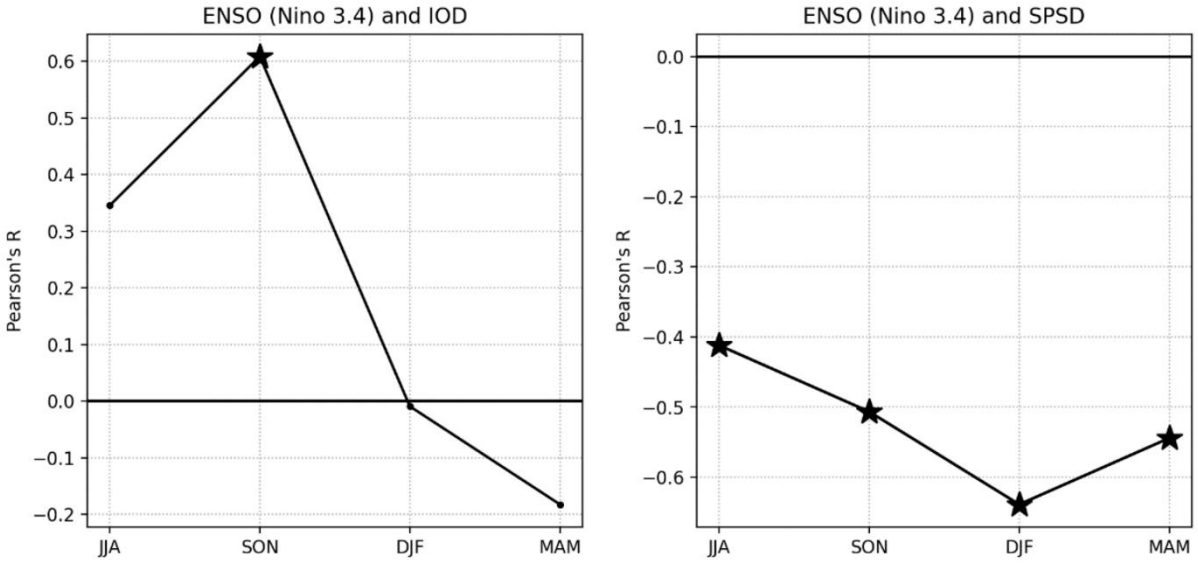

Figure 2-3: Correlation coefficient between Niño 3.4 and IOD (left) and SPSD (right). Stars indicate correlations significant at the 99% level.

The SAM is characterised by a significant positive trend over recent decades. As such, the positive composite samples tend to be concentrated on latest decades. For example, of the composites samples matching the operational VCSN dataset (1961-2024), the (top-7) positive years for DJF are 1982, 1995, 1998, 2015, 2016, 2023 and 2024, while the (bottom-7) negative years are 1964, 1965, 1967, 1969, 1971, 1972 and 1977. The positive SAM trend is a defining characteristic of this mode and is well understood to result both from anthropogenic global warming and ozone depletion. For this report, the SAM index has not been detrended. Therefore, the uneven distribution of positive and negative phases of the SAM needs to be kept in mind when interpreting the results.

Figure 2-4 presents the seasonal time-series of the SAM index, with the linear trend line overlaid. The red and blue markers highlight the top- and bottom-seven seasons selected for the composites respectively.

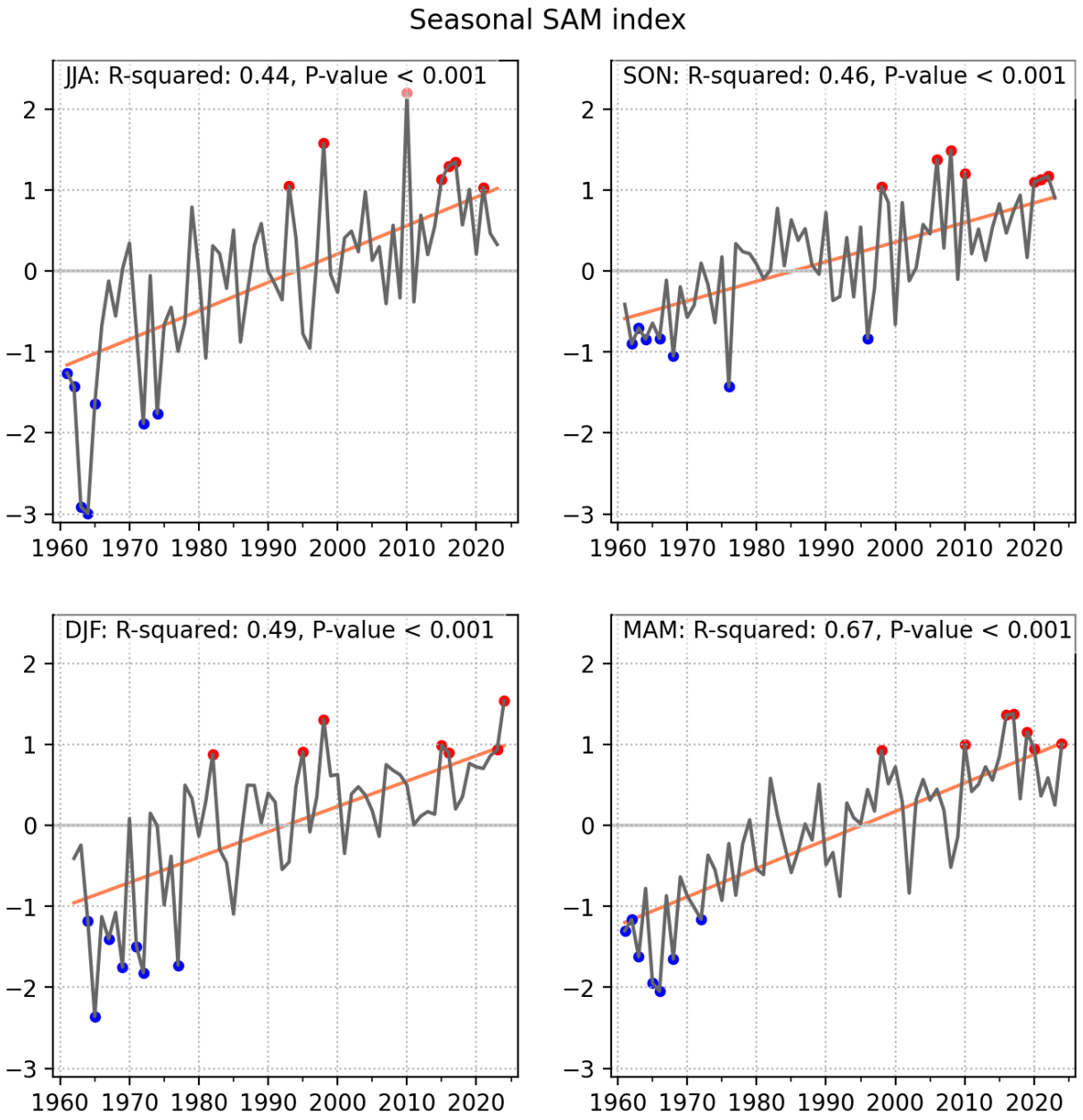

Figure 2-4: Seasonal time-series of the SAM index.

As described in Section 2.1, rainfall data from the three different datasets are available over different periods of time. As such, there cannot be a one-to-one correspondence between the composite samples selected for each rainfall dataset when selected the top / bottom values of the climate modes.

One also must note that the sign of the composite anomaly between the different rainfall parameters might not always be consistent, especially when it comes to heavy rain days, which by definition (the top 10% of daily rainfall accumulations) are relatively rare.

While statistical significance is indicated by stippling in the composite maps (with a 90% confidence level chosen) it also must be interpreted with caution. The emphasis therefore needs to be on the high-level interpretation of the patterns emerging from the following composite analyses. Elements of interpretation are provided in each of the sections (parameters + climate driver) in aid of this.

2.6 Observed rainfall trends

Of the three rainfall datasets used here, the operational VCSN (at 5 km resolution) is available over the longest period (1961-2024). During this time, some areas of the Greater Wellington region show small but significant trends in some rainfall parameters. Figure 2-5, Figure 2-6 and Figure 2-7 present the seasonal trends for rainfall accumulation, number of dry days and number very wet days (rainfall > 90th percentile) respectively.

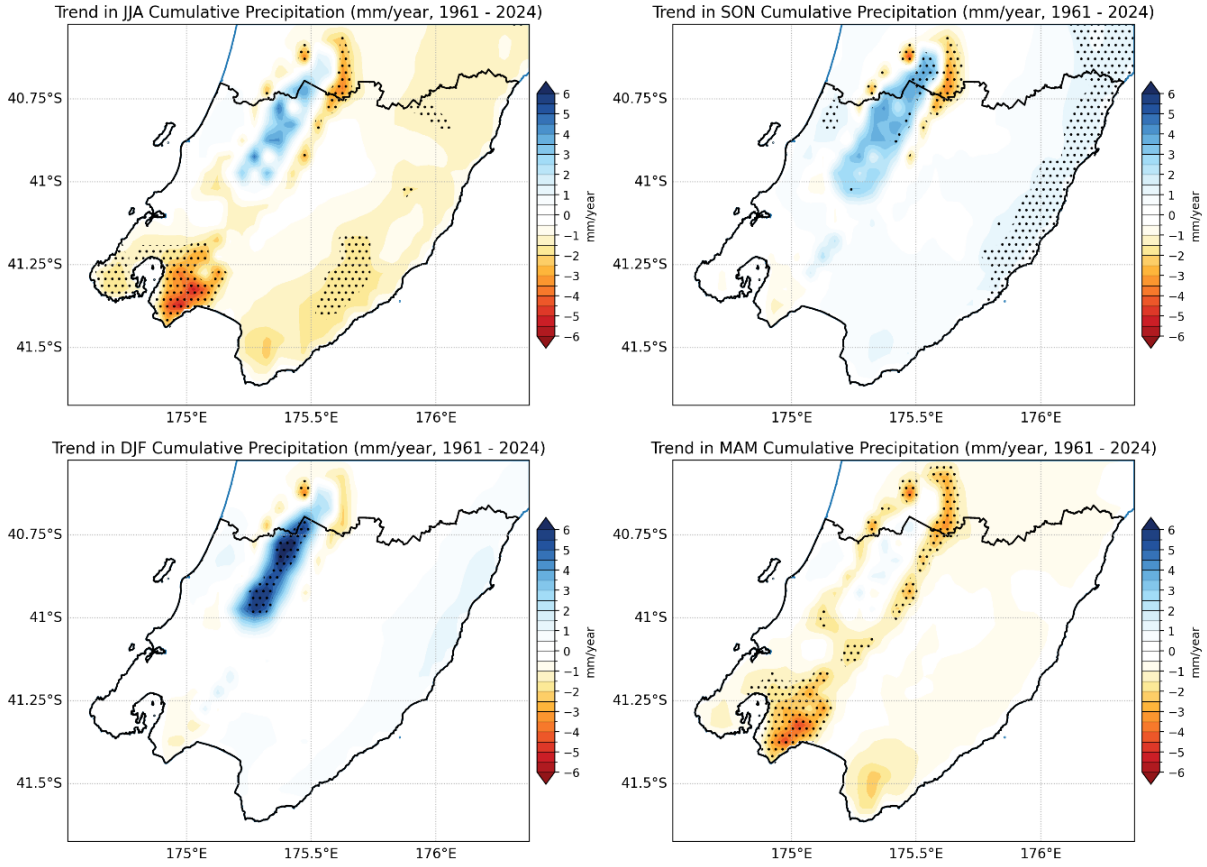

Figure 2-5: Trends in seasonal rainfall accumulation.

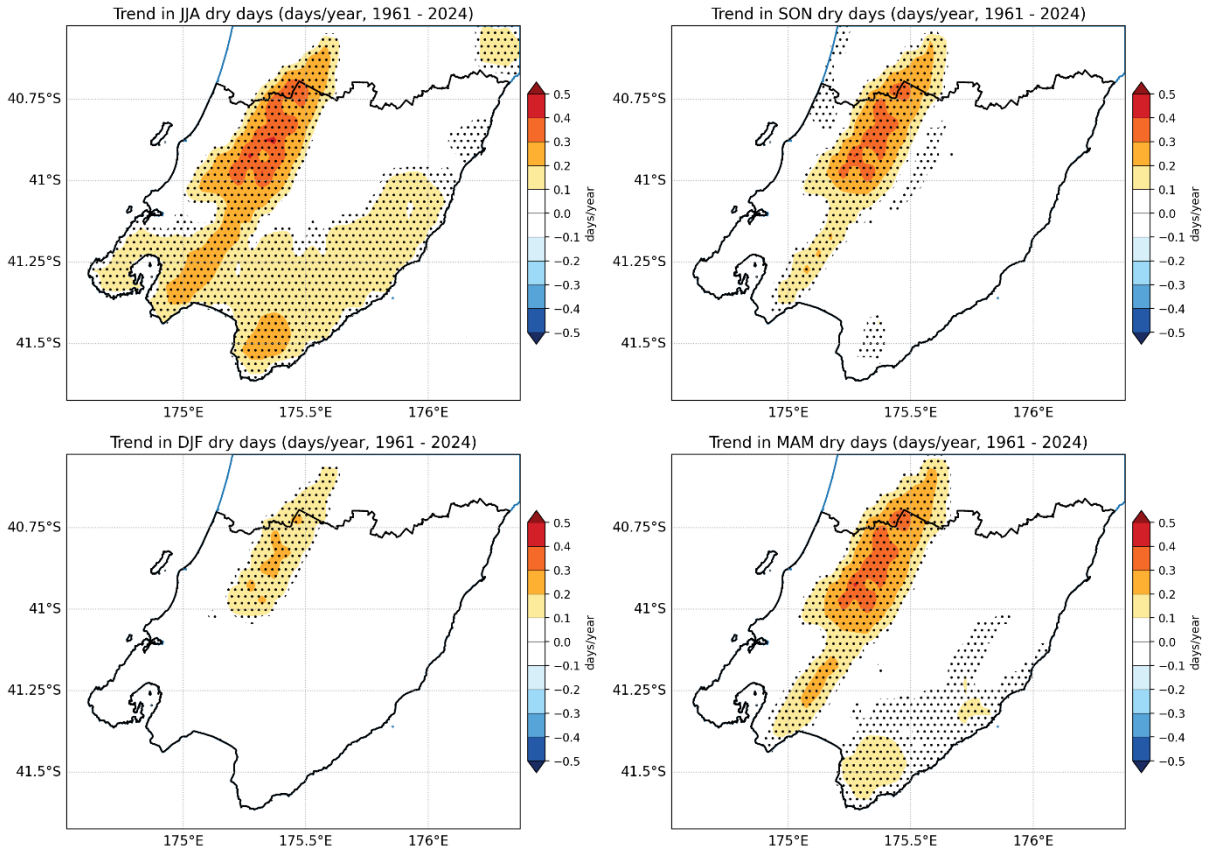

Figure 2-6: Trends in seasonal number of dry days.

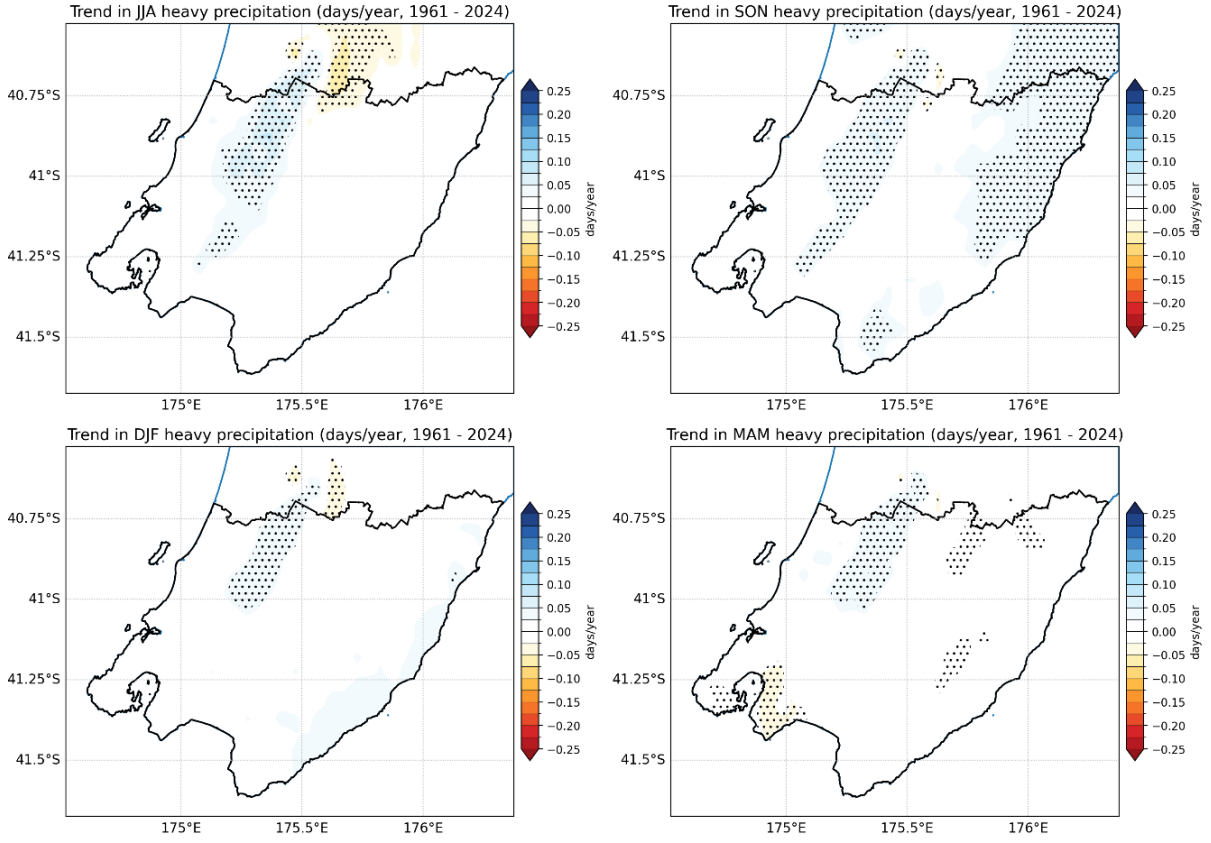

Figure 2-7: Trends in seasonal number of very wet days.

To illustrate the magnitude of the trend in context of the interannual variability, we have calculated a sub-regional index (outlined in black Figure 2-8 below) and overlaid the linear trend in winter (JJA) rainfall accumulation. The trend is about -3.3 mm/year, which corresponds to a decrease of about 200 mm accumulated seasonal precipitation over the 1961-2024 period, noting that this trend takes place in the context of large interannual (year to year) variability.

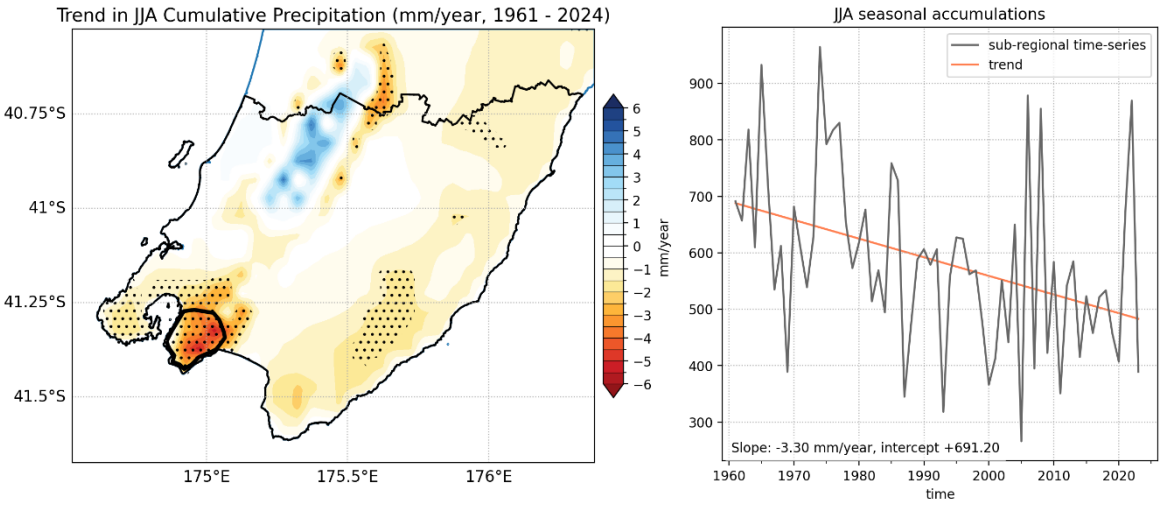

Figure 2-8: Sub-regional trend in winter (JJA) rainfall.

3 Total Rainfall

3.1 ENSO – positive phase (El Niño)

In this section, we compiled composite maps for seasonal rainfall anomalies (expressed in percentage of normal) for the positive phases of ENSO (El Niño).

The analyses show a relatively consistent signal over the Greater Wellington region during the positive phases of ENSO, both for the operational VCSN (Figure 3-1) and for the augmented VCSN (Figure 3-2). In both cases, a dry signal is evident, especially for spring (SON) and summer (DJF) and for the eastern half of the Greater Wellington region (i.e., east of the Tararua ranges). Also present is a wet signal (albeit statistically non-significant) west of the Tararua ranges in autumn (MAM).

The signal is embedded in a large-scale, Pacific-wide signal as evidenced by the composite anomalies from the MSWEP dataset (Figure 3-3): Drier than normal conditions occur in the Southwest Pacific, approximately from Vanuatu to French Polynesia, during positive phases of ENSO. This pattern therefore is relatively robust.

3.1.1 Operational VCSN

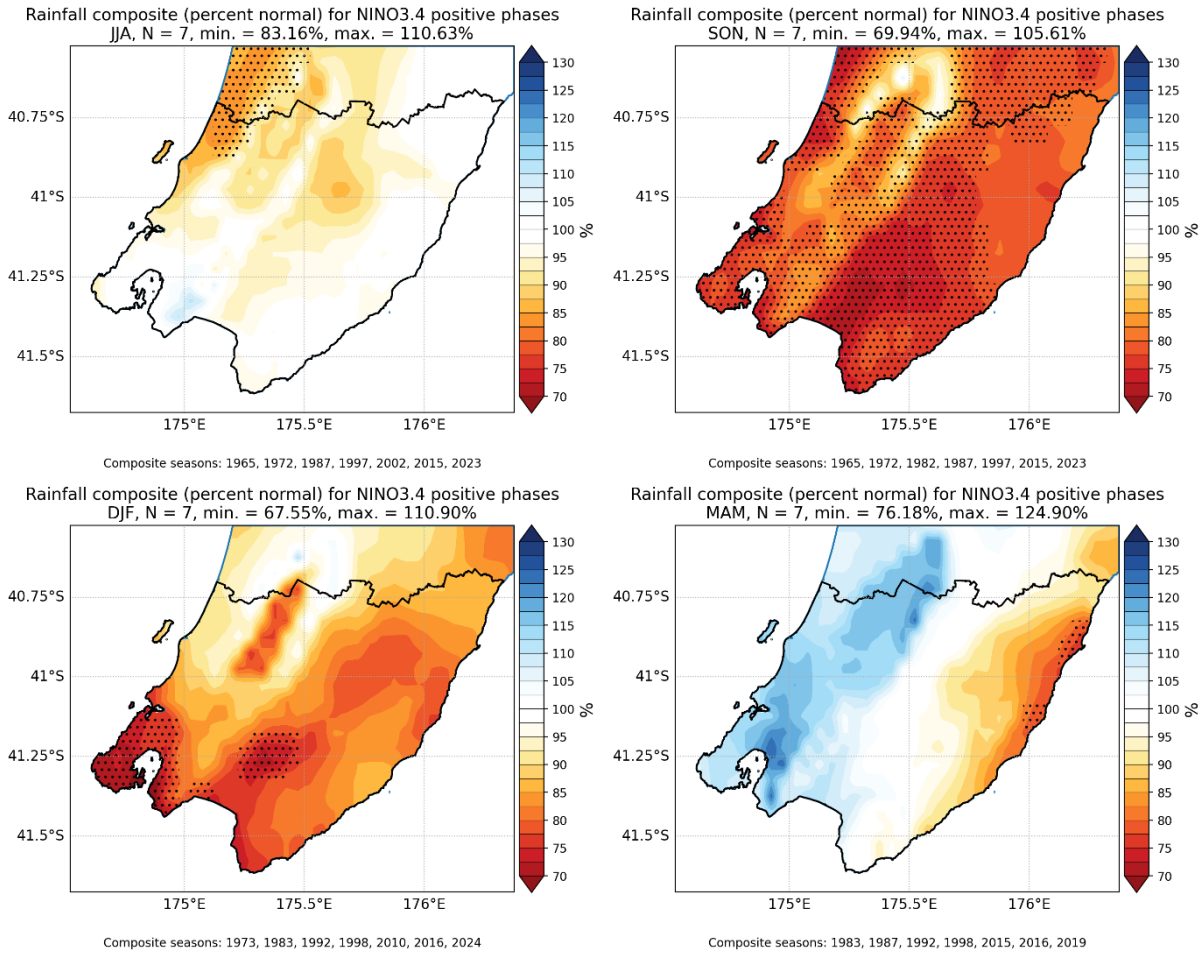

Figure 3-1: Rainfall anomalies (operational VCSN) during El Niño. Stippling indicates areas of statistical significance at $p \leq 0.10$. The years indicated under each figure are those of the last month in the season (e.g., DJF 1973 refers to December 1972 – February 1973).

3.1.2 Augmented VCSN

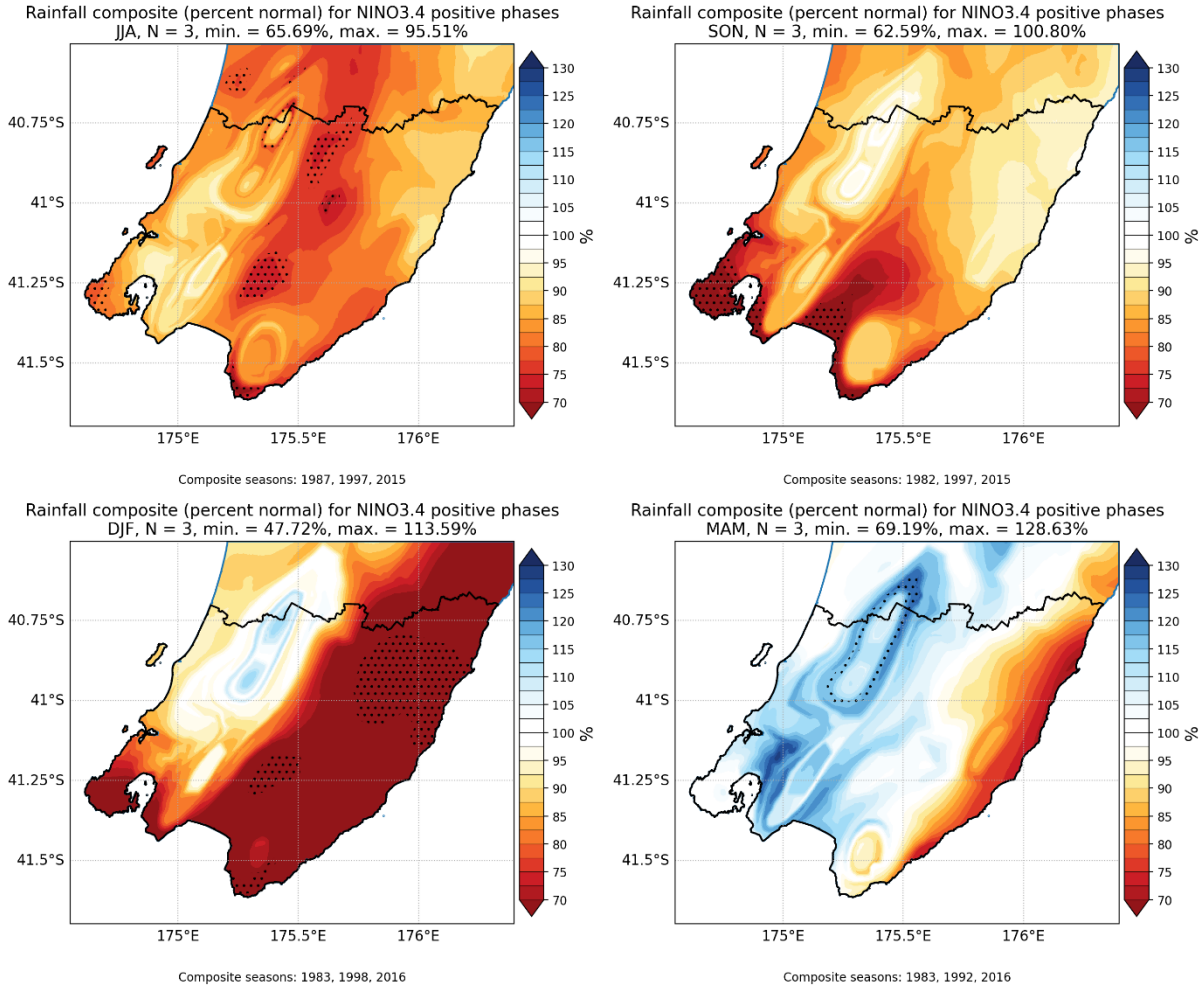

Figure 3-2: Rainfall anomalies (augmented VCSN) during El Niño. The legend range of 70-130% was selected to match the range presented for the operational VCSN maps above (Figure 3-1).

3.1.3 MSWEP

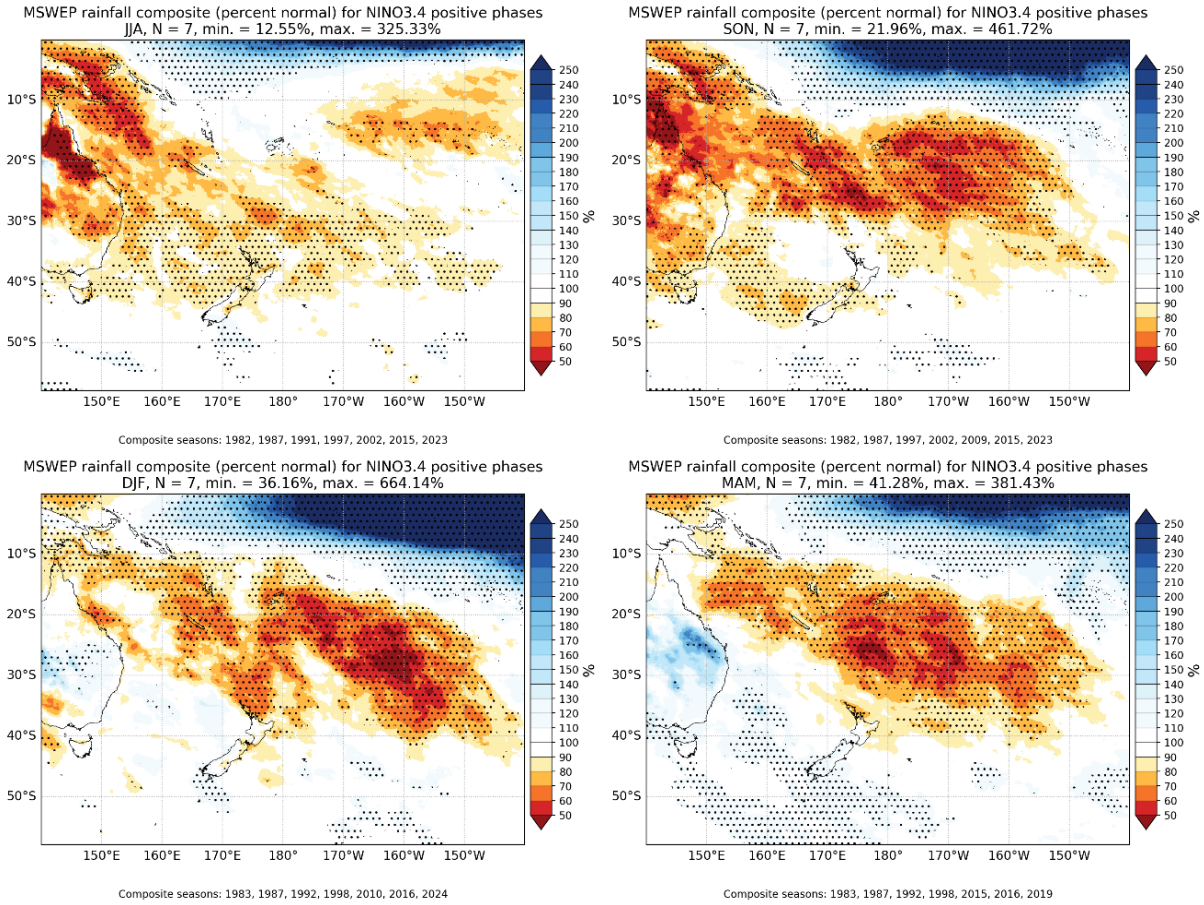

Figure 3-3: Rainfall anomalies (MSWEP) during El Niño.

3.2 ENSO – negative phase (La Niña)

In this section, we compiled composite maps for seasonal rainfall anomalies (expressed in percentage of normal) for the negative phases of ENSO (La Niña).

Notably, the composite anomalies observed during La Niña (Figure 3-4 to Figure 3-5) show that these events are not necessarily associated with anomalies of the opposite sign of El Niño events. This is especially the case during spring (SON) and summer (DJF), where significant areas of the Greater Wellington region show drier than normal conditions during both El Niño and La Niña events, although the anomalies are not necessarily significant. A small wet signal is also present in autumn (MAM) and winter (JJA) especially in the Wellington region, although here again the anomalies are not statistically significant.

The amplitude of the anomalies is also generally smaller during La Niña than during El Niño.

It is also consistent with a large-scale signal in the southwest Pacific that is less extant and more muted during La Niña than during El Niño, as evidenced by the composite anomalies in the MSWEP dataset (Figure 3-6).

3.2.1 Operational VCSN

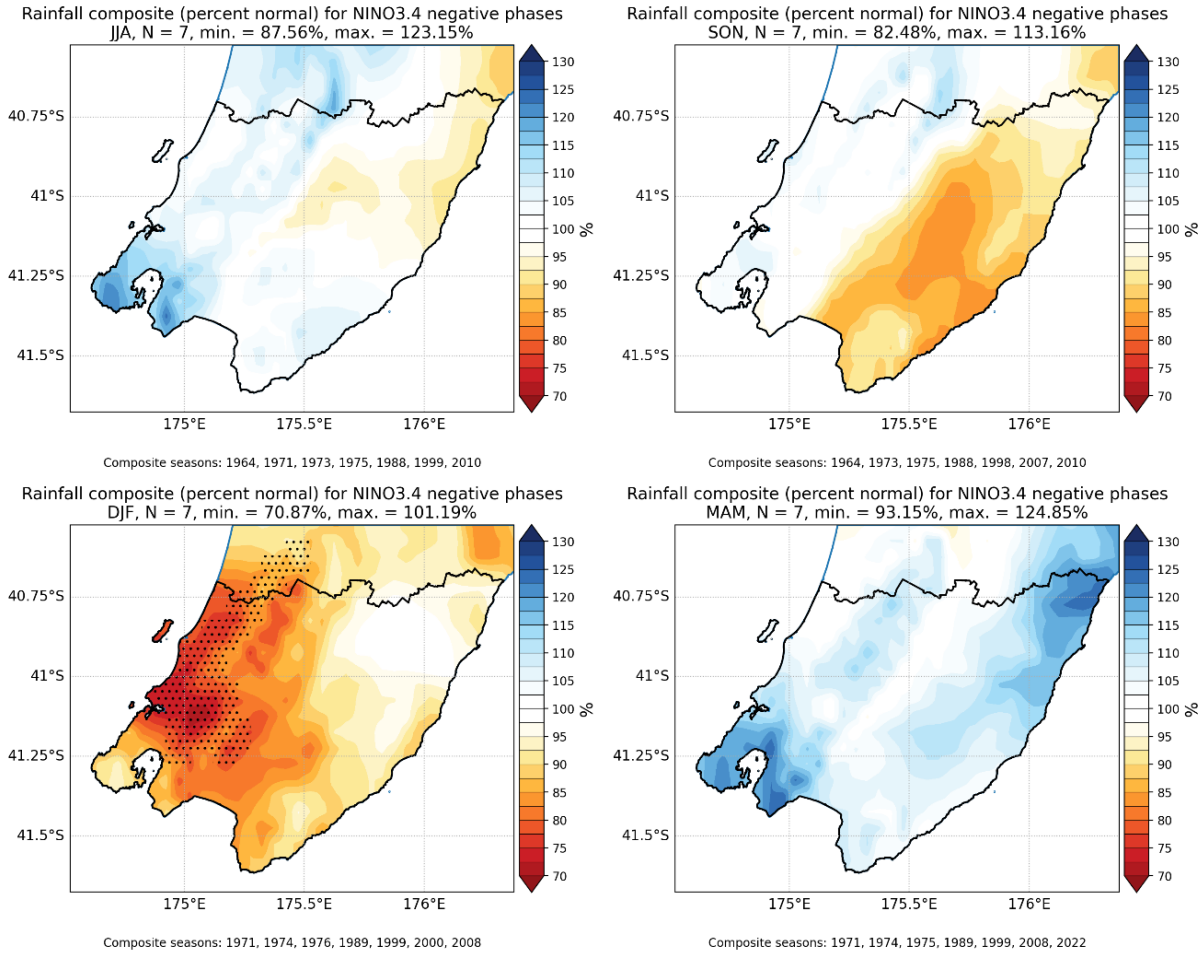

Figure 3-4: Rainfall anomalies (operational VCSN) during La Niña.

3.2.2 Augmented VCSN

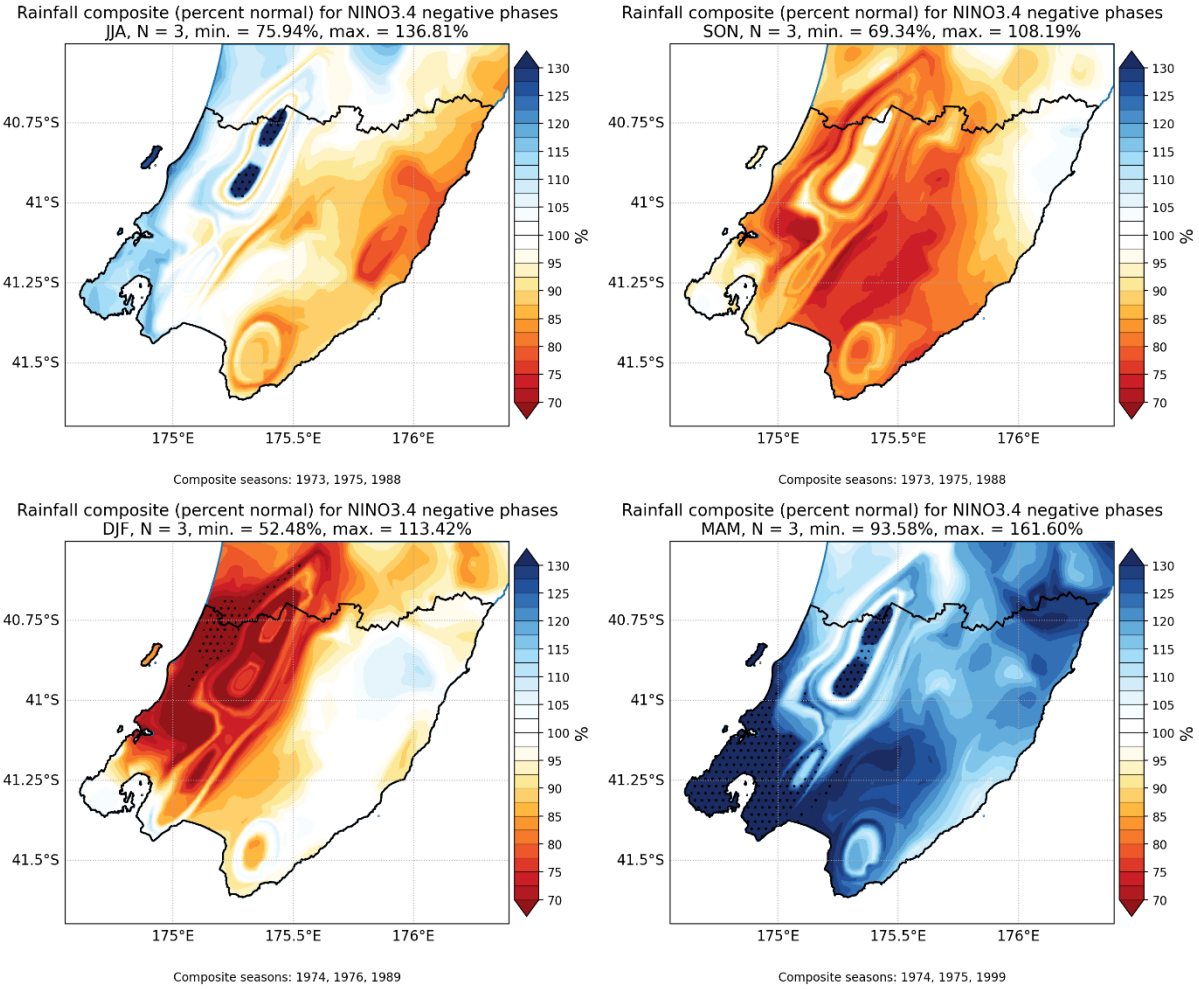

Figure 3-5: Rainfall anomalies (augmented VCSN) during La Niña. The legend range of 70-130% was selected to match the range presented for the operational VCSN maps above (Figure 3-4).

3.2.3 MSWEP

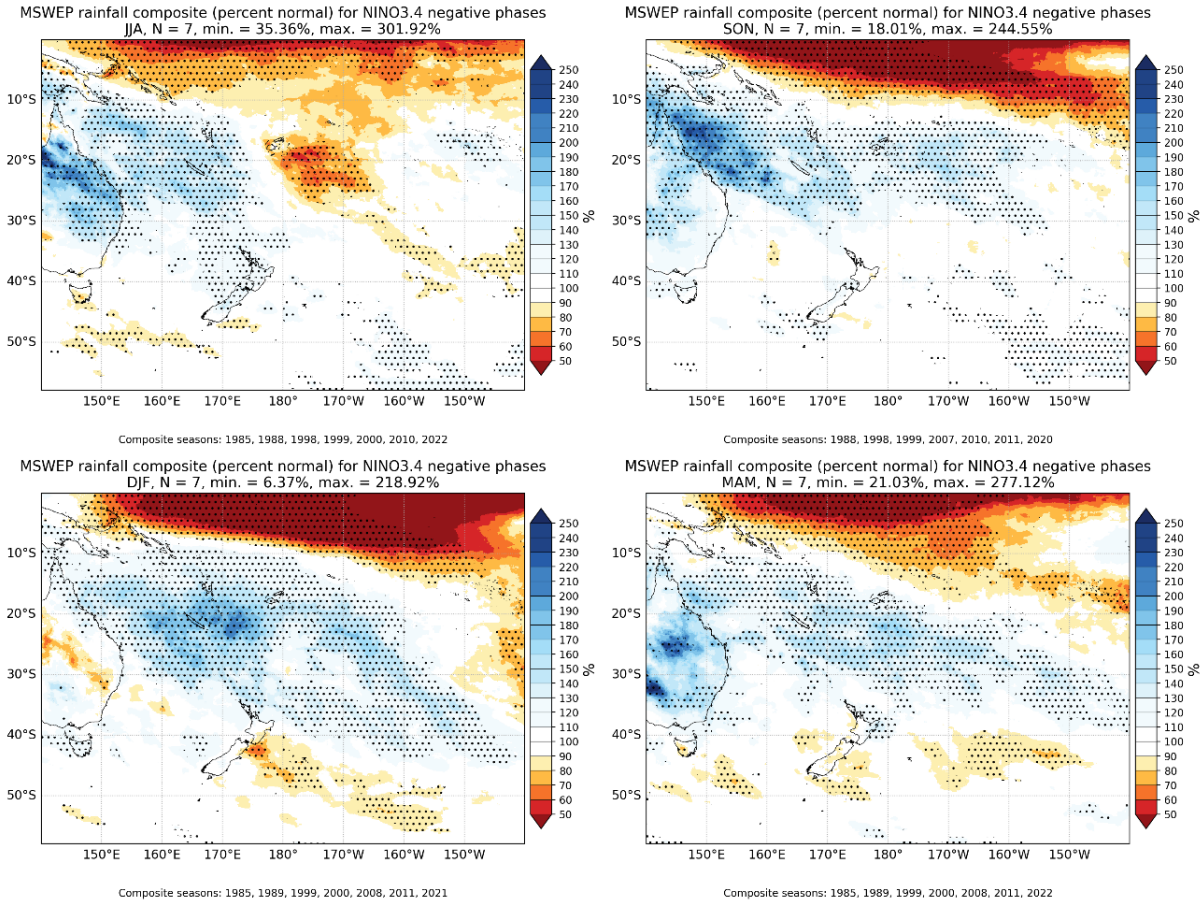

Figure 3-6: Rainfall anomalies (MSWEP) during La Niña.

3.3 IOD – positive phase

As highlighted above (see Section 2.5), the IOD is not strictly independent from ENSO, with IOD positive phases in spring (SON) often coinciding with the development phase of positive ENSO events, and vice-versa.

As expected from this relationship, positive IOD events tend to be associated with drier than normal conditions for the Greater Wellington region especially during spring (SON) and more so summer (DJF) (Figure 3-7). In winter (JJA) though, wetter than normal conditions tend to be associated with the positive phases of the IOD, but we note that the IOD, given its strong phase-locking onto the spring (SON) and the pattern of its relationship with ENSO, is not consistently expressed in winter (JJA).

However, the MSWEP composites highlight the fact that large-scale coherent rainfall anomalies associated with the IOD are mostly restricted to spring (SON) (Figure 3-8), reflecting the strong phase locking of the IOD phenomenon on the seasonal cycle.

In summary, the composite anomalies associated with the IOD positive phases largely reflect the relationship between the IOD and ENSO.

3.3.1 Operational VCSN

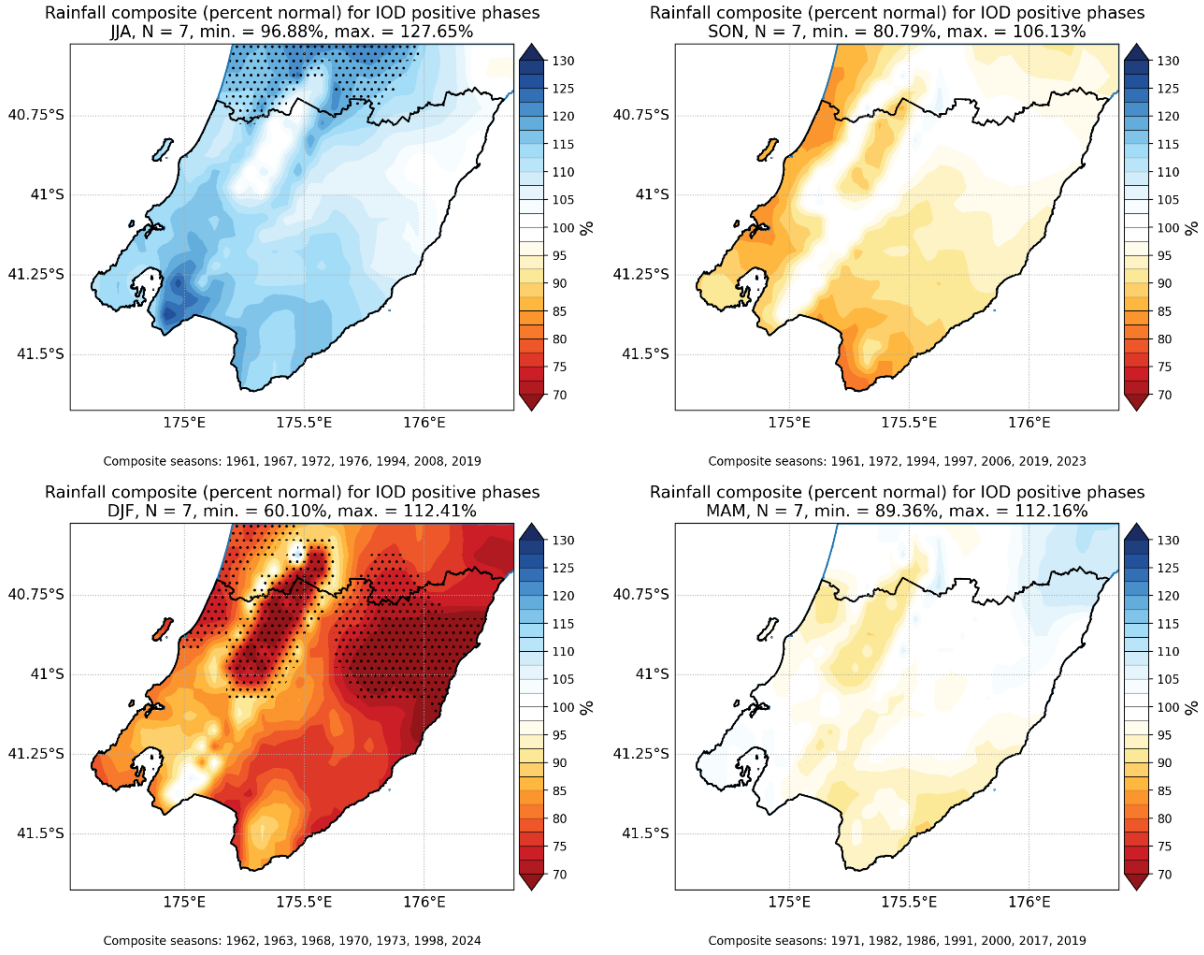

Figure 3-7: Rainfall anomalies (operational VCSN) during the positive phase of IOD.

3.3.2 MSWEP

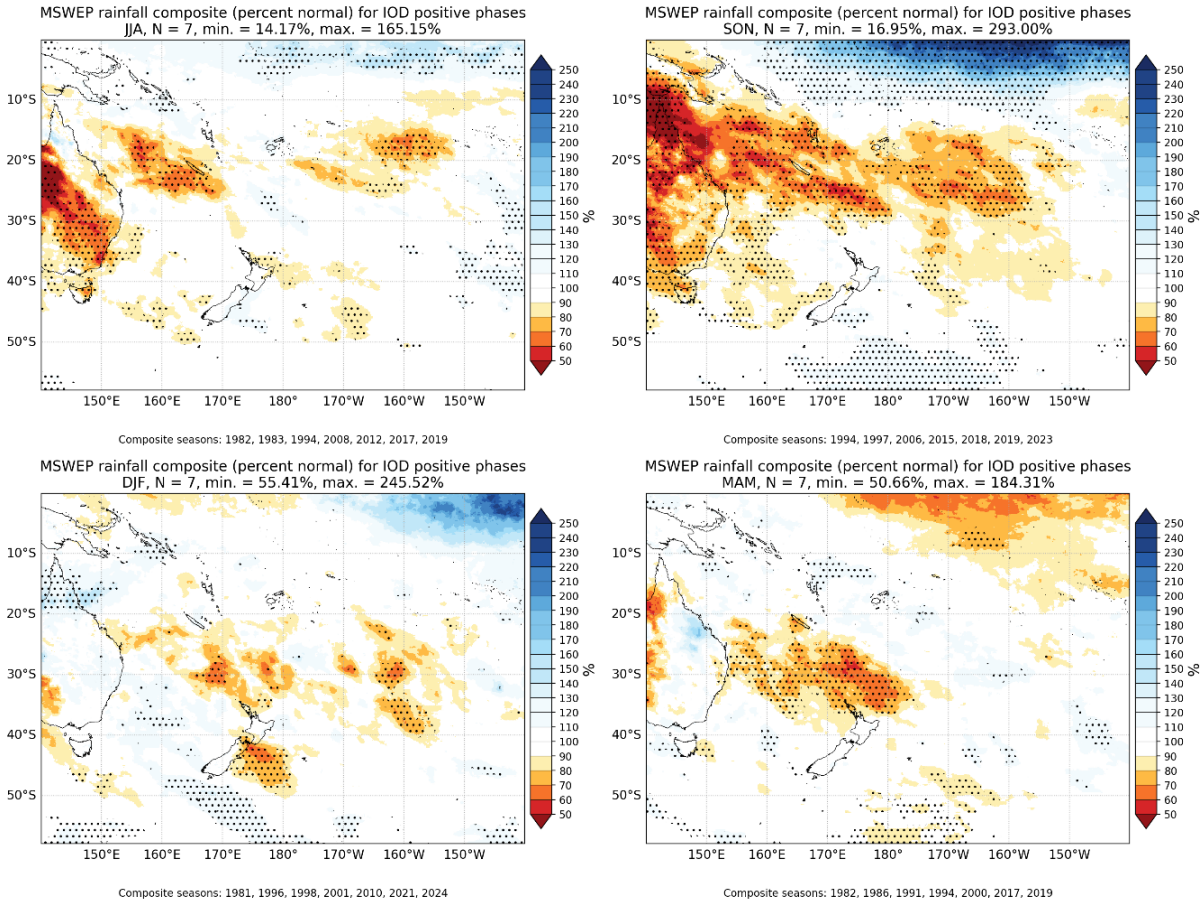

Figure 3-8: Rainfall anomalies (MSWEP) during the positive phase of IOD.

3.4 IOD – negative phase

In contrast with the positive phases of the IOD, negative phases of the IOD tend to be associated with wetter than normal conditions over the Greater Wellington region, although the anomalies are not significant (Figure 3-9). As observed above for the positive phases of the IOD, large-scale/basin-scale coherent rainfall anomalies are mostly observed during the peak of IOD events in spring (SON), with summer (DJF) and autumn (MAM) especially being characterised by much less spatially coherent anomalies (Figure 3-10).

3.4.1 Operational VCSN

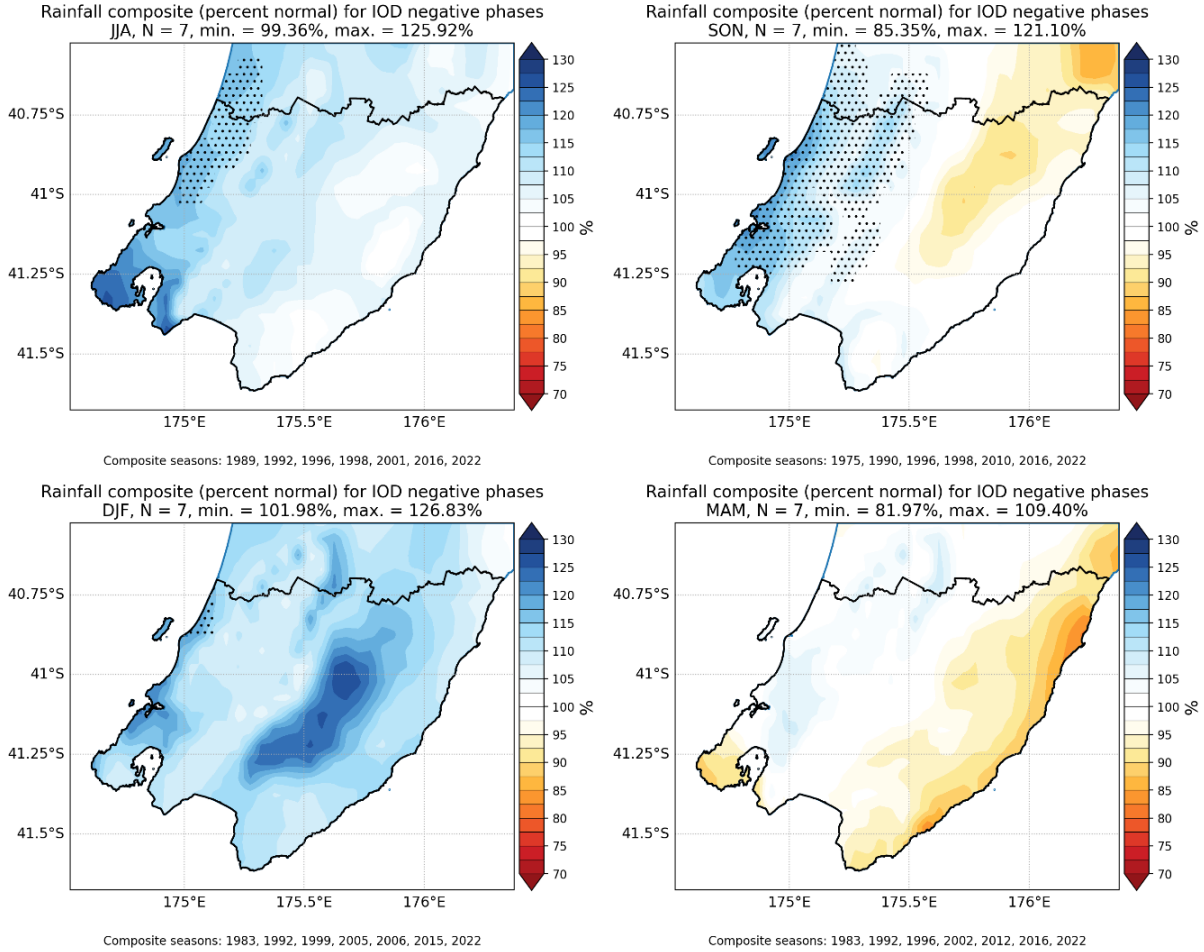

Figure 3-9: Rainfall anomalies (operational VCSN) during the negative phase of IOD.

3.4.2 MSWEP

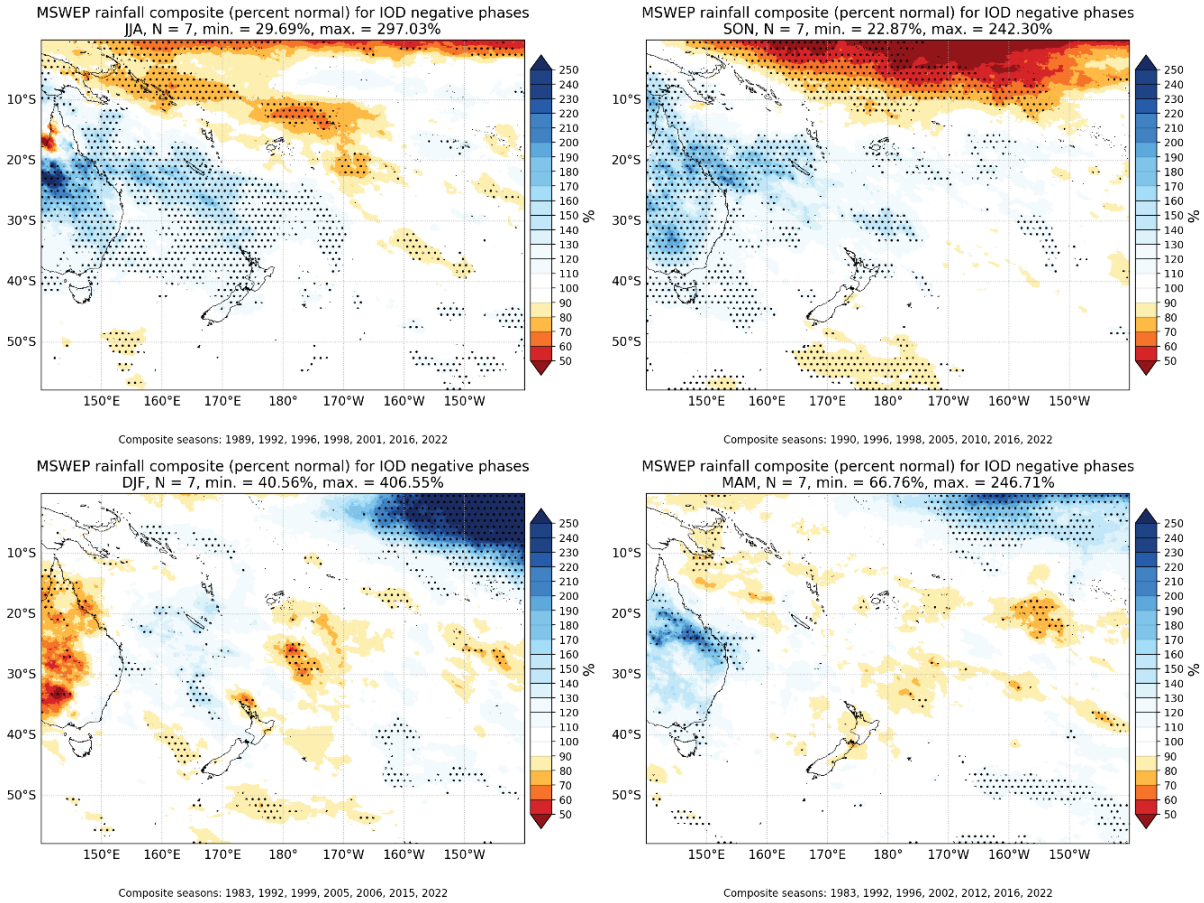

Figure 3-10: Rainfall anomalies (MSWEP) during the negative phase of IOD.

3.5 SAM – positive phase

The positive phases of the SAM tends to be associated with drier than normal conditions during the winter (JJA) and summer (DJF), while wetter than normal conditions, especially in the western part of the Greater Wellington region, are recorded in spring (SON) (Figure 3-11 and Figure 3-12).

3.5.1 Operational VCSN

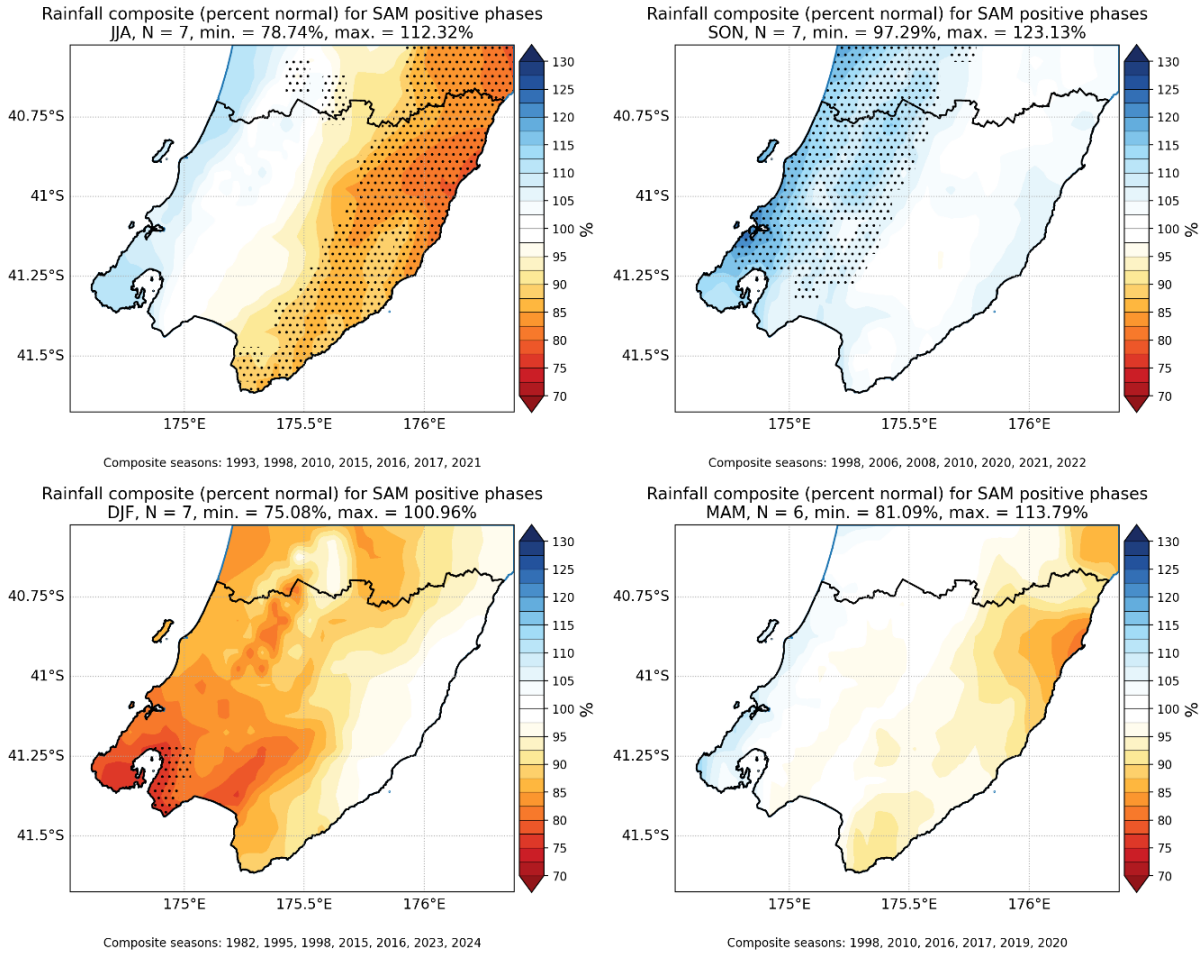

Figure 3-11: Rainfall anomalies (operational VCSN) during the positive phase of SAM.

3.5.2 MSWEP

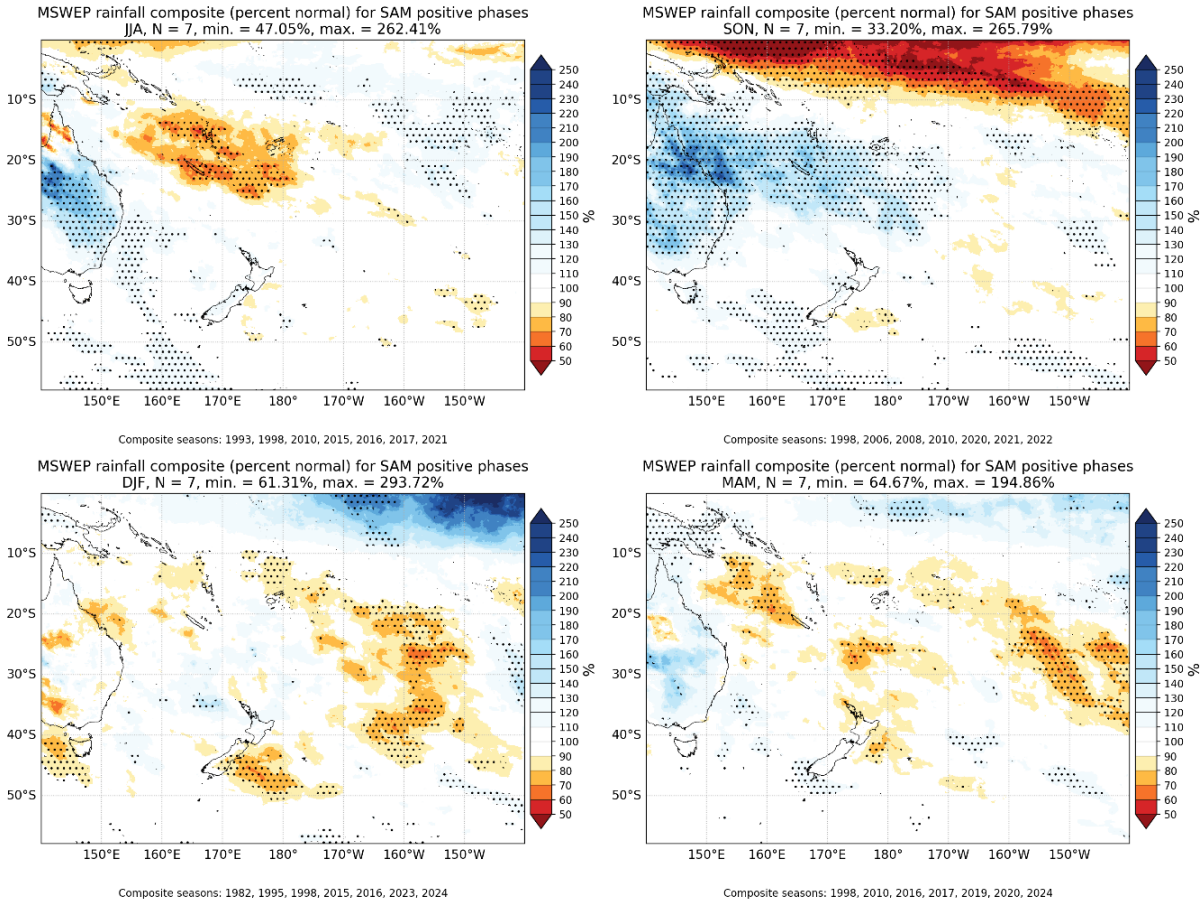

Figure 3-12: Rainfall anomalies (MSWEP) during the positive phase of SAM.

3.6 SAM – negative phase

Wetter conditions are generally experienced in the Greater Wellington region (with the exception of spring (SON)) during the negative phase of SAM (Figure 3-13 and Figure 3-14). This can be contrasted with the generally dry conditions experienced during the positive phases of the SAM (again, except for spring (SON)). Several points however must be recalled:

1. The SAM shows a strong positive trend over the period of analysis (Section 2.5; Figure 2-4).
2. Negative phases of the SAM are therefore clustered during the first decades of the period, while positive phases of the SAM are clustered during the last decades.
3. Some rainfall parameters – although not for all areas of the Greater Wellington region – show a weak negative trend (i.e., a trend overall towards drier conditions) over the same period.

Overall, these signals (positive SAM trend, and a positive SAM tending to be associated with drier conditions, and an observed negative trend in rainfall) appear to be consistent. One hypothesis could be that part of the rainfall trends observed in some regions and parameters are causally related to the observed positive SAM trend.

3.6.1 Operational VCSN

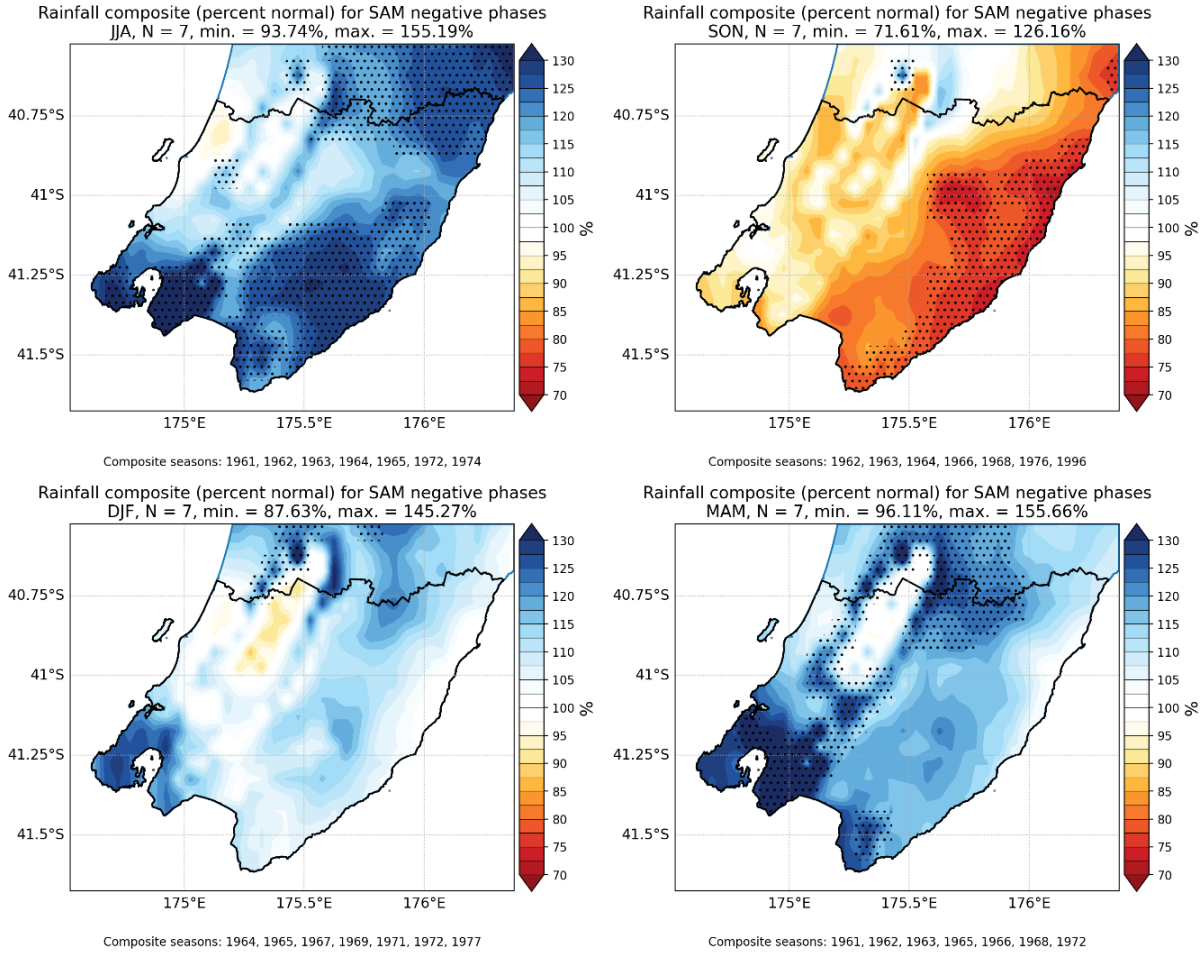

Figure 3-13: Rainfall anomalies (operational VCSN) during the negative phase of SAM.

3.6.2 MSWEP

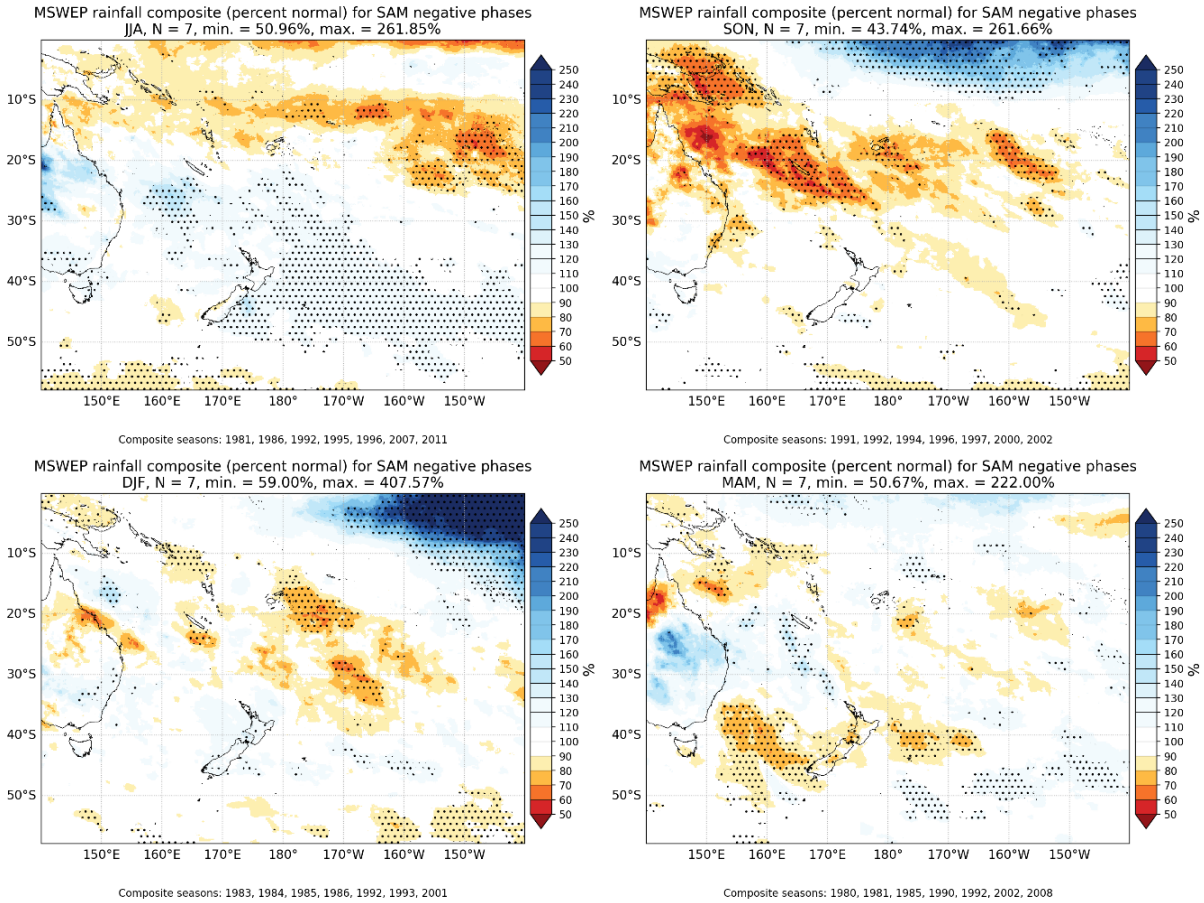

Figure 3-14: Rainfall anomalies (MSWEP) during the negative phase of SAM.

3.7 SPSD – positive phase

The positive phases of the SPSD tends to be associated with wetter than normal conditions during summer (DJF), especially in the eastern and southern parts of the Greater Wellington region (Figure 3-15). These wetter than normal conditions extend towards the northwest of the North Island over parts of the Tasman Sea (Figure 3-16).

3.7.1 Operational VCSN

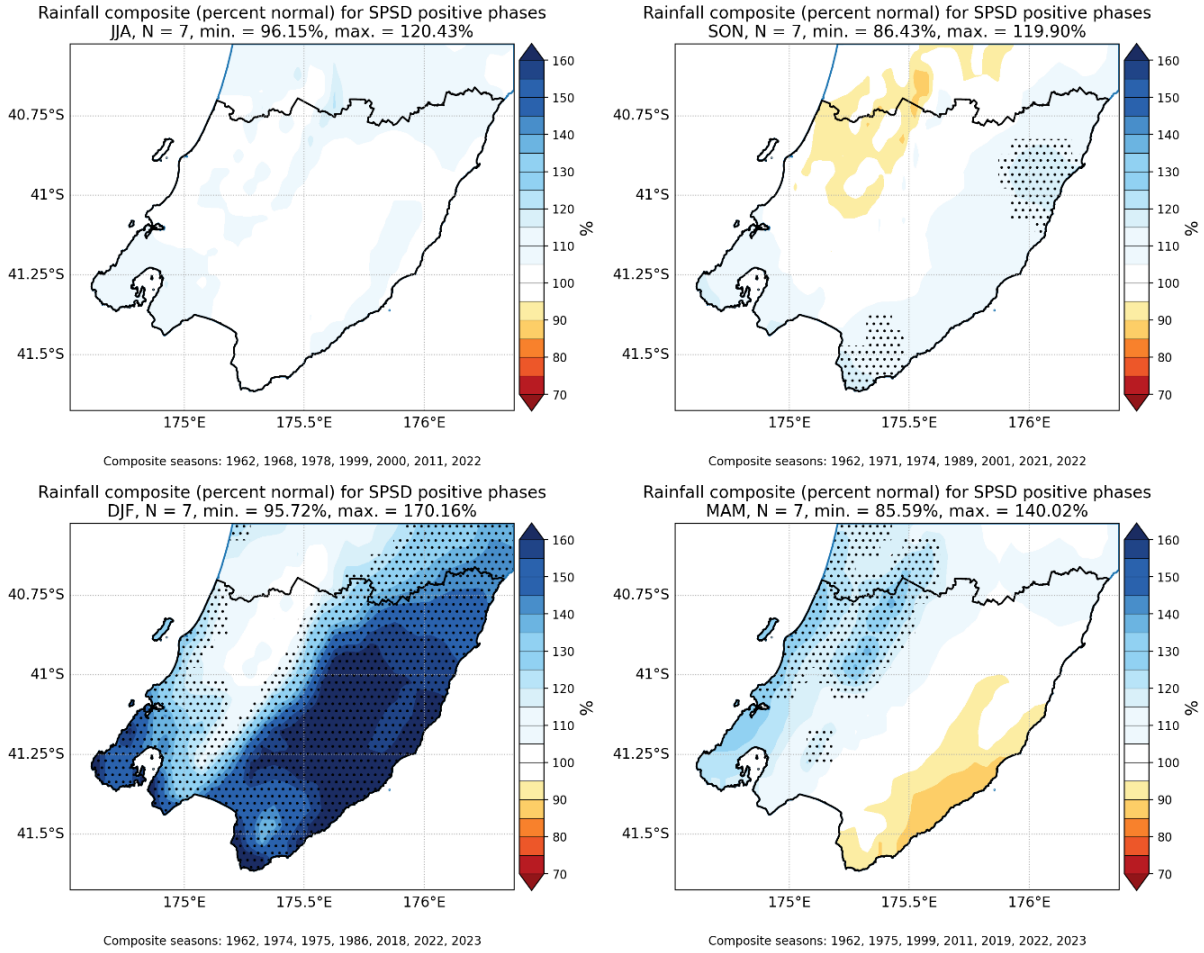

Figure 3-15: Rainfall anomalies (operational VCSN) during the positive phase of SPSD.

3.7.2 MSWEP

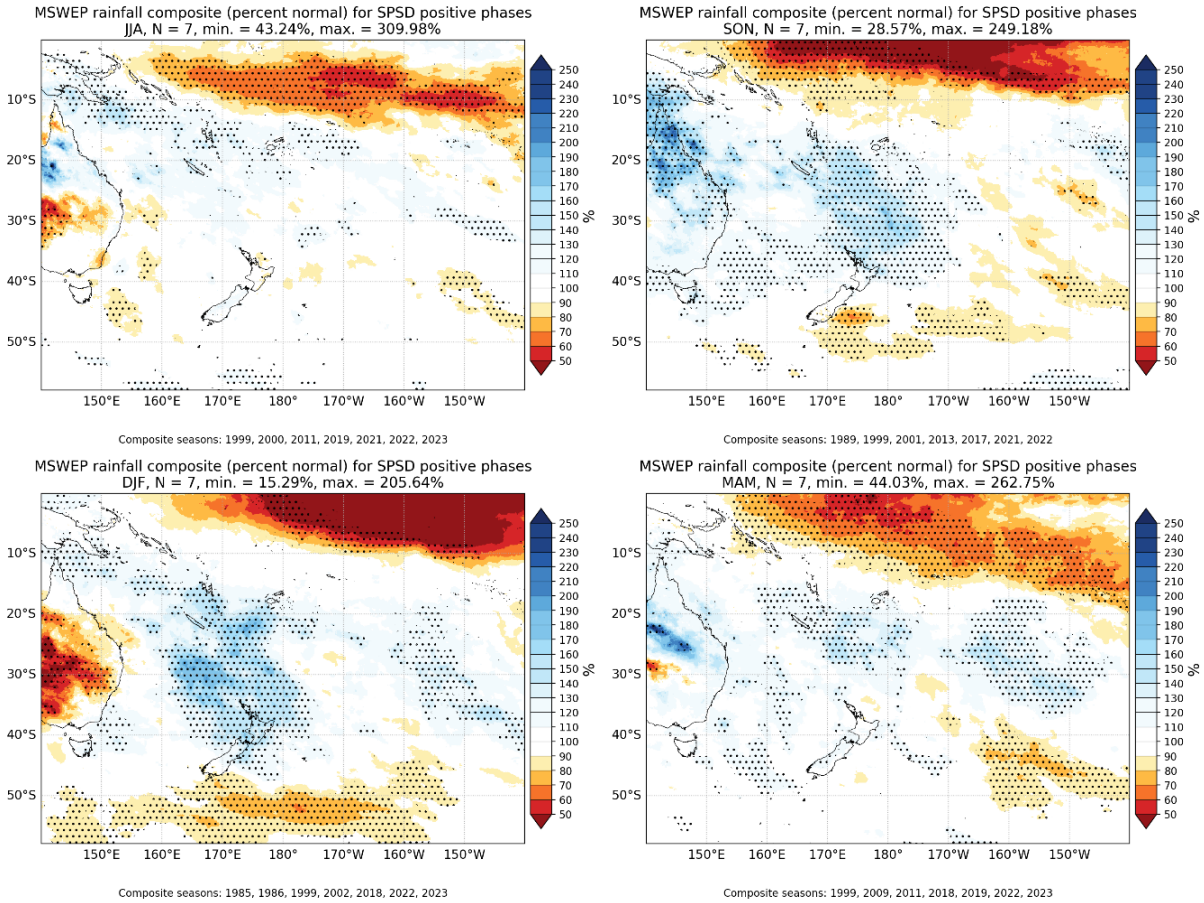

Figure 3-16: Rainfall anomalies (MSWEP) during the positive phase of SPSD.

3.8 SPSD – negative phase

The negative phases of the SPSD tends to be associated with drier than normal conditions during spring (SON) for western and southern parts of the Greater Wellington region (Figure 3-17), although this anomaly isn't statistically significant for most parts. Drier than normal conditions are typically observed north of New Zealand during the negative phase of SPSD (Figure 3-18).

3.8.1 Operational VCSN

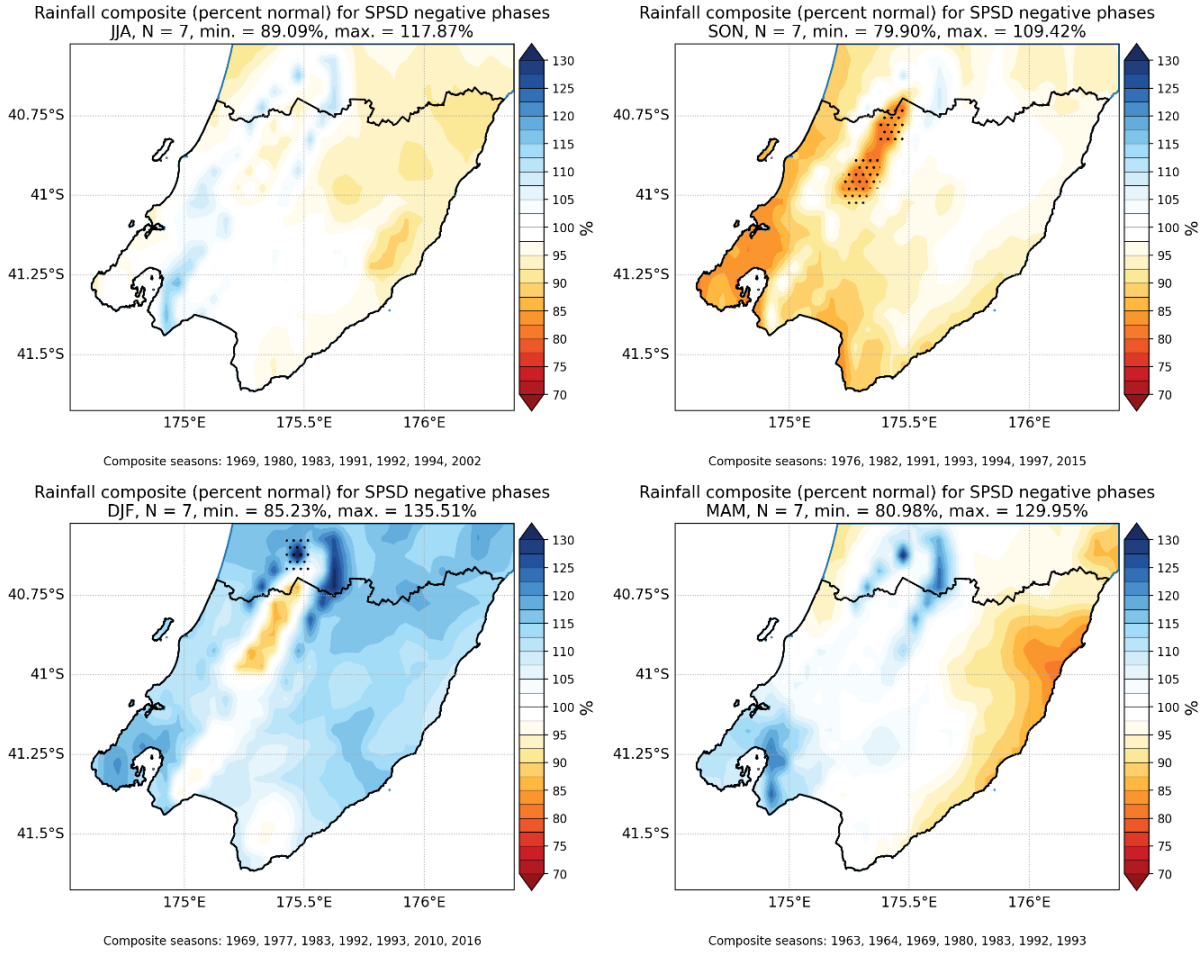

Figure 3-17: Rainfall anomalies (operational VCSN) during the negative phase of SPSD.

3.8.2 MSWEP

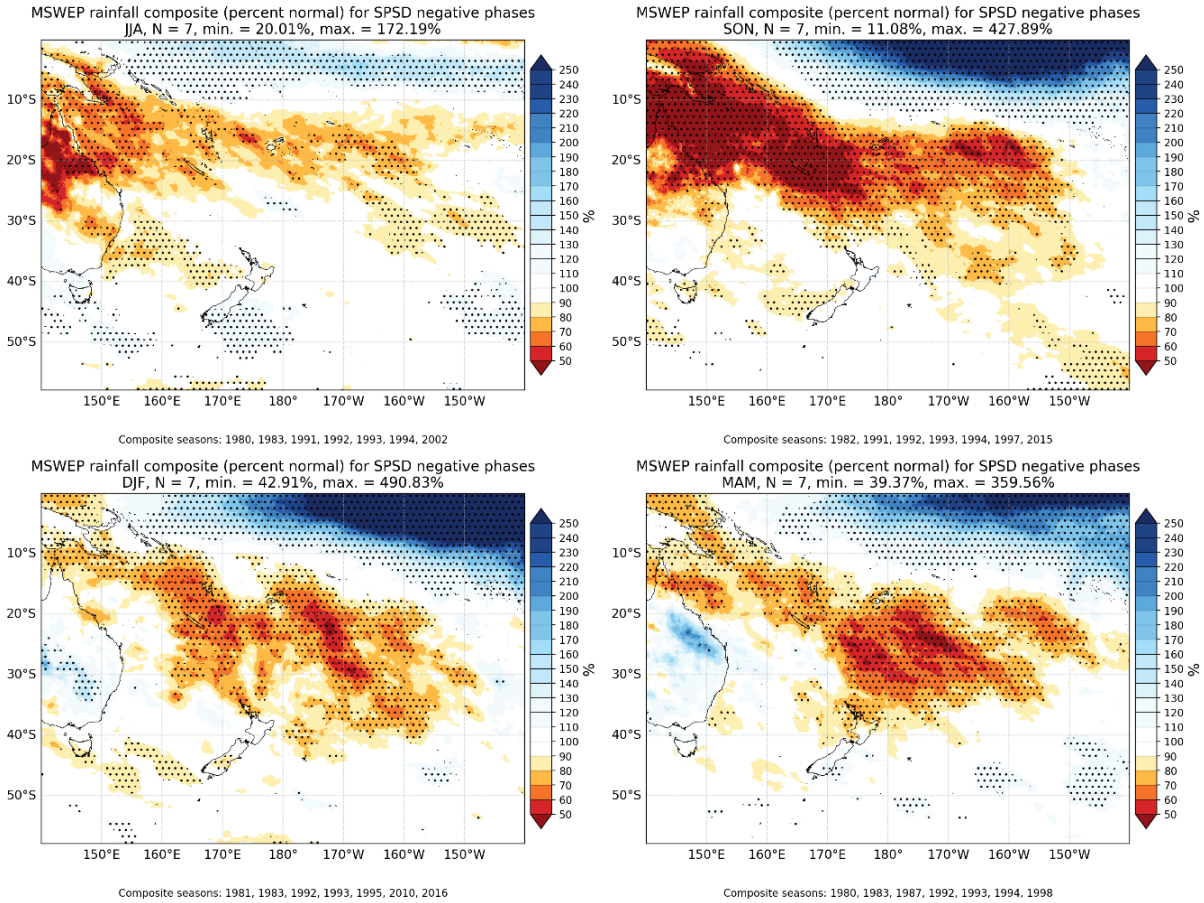

Figure 3-18: Rainfall anomalies (MSWEP) during the negative phase of SPSD.

4 Rain days

4.1 ENSO – positive phase (El Niño)

During the positive phases of ENSO, many parts of the region observe a reduction in spring (SON) and summer (DJF) rain days (Figure 4-1 and Figure 4-2). In both cases, this reduction in rain days does not appear to extend to cover the Tararua ranges.

The signal is embedded in a large-scale, Pacific-wide signal as evidenced by the composites anomalies from the MSWEP dataset (Figure 4-3): fewer rain days are generally observed over and to the north of the North Island during positive phases of ENSO.

4.1.1 Operational VCSN

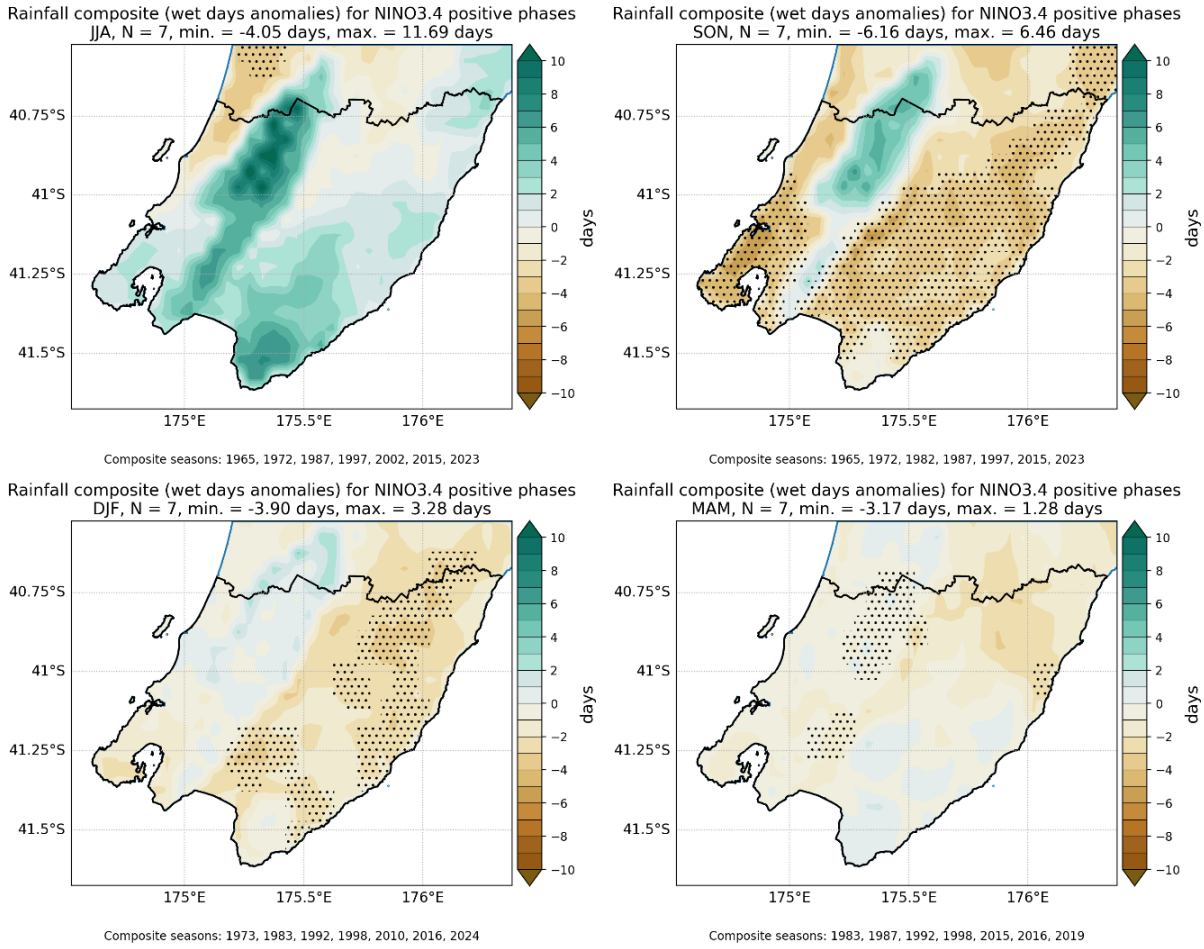

Figure 4-1: Rain day anomalies (operational VCSN) during El Niño. Stippling indicates areas of statistical significance at $p \leq 0.10$. The years indicated under each figure are those of the last month in the season (e.g., DJF 1973 refers to December 1972 – February 1973).

4.1.2 Augmented VCSN

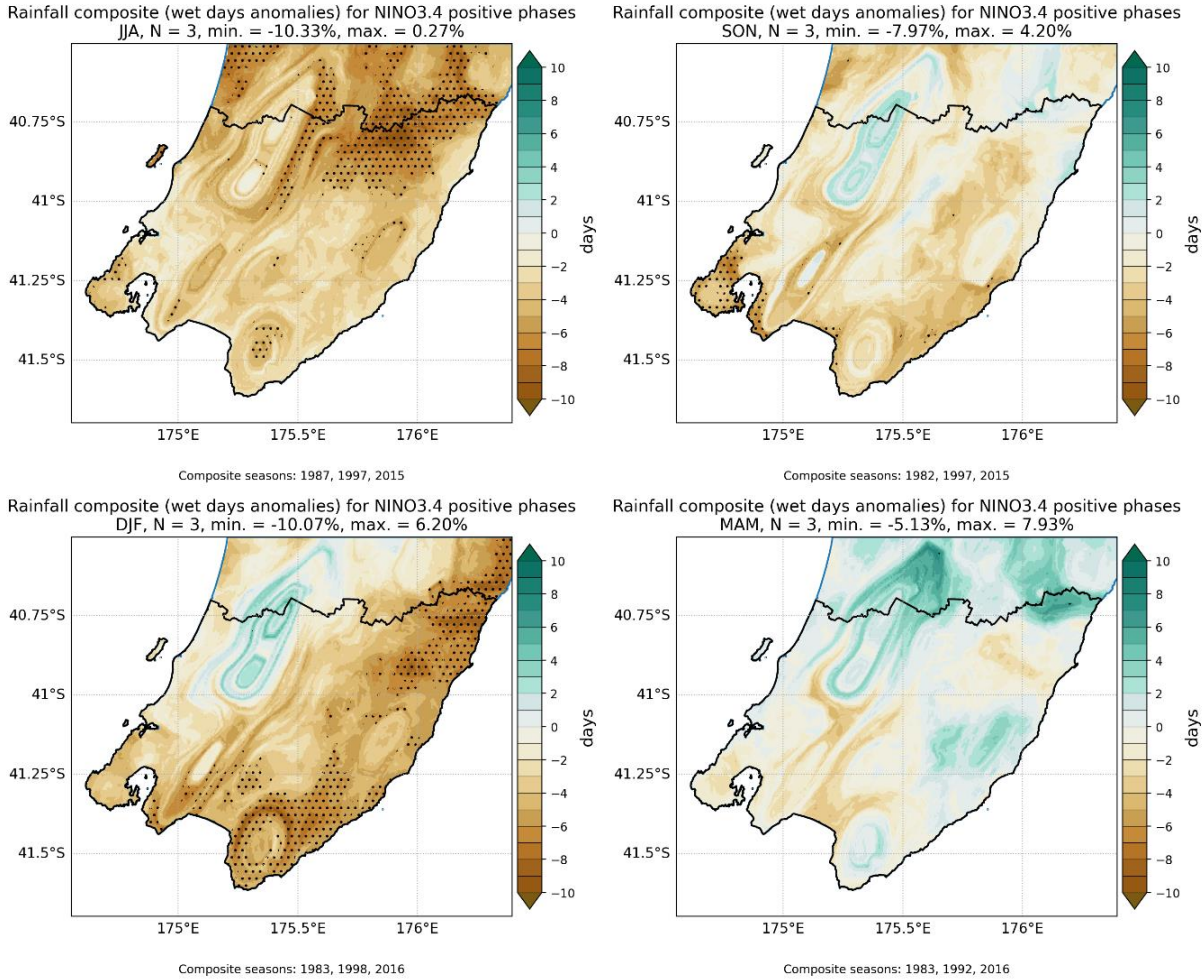

Figure 4-2: Rain day anomalies (augmented VCSN) during El Niño.

4.1.3 MSWEP

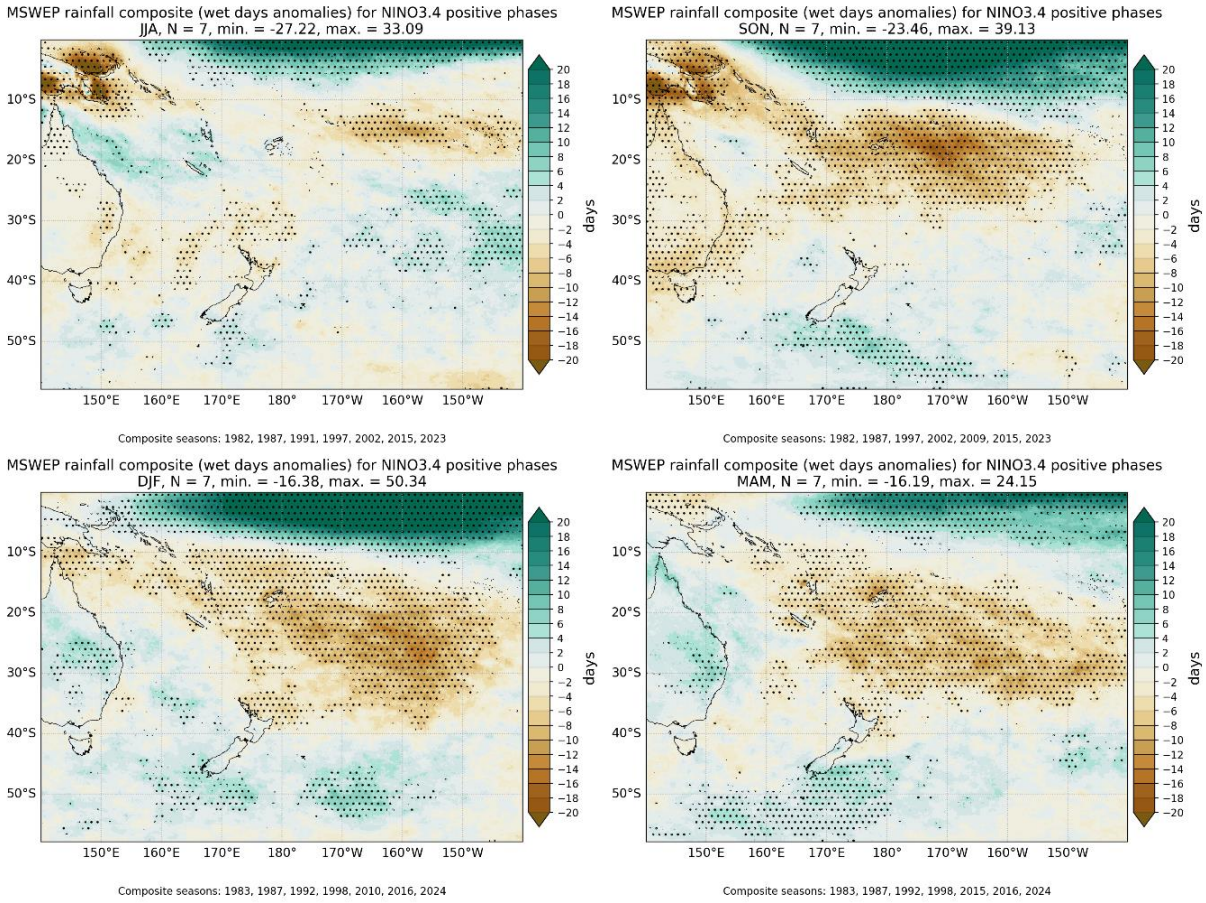

Figure 4-3: Rain day anomalies (MSWEP) during El Niño.

4.2 ENSO – negative phase (La Niña)

La Niña tends to be associated with a decrease in summer (DJF) rain days for western parts of the Greater Wellington region, and a decrease in spring (SON) rain days for eastern parts (Figure 4-4 and Figure 4-5). Many parts of the region observe an increase in winter (JJA) rain days, especially about the Tararua Range. Summer (DJF) and autumn (MAM) rain days tend to decrease east of the South Island and increase to the north of New Zealand during La Niña (Figure 4-6).

4.2.1 Operational VCSN

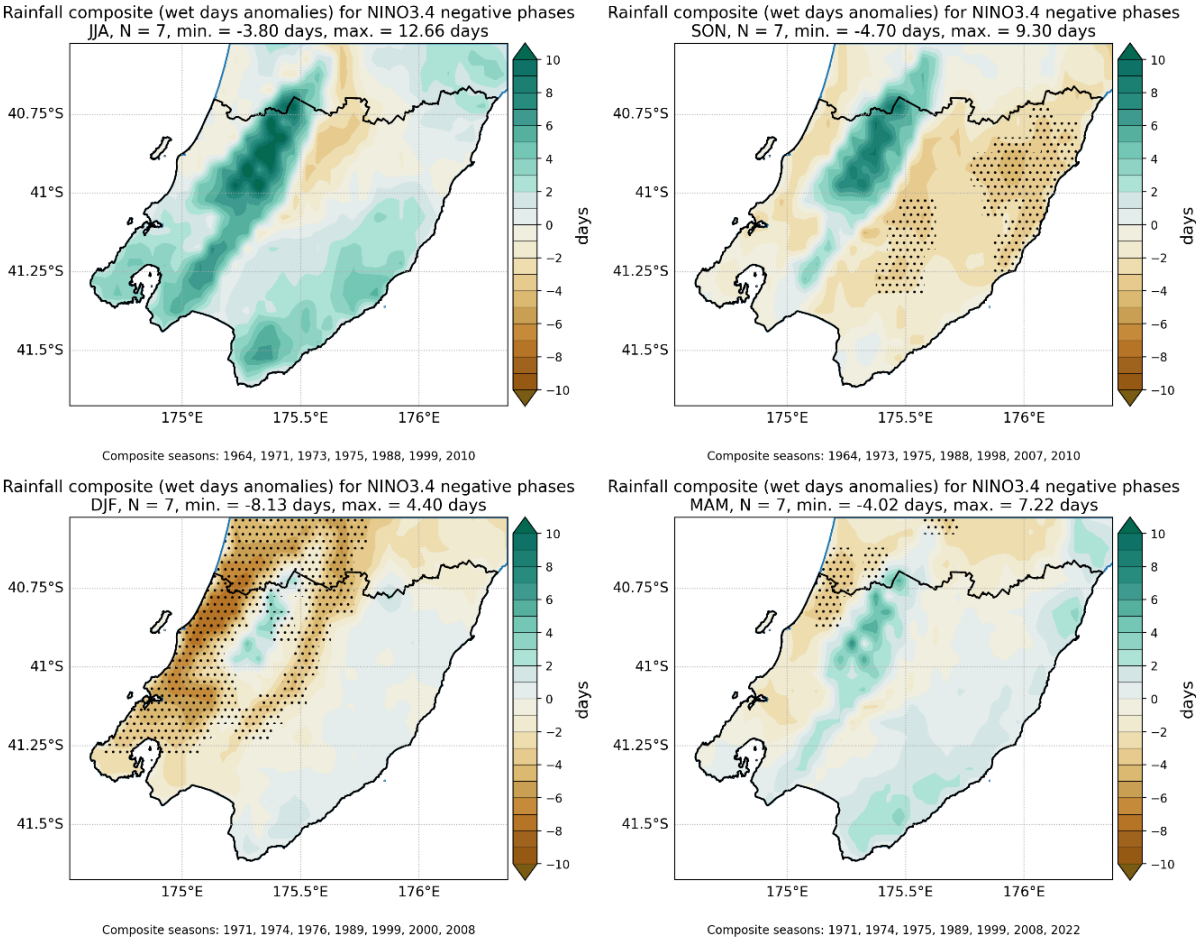

Figure 4-4: Rain day anomalies (operational VCSN) during La Niña.

4.2.2 Augmented VCSN

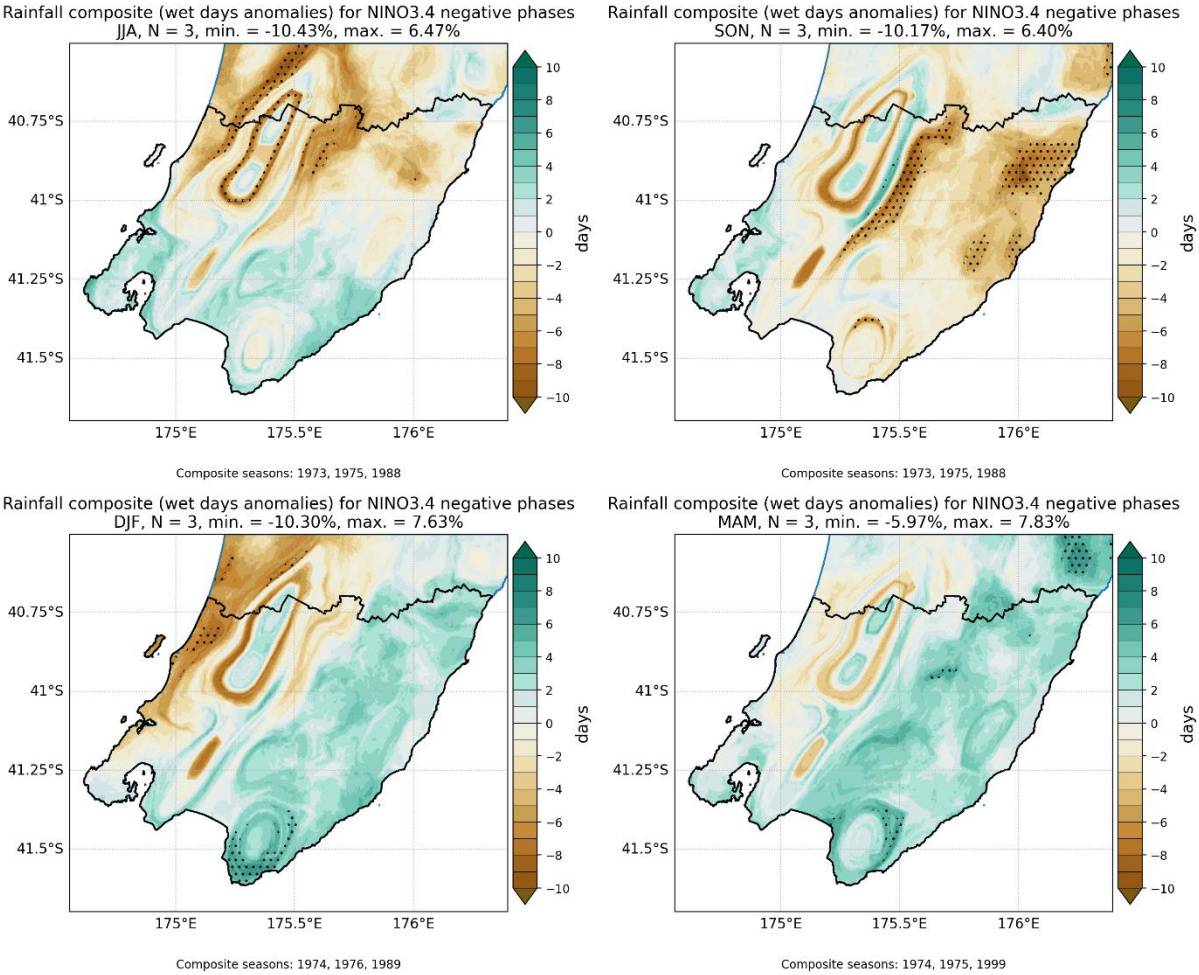

Figure 4-5: Rain day anomalies (augmented VCSN) during La Niña.

4.2.3 MSWEP

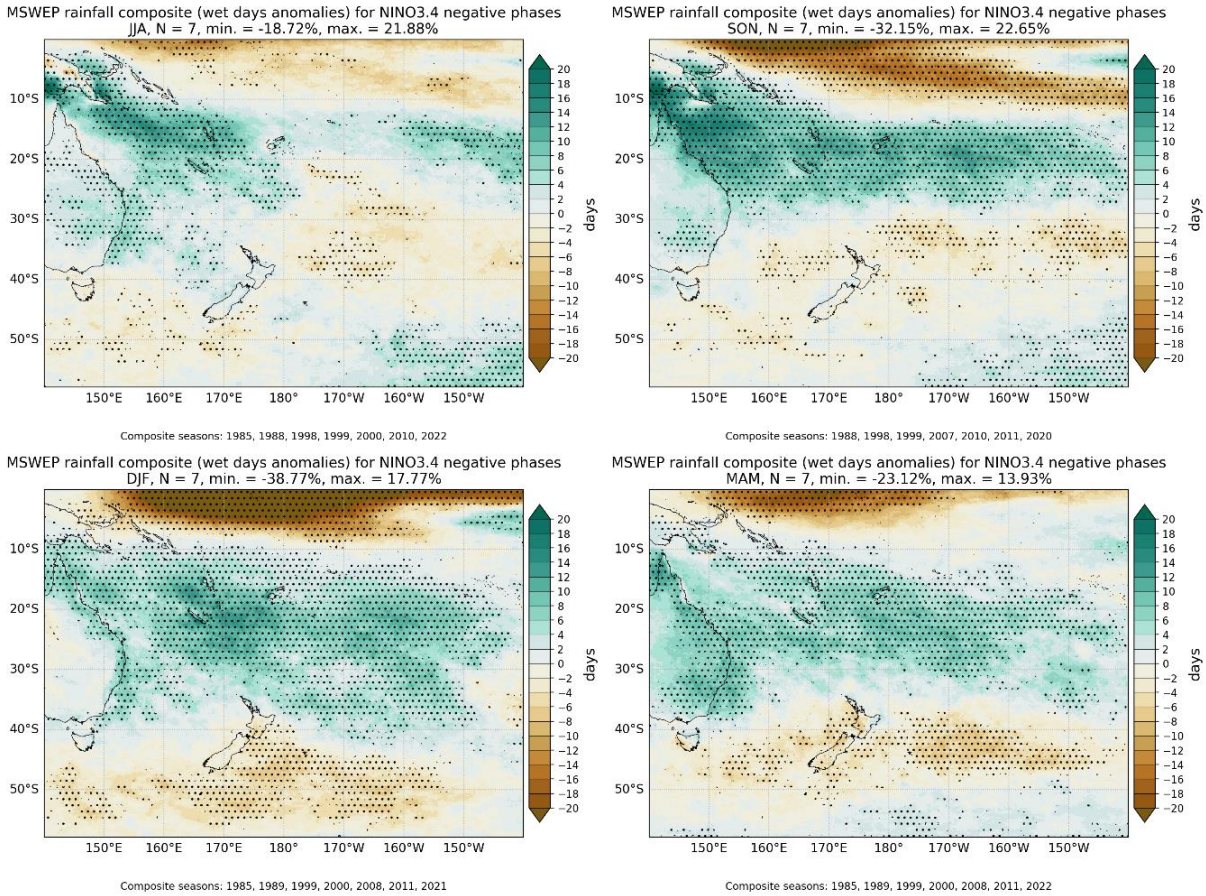

Figure 4-6: Rain day anomalies (MSWEP) during La Niña.

4.3 IOD – positive phase

Positive IOD events tend to be associated with fewer than normal spring (SON) and summer (DJF) rain days for most of the region, except for the Tararua Range (Figure 4-7). The MSWEP composites highlight a reduction in spring (SON) rain days for much of the southwest Pacific and Australia (Figure 4-8).

4.3.1 Operational VCSN

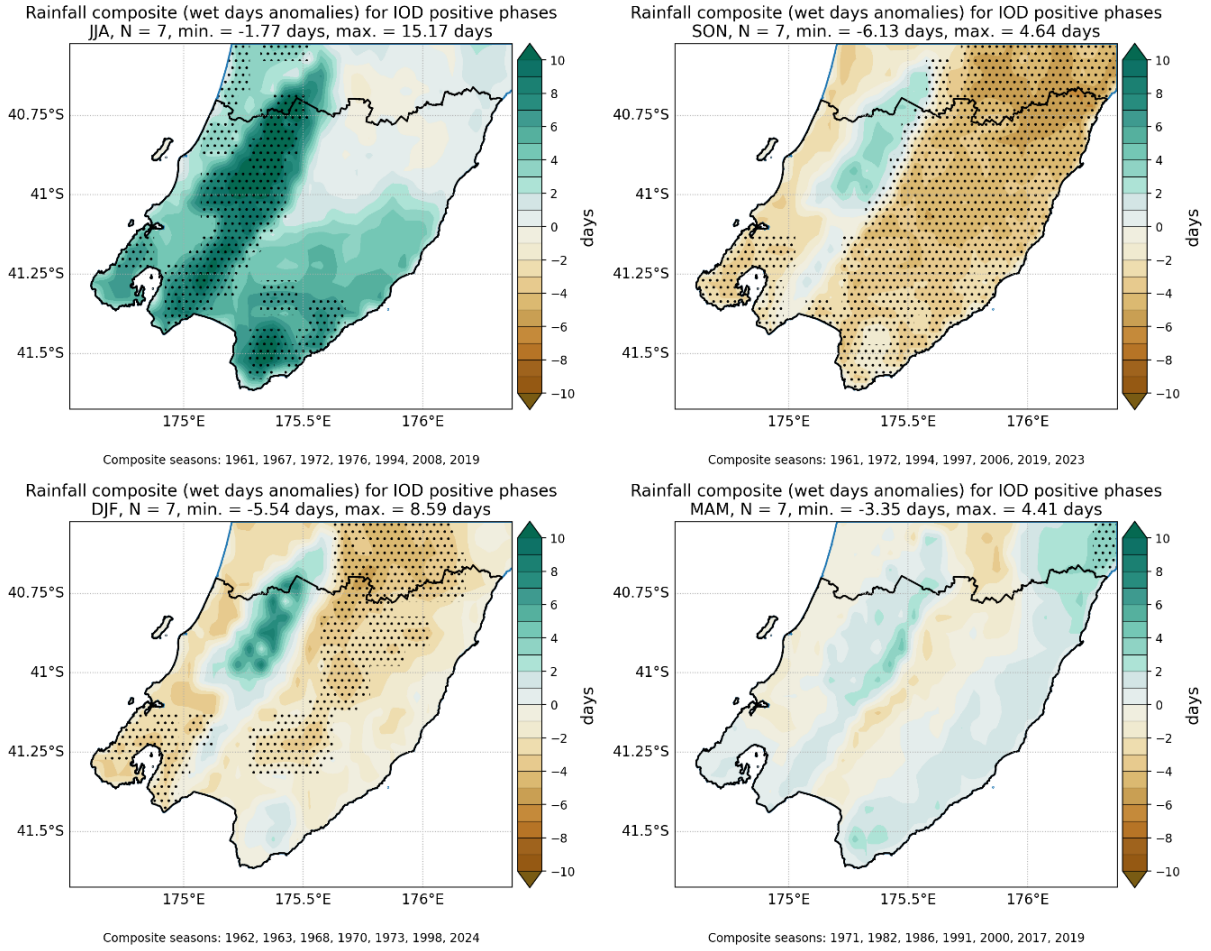

Figure 4-7: Rain day anomalies (operational VCSN) during the positive phase of IOD.

4.3.2 MSWEP

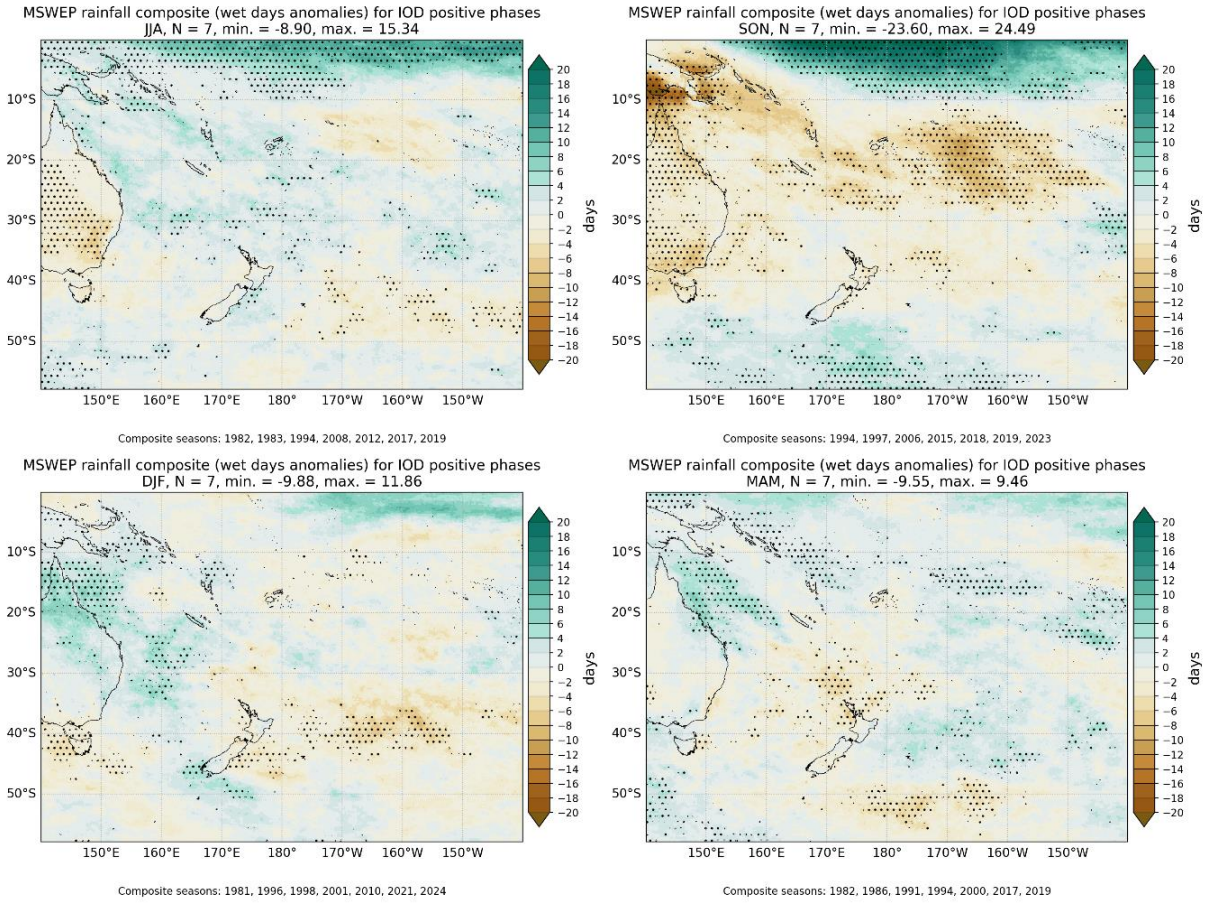

Figure 4-8: Rain day anomalies (MSWEP) during the positive phase of IOD.

4.4 IOD – negative phase

Negative phases of the IOD tend to be associated with increases in winter (JJA) rain days over the Greater Wellington region, although the anomalies are generally not significant (Figure 4-9). Large-scale/basin-scale coherent rain day anomalies are mostly observed during the peak of IOD events in spring (SON), with autumn (MAM) especially being characterised by much less spatially coherent anomalies (Figure 4-10).

4.4.1 Operational VCSN

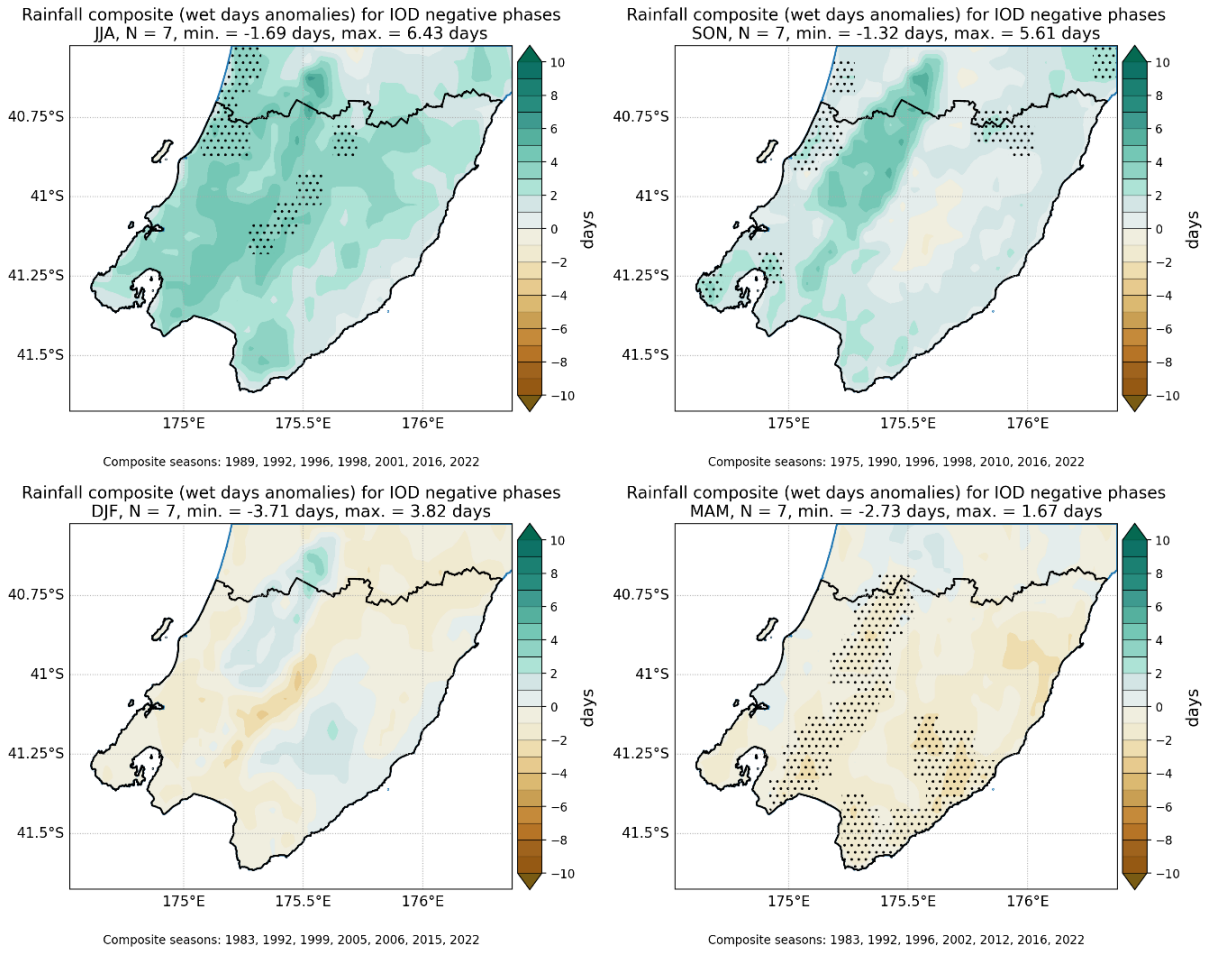

Figure 4-9: Rain day anomalies (operational VCSN) during the negative phase of IOD.

4.4.2 MSWEP

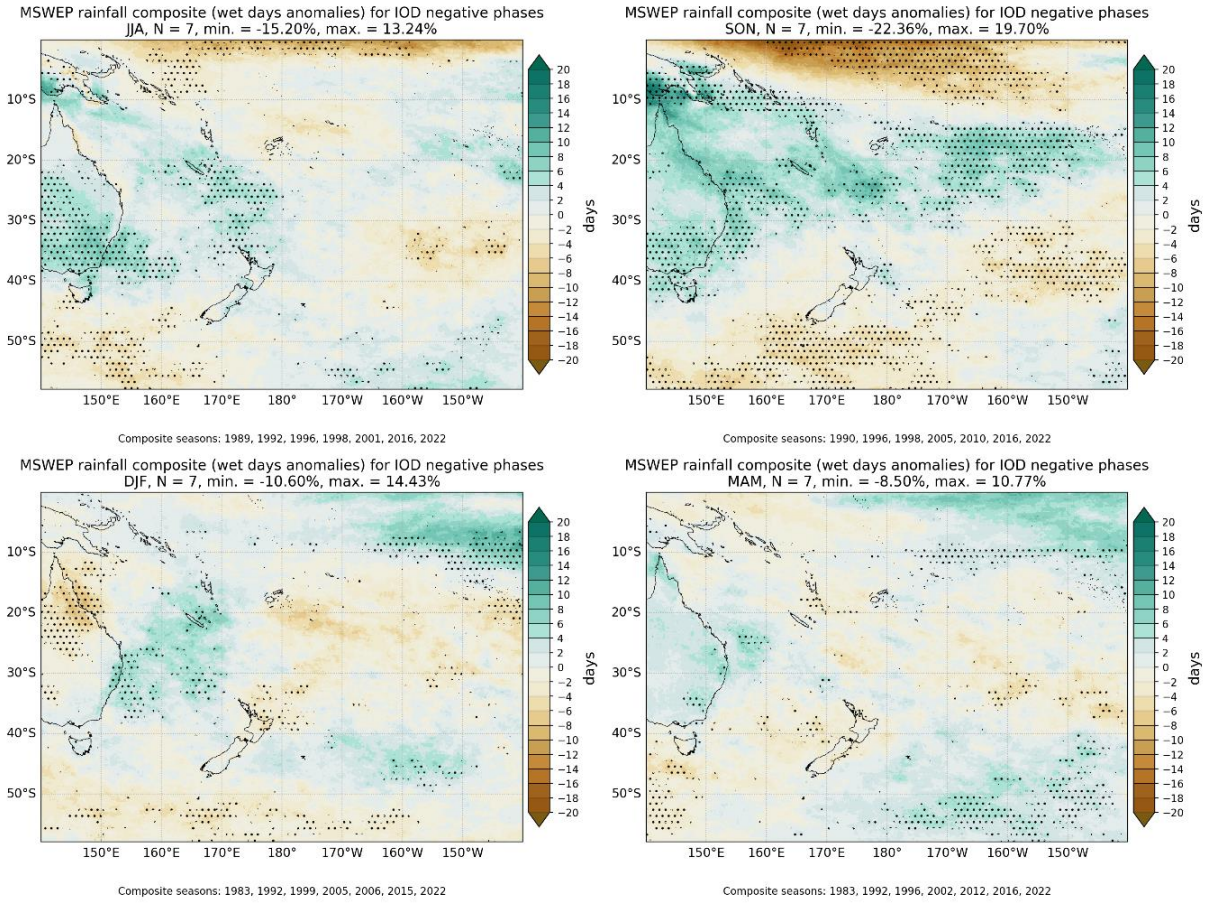

Figure 4-10: Rain day anomalies (MSWEP) during the negative phase of IOD.

4.5 SAM – positive phase

The positive phase of the SAM tends to be associated with fewer than normal rain days during the summer (DJF) and autumn (MAM) (Figure 4-11 and Figure 4-12).

4.5.1 Operational VCSN

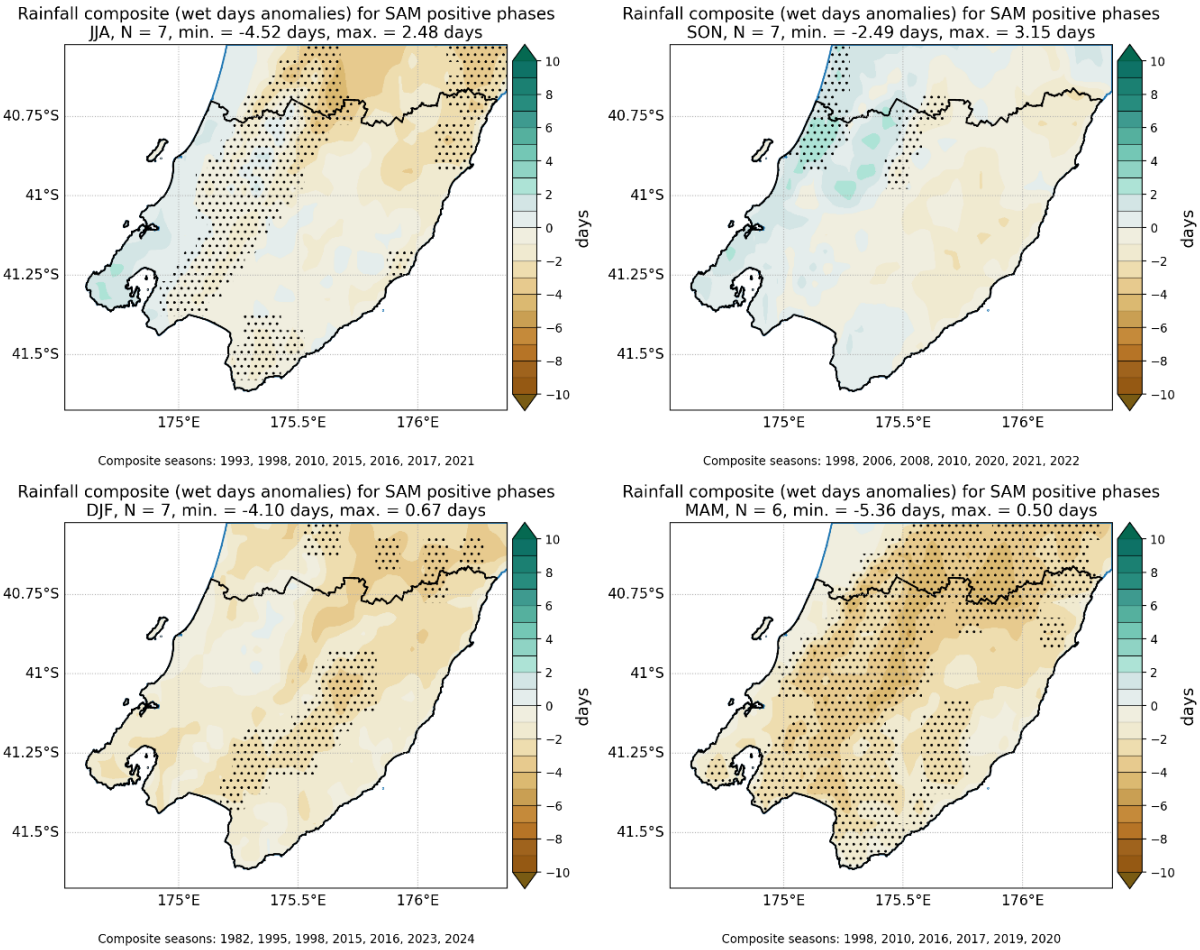

Figure 4-11: Rain day anomalies (operational VCSN) during the positive phase of SAM.

4.5.2 MSWEP

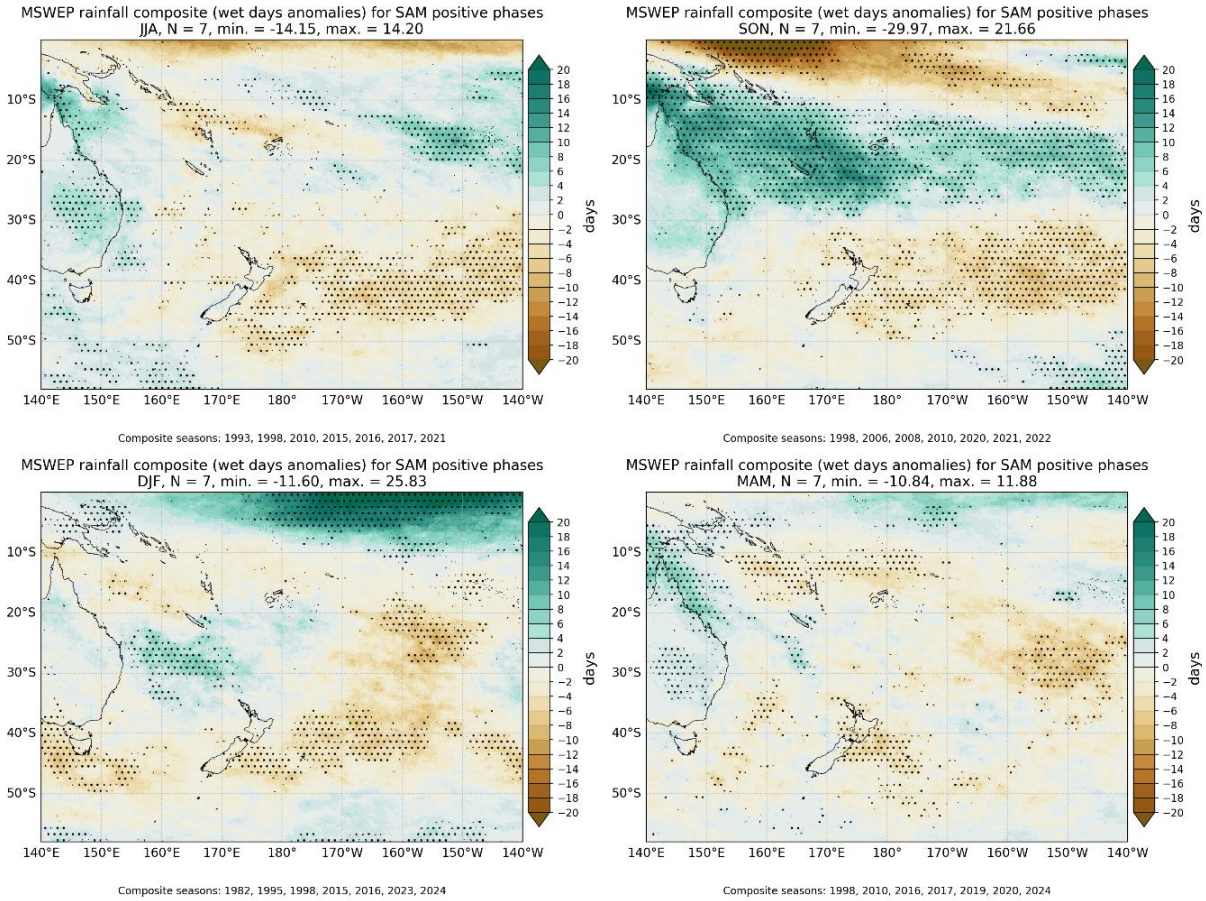

Figure 4-12: Rain day anomalies (MSWEP) during the positive phase of SAM.

4.6 SAM – negative phase

The Greater Wellington region typically observes more rain days than normal during the negative phase of SAM, particularly during winter (JJA) (Figure 4-13 and Figure 4-14).

4.6.1 Operational VCSN

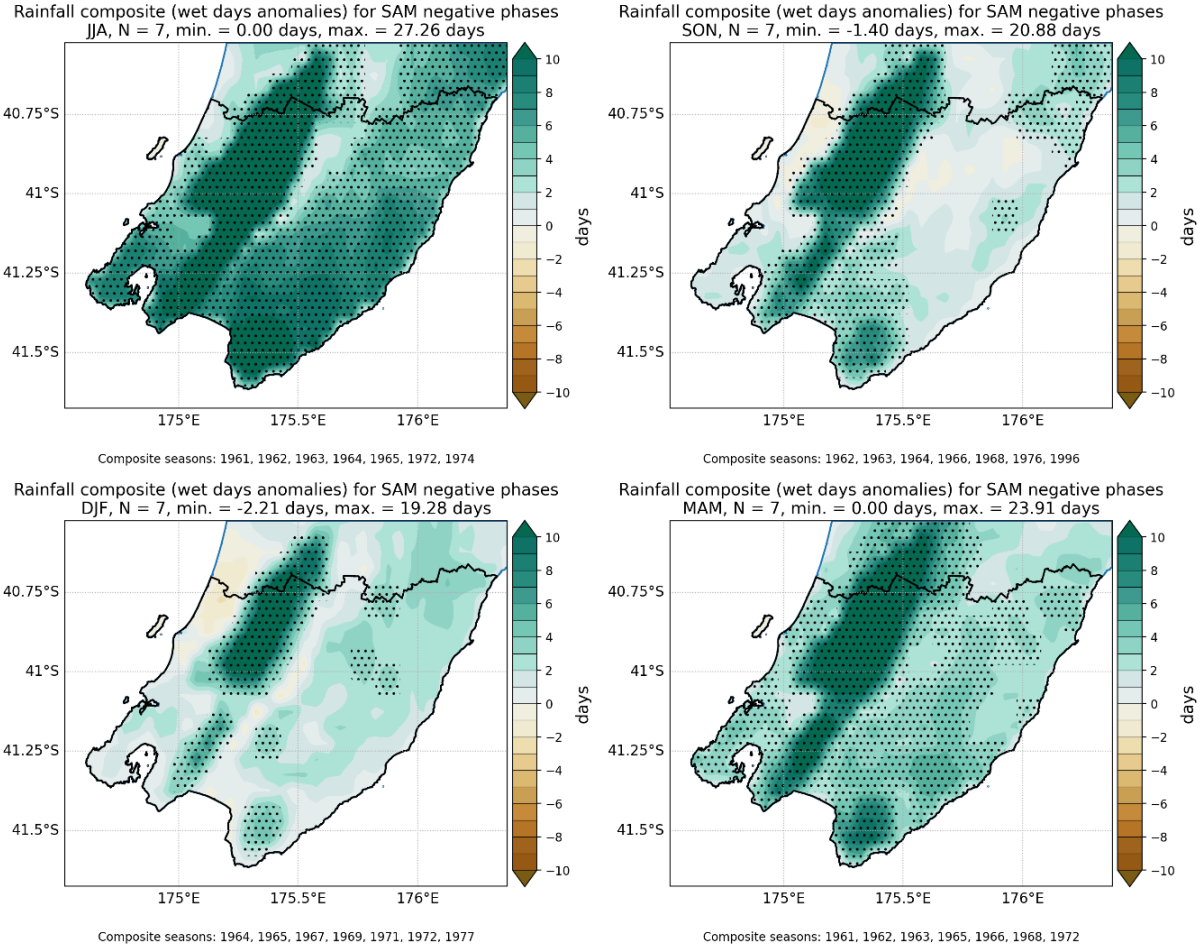

Figure 4-13: Rain day anomalies (operational VCSN) during the negative phase of SAM.

4.6.2 MSWEP

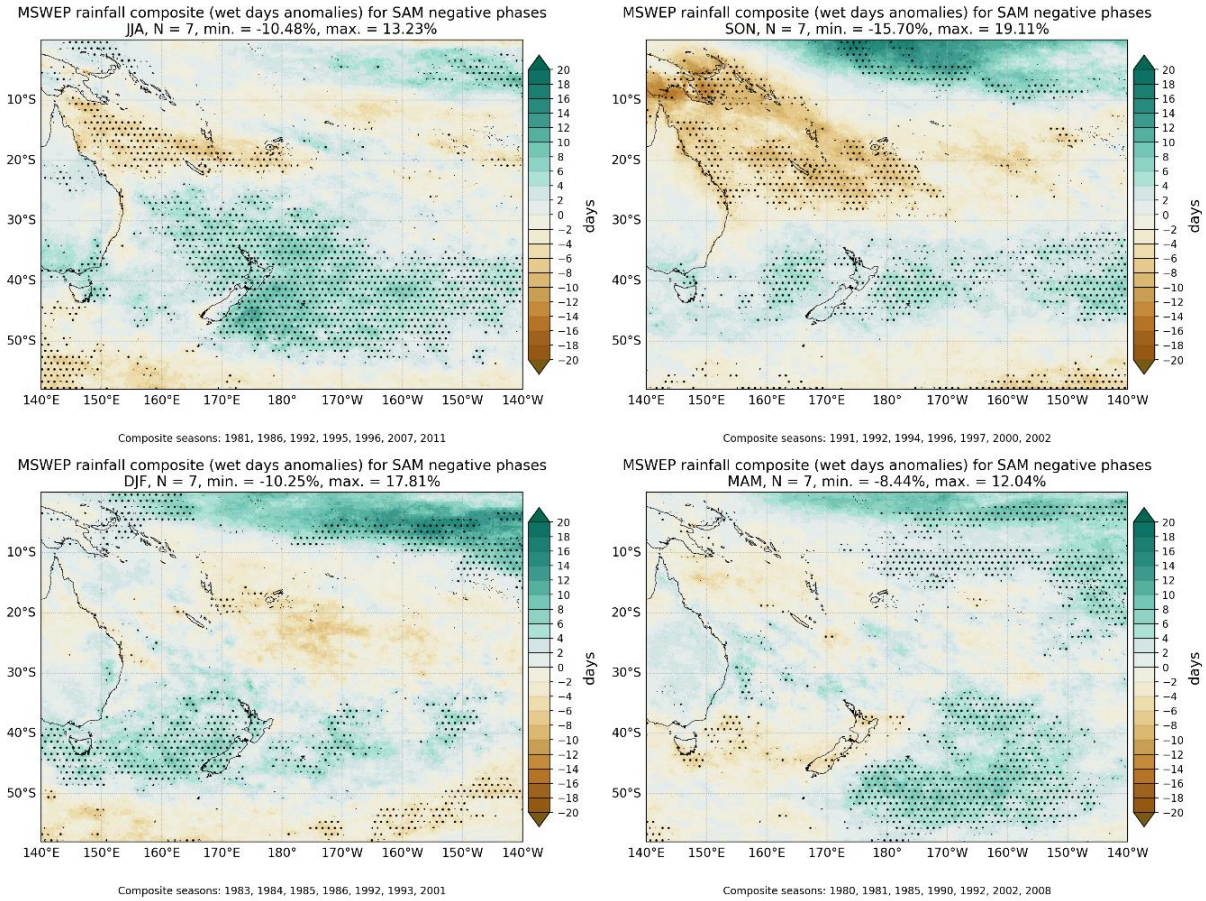

Figure 4-14: Rain day anomalies (MSWEP) during the negative phase of SAM.

4.7 SPSD – positive phase

Positive phases of the SPSD tends to be associated with more rain days than normal for the Greater Wellington region (Figure 4-15). The notable exception is during summer (DJF), when western parts of the region tend to observe fewer rain days. These increases in rain days extend towards central and northern parts of the Tasman Sea, particularly during spring (SON) and summer (DJF) (Figure 4-16).

4.7.1 Operational VCSN

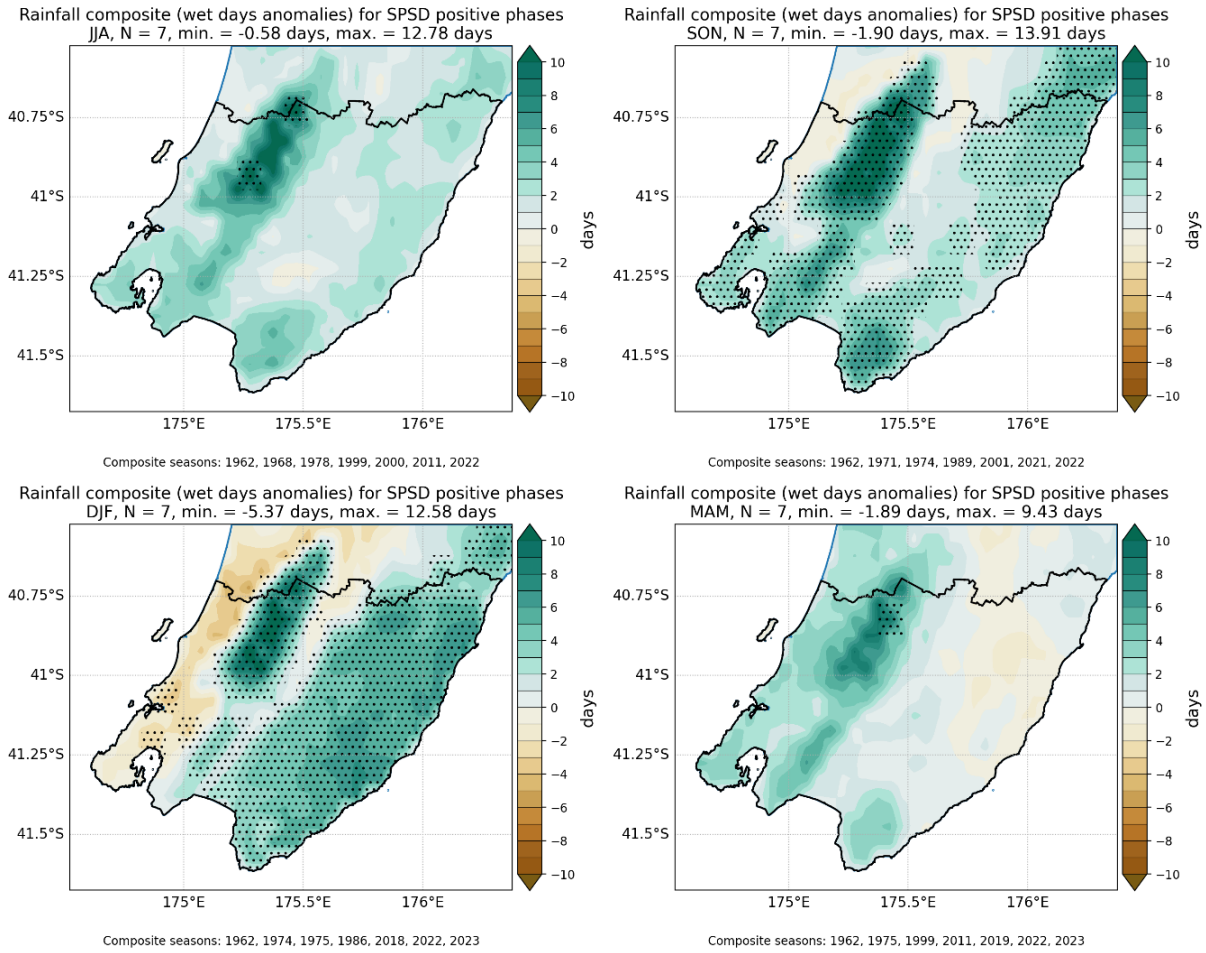

Figure 4-15: Rain day anomalies (operational VCSN) during the positive phase of SPSD.

4.7.2 MSWEP

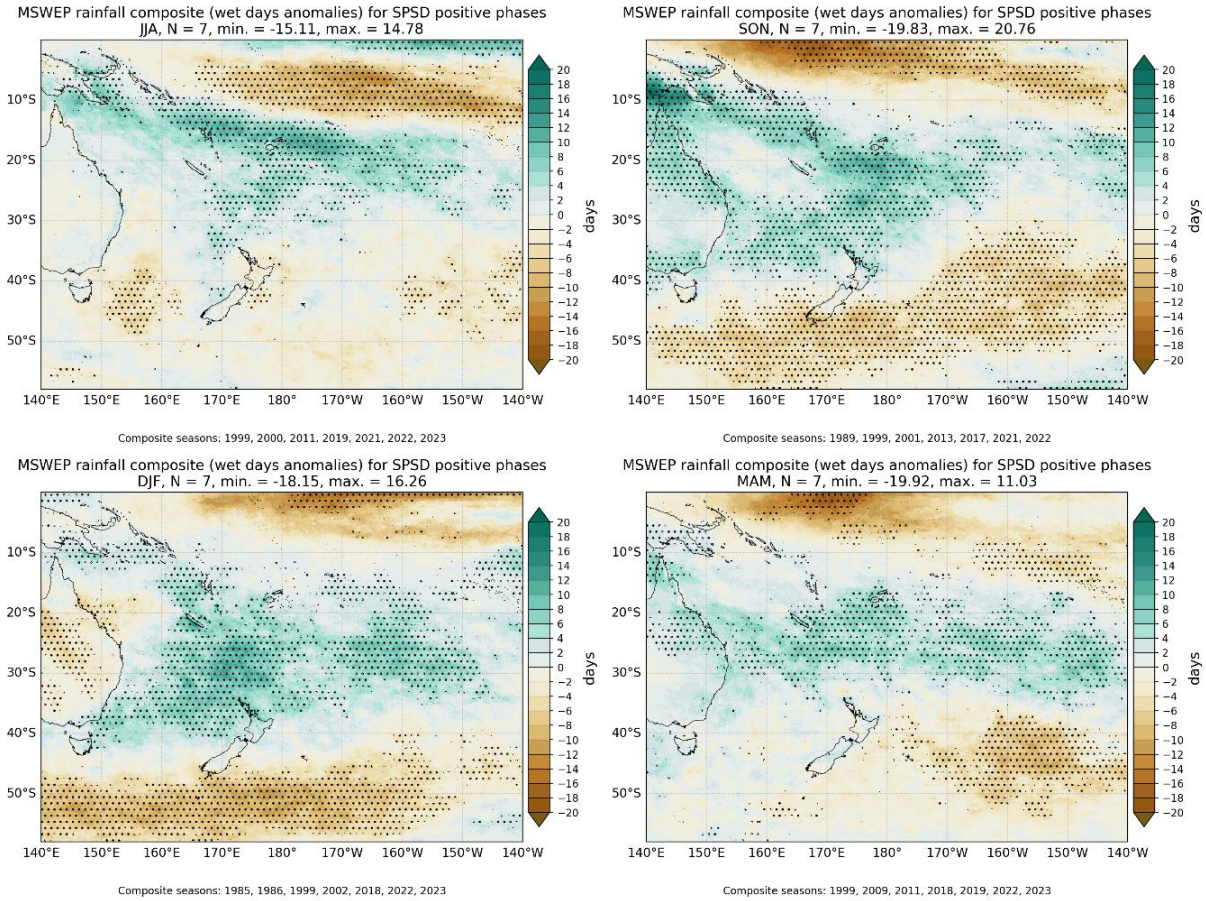

Figure 4-16: Rain day anomalies (MSWEP) during the positive phase of SPSD.

4.8 SPSD – negative phase

Negative phases of the SPSD are associated with more winter (JJA) and summer (DJF) rain days than normal for the Greater Wellington region (Figure 4-17). Fewer than normal rain days are typically observed about the Pacific Islands during the negative phase of SPSD (Figure 4-18).

4.8.1 Operational VCSN

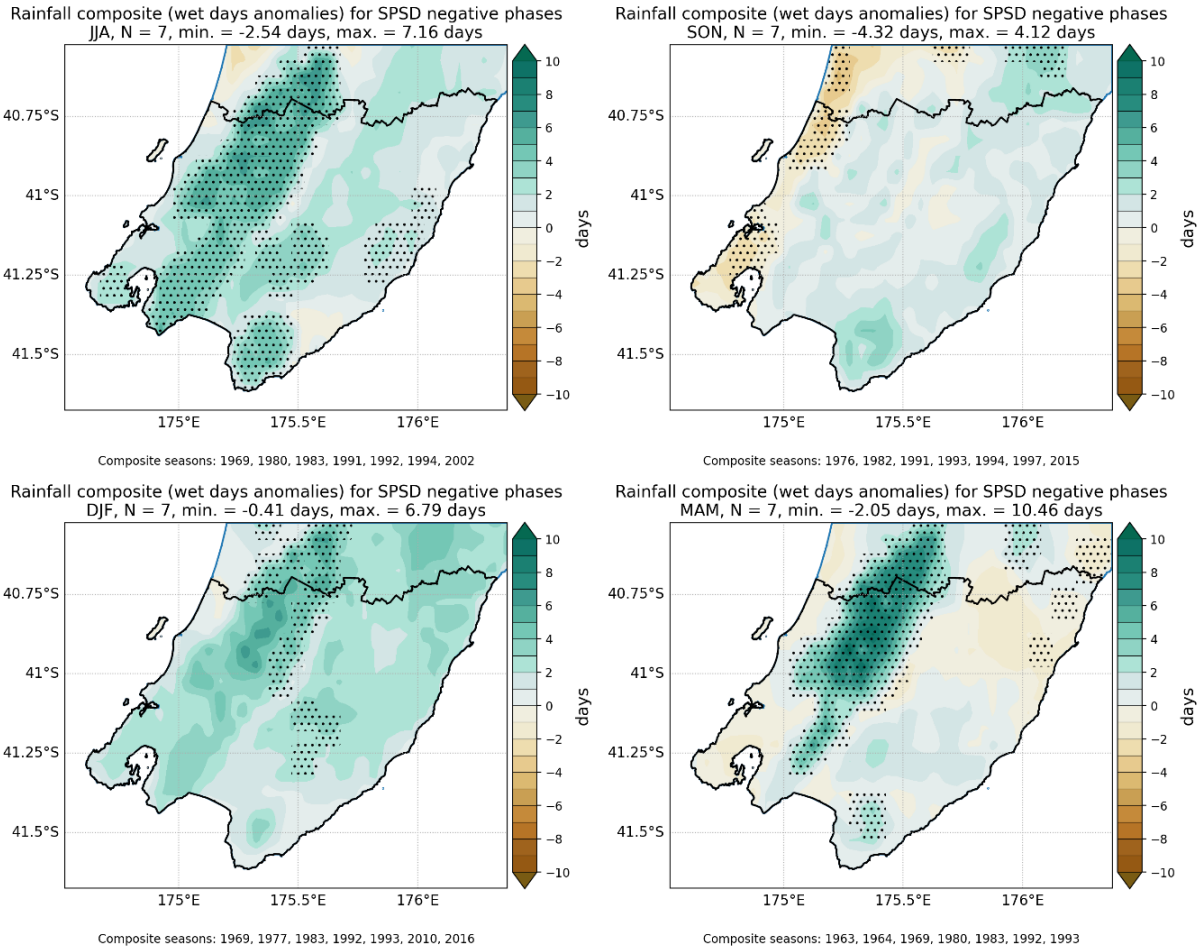

Figure 4-17: Rain day anomalies (operational VCSN) during the negative phase of SPSD.

4.8.2 MSWEP

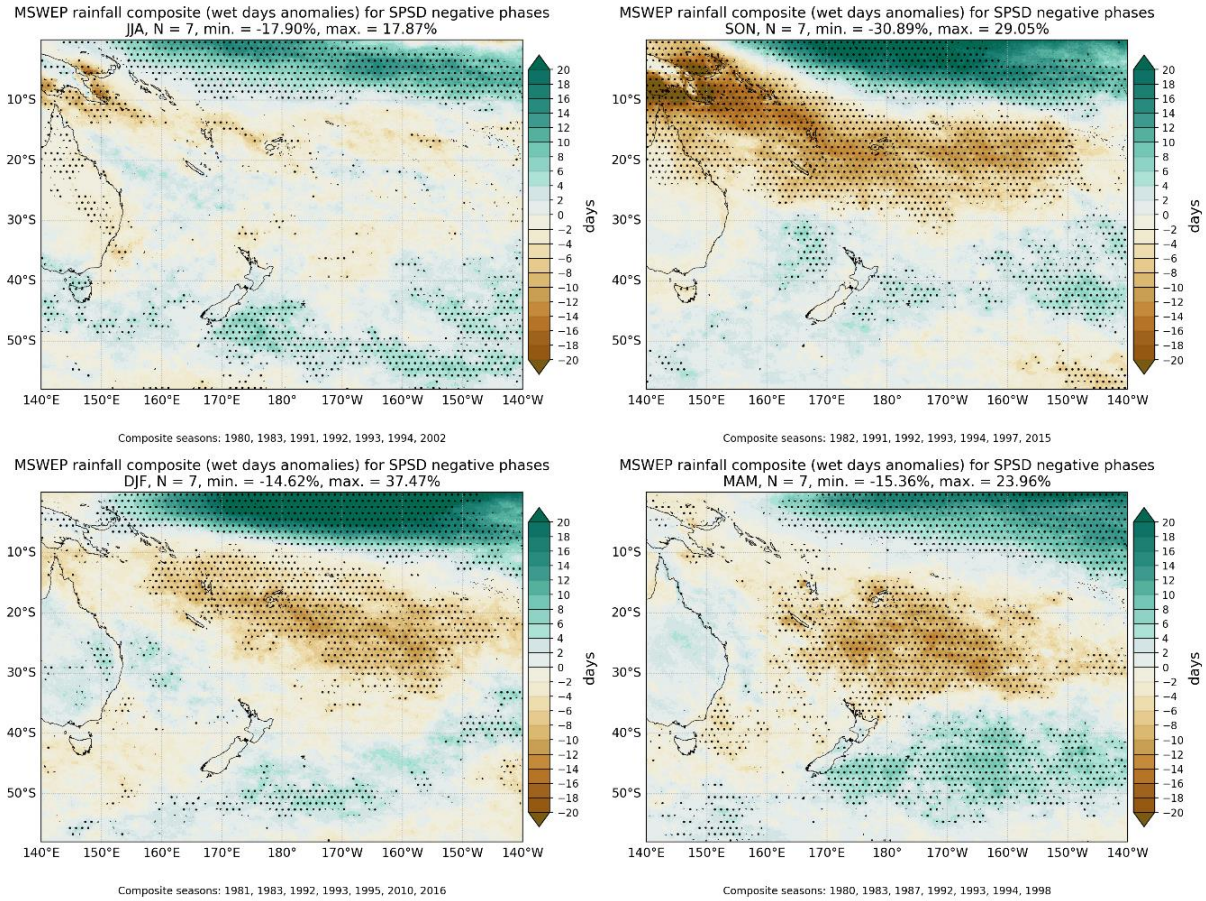

Figure 4-18: Rain day anomalies (MSWEP) during the negative phase of SPSD.

5 Heavy rain days

5.1 ENSO – positive phase (El Niño)

During the positive phases of ENSO, many parts of the region observe a reduction in winter (JJA), spring (SON) and summer (DJF) heavy rain days (Figure 5-1 and Figure 5-2). Western parts of the region tend to observe an increase in autumn (MAM) heavy rain days during El Niño, although this pattern isn't statistically significant.

The signal is embedded in a large-scale, Pacific-wide signal as evidenced by the composites anomalies from the MSWEP dataset (Figure 5-3): fewer heavy rain days are generally observed over and to the north of the North Island during positive phases of ENSO.

5.1.1 Operational VCSN

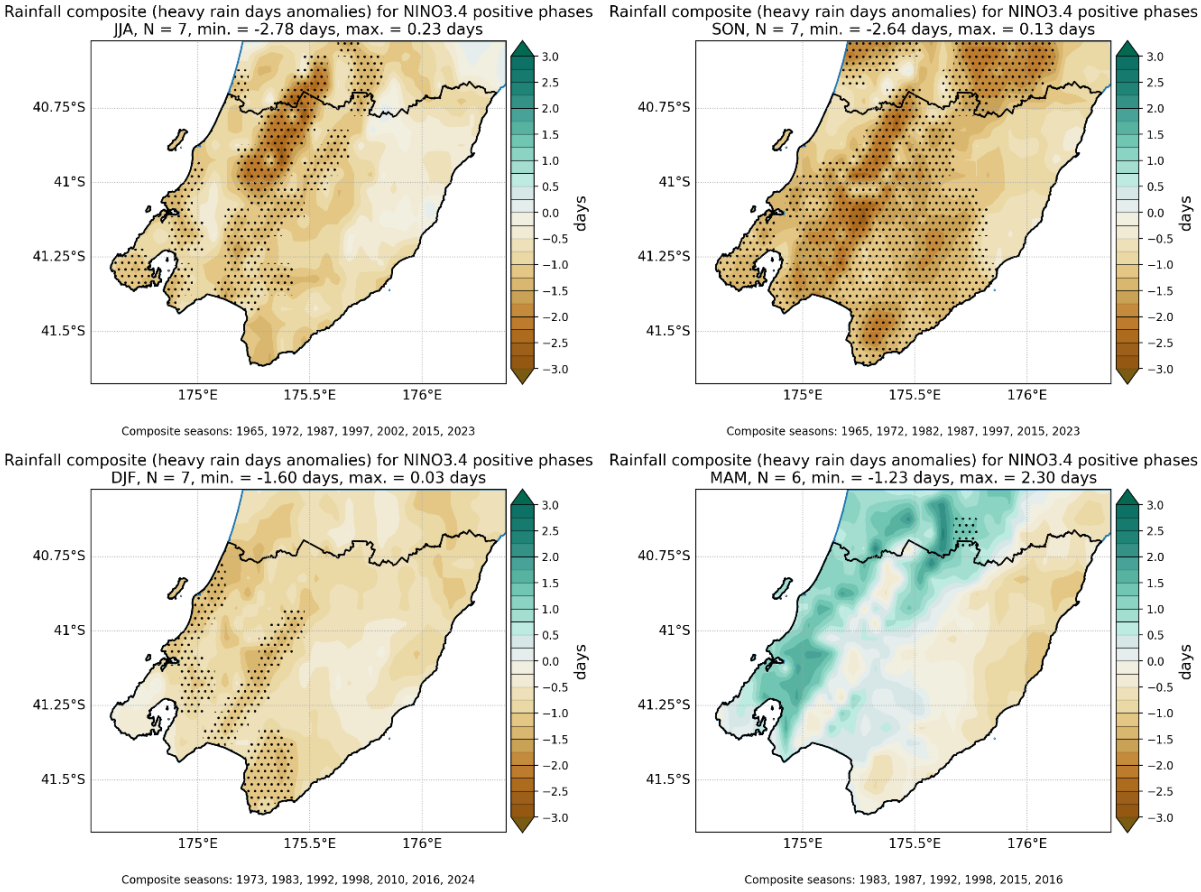

Figure 5-1: Heavy rain day anomalies (operational VCSN) during El Niño. Stippling indicates areas of statistical significance at $p \leq 0.10$. The years indicated under each figure are those of the last month in the season (e.g., DJF 1973 refers to December 1972 – February 1973).

5.1.2 Augmented VCSN

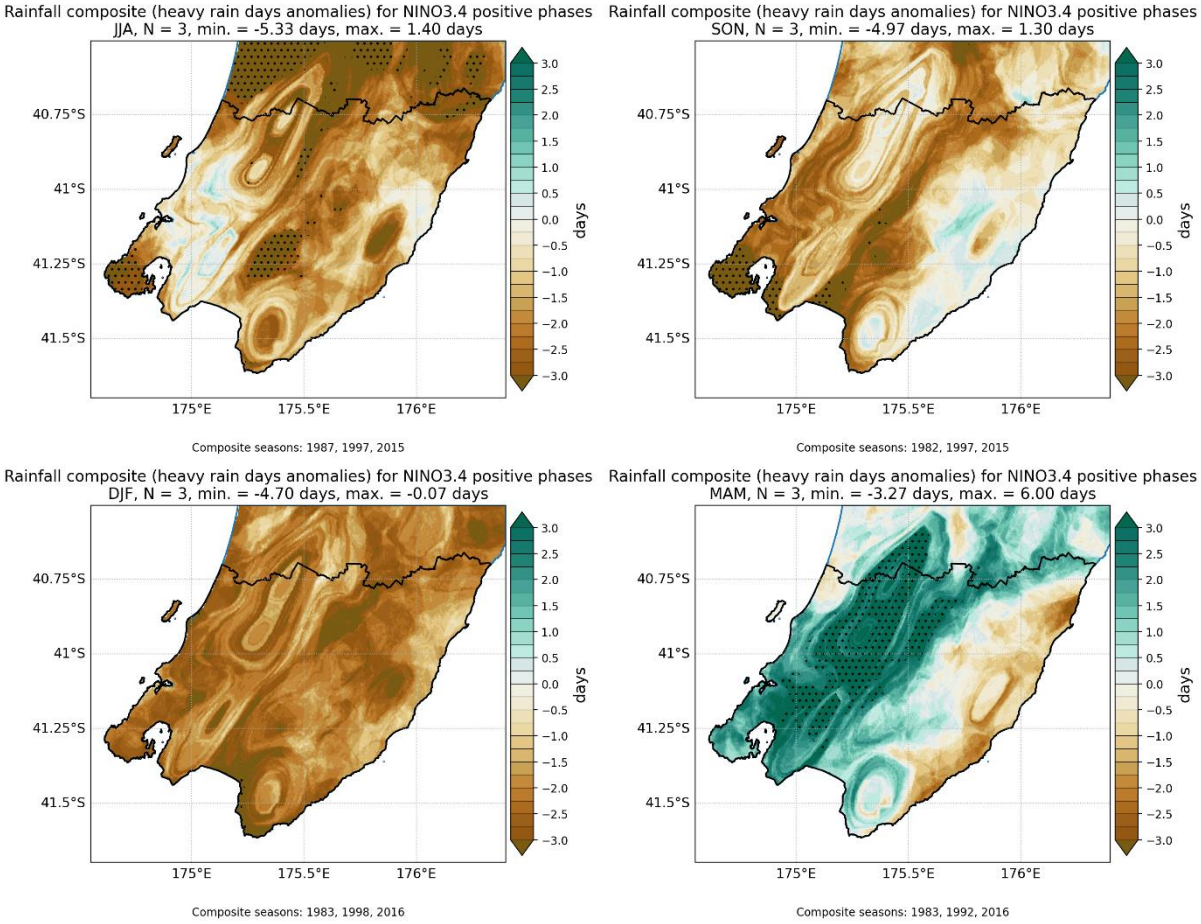

Figure 5-2: Heavy rain day anomalies (augmented VCSN) during El Niño. The legend range of ± 3 days was selected to match the range presented for the operational VCSN maps above (Figure 5-1).

5.1.3 MSWEP

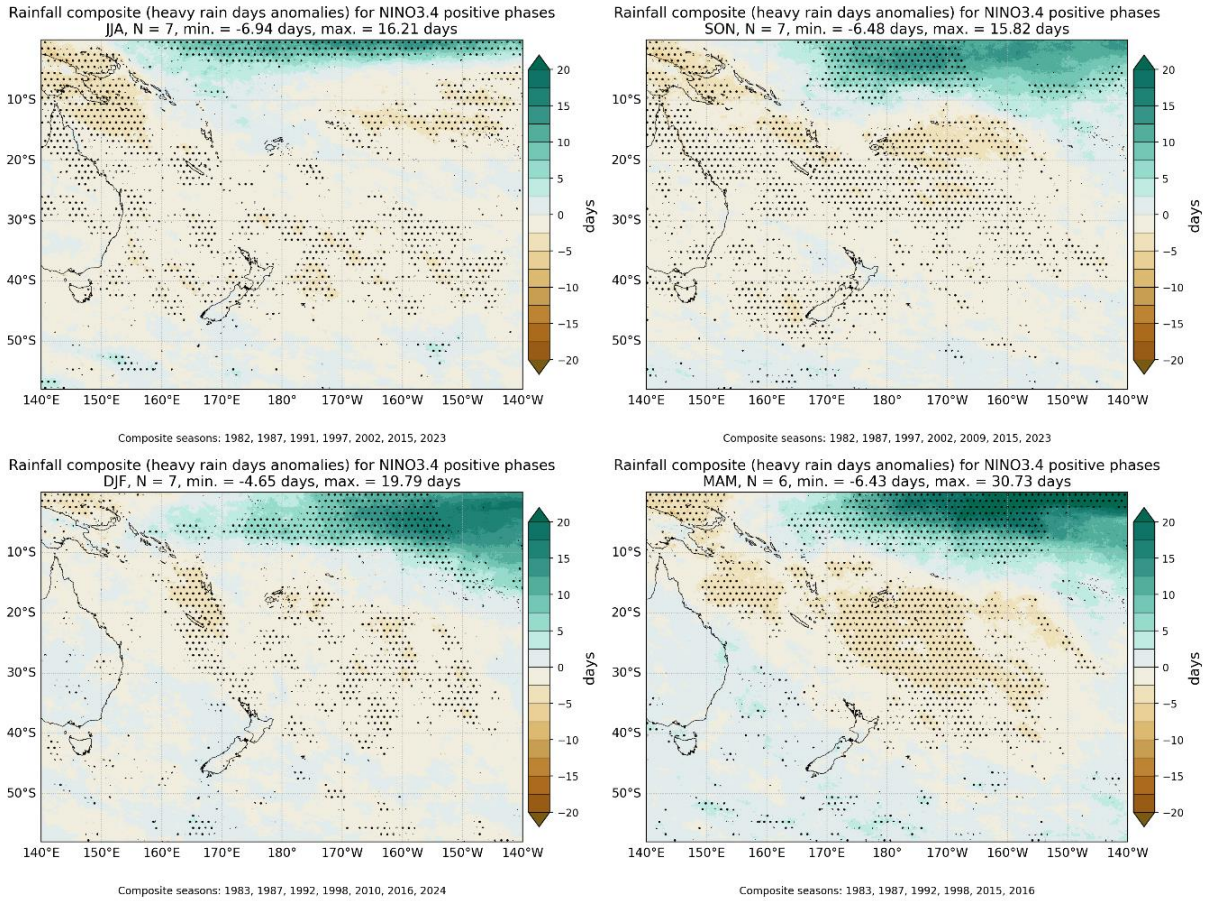

Figure 5-3: Heavy rain day anomalies (MSWEP) during El Niño.

5.2 ENSO – negative phase (La Niña)

La Niña tends to be associated with a decrease in winter (JJA) and spring (SON) heavy rain days for eastern parts of the Greater Wellington region (Figure 5-4 and Figure 5-5). Many parts of the region observe an increase in autumn (MAM) heavy rain days. Summer (DJF) and autumn (MAM) heavy rain days tend to increase to the north of New Zealand during La Niña (Figure 5-6).

5.2.1 Operational VCSN

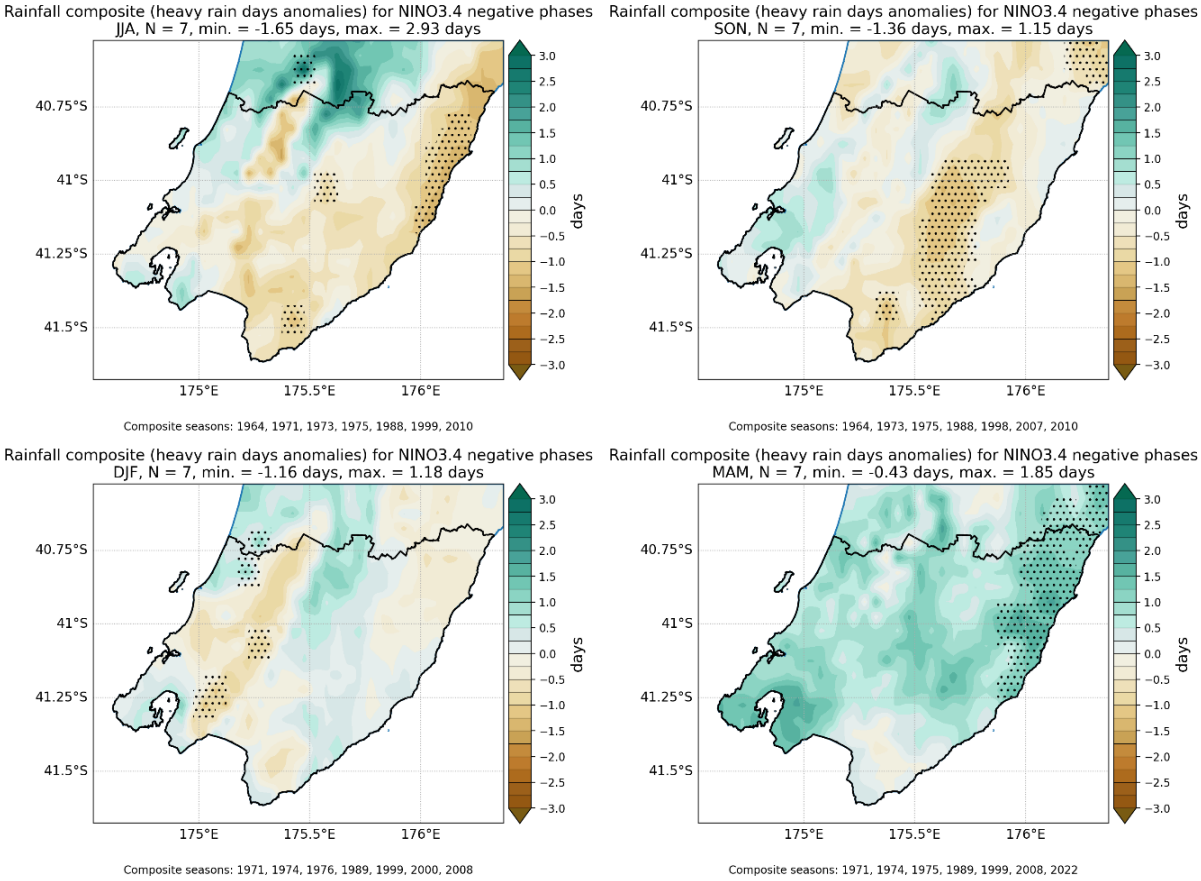

Figure 5-4: Heavy rain day anomalies (operational VCSN) during La Niña.

5.2.2 Augmented VCSN

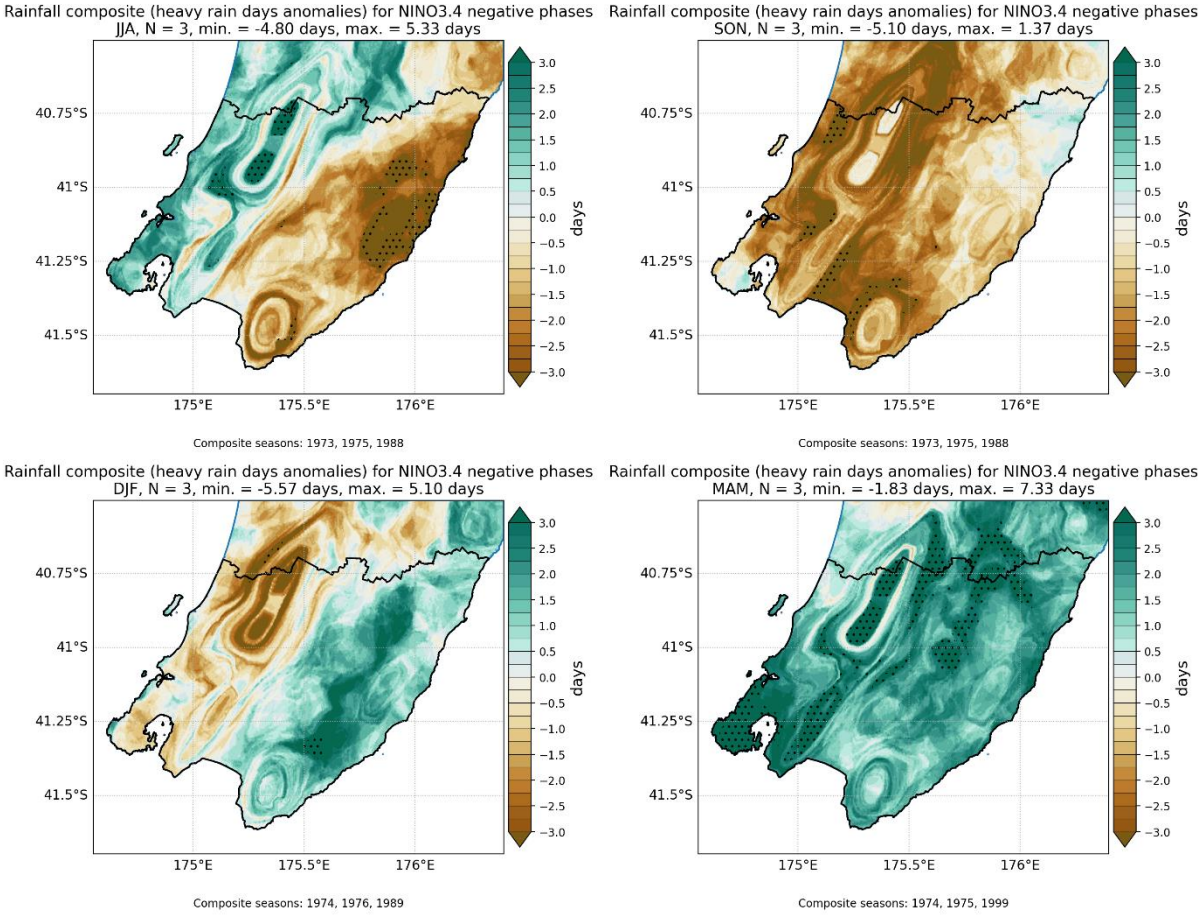

Figure 5-5: Heavy rain day anomalies (augmented VCSN) during La Niña. The legend range of ± 3 days was selected to match the range presented for the operational VCSN maps above (Figure 5-4).

5.2.3 MSWEP

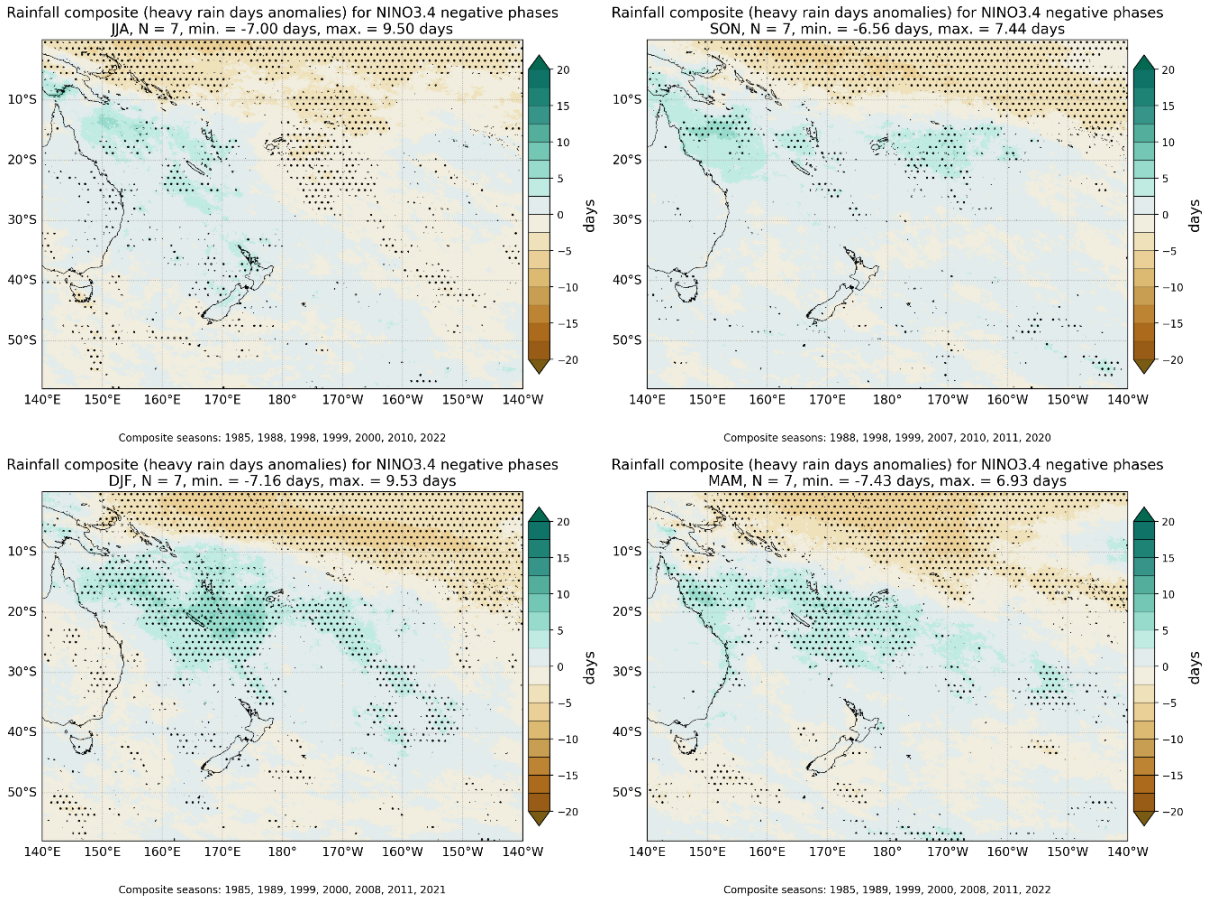

Figure 5-6: Heavy rain day anomalies (MSWEP) during La Niña.

5.3 IOD – positive phase

Positive IOD events tend to be associated with fewer than normal summer (DJF) heavy rain days for most of the region, especially for the Tararua Range (Figure 5-7). The MSWEP composites highlight a reduction in winter (JJA) and spring (SON) heavy rain days for much of the Tasman Sea and eastern Australia (Figure 5-8).

5.3.1 Operational VCSN

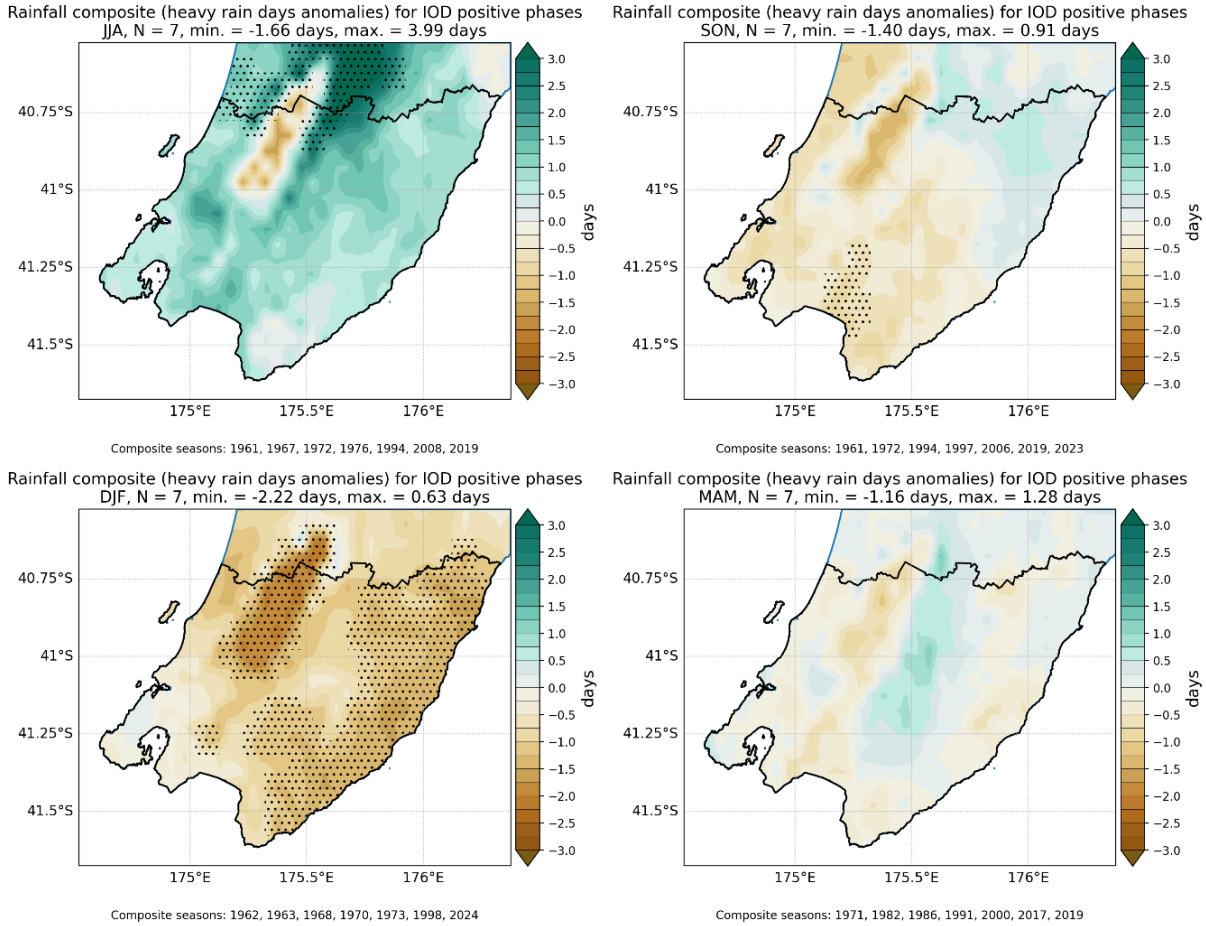

Figure 5-7: Heavy rain day anomalies (operational VCSN) during the positive phase of IOD.

5.3.2 MSWEP

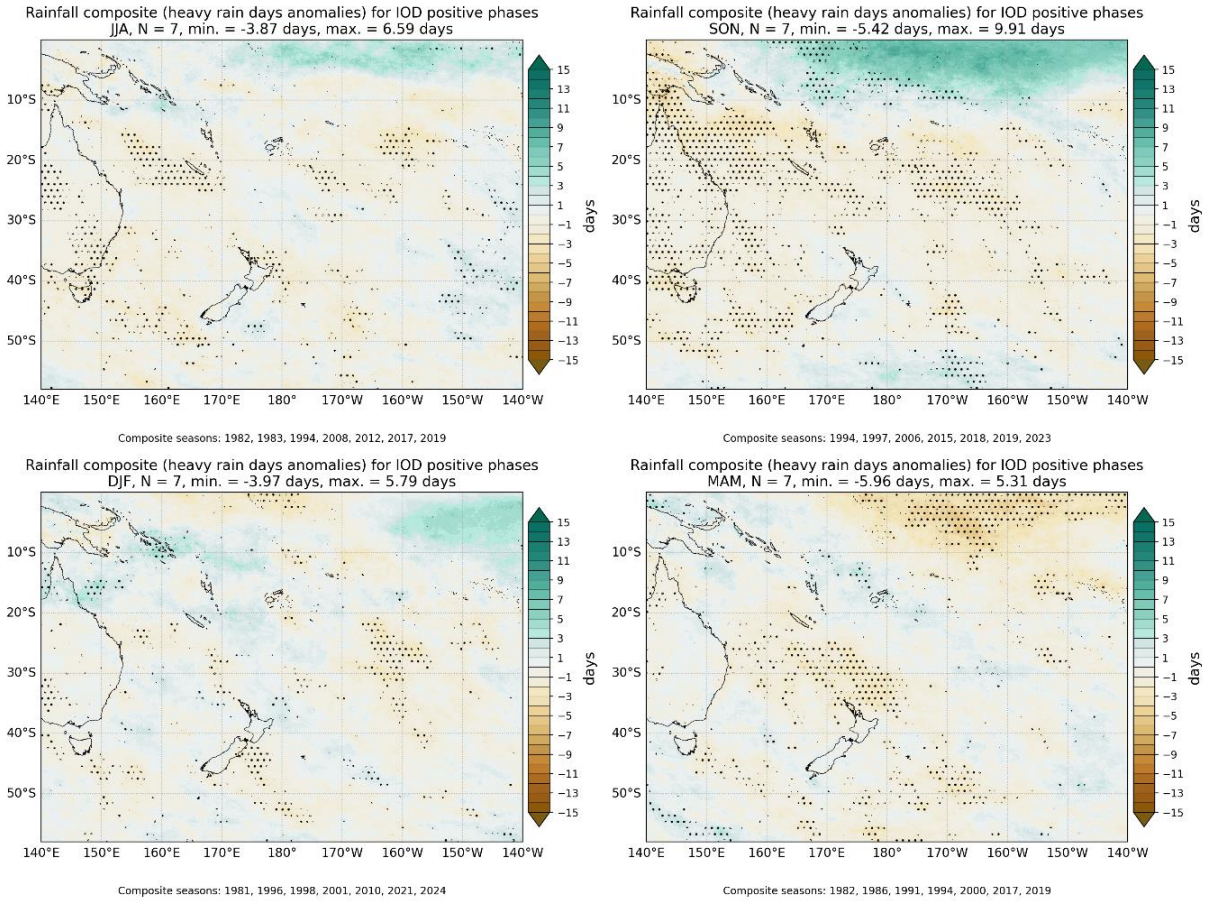

Figure 5-8: Heavy rain day anomalies (MSWEP) during the positive phase of IOD.

5.4 IOD – negative phase

Negative phases of the IOD tend to be associated with increases in winter (JJA) heavy rain days for western parts of the Greater Wellington region (Figure 5-9). The equatorial Pacific tends to observe fewer heavy rain days in spring (SON) (Figure 5-10).

5.4.1 Operational VCSN

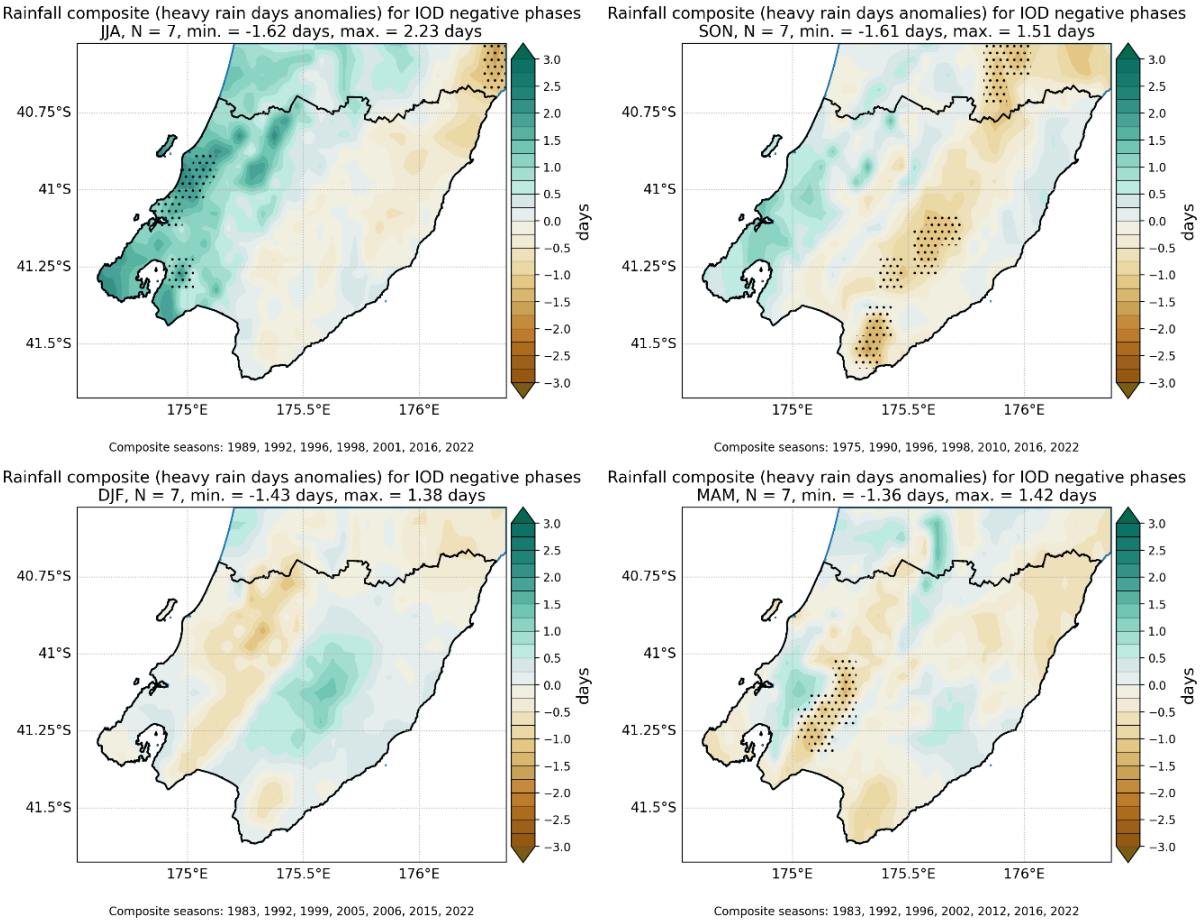

Figure 5-9: Heavy rain day anomalies (operational VCSN) during the negative phase of IOD.

5.4.2 MSWEP

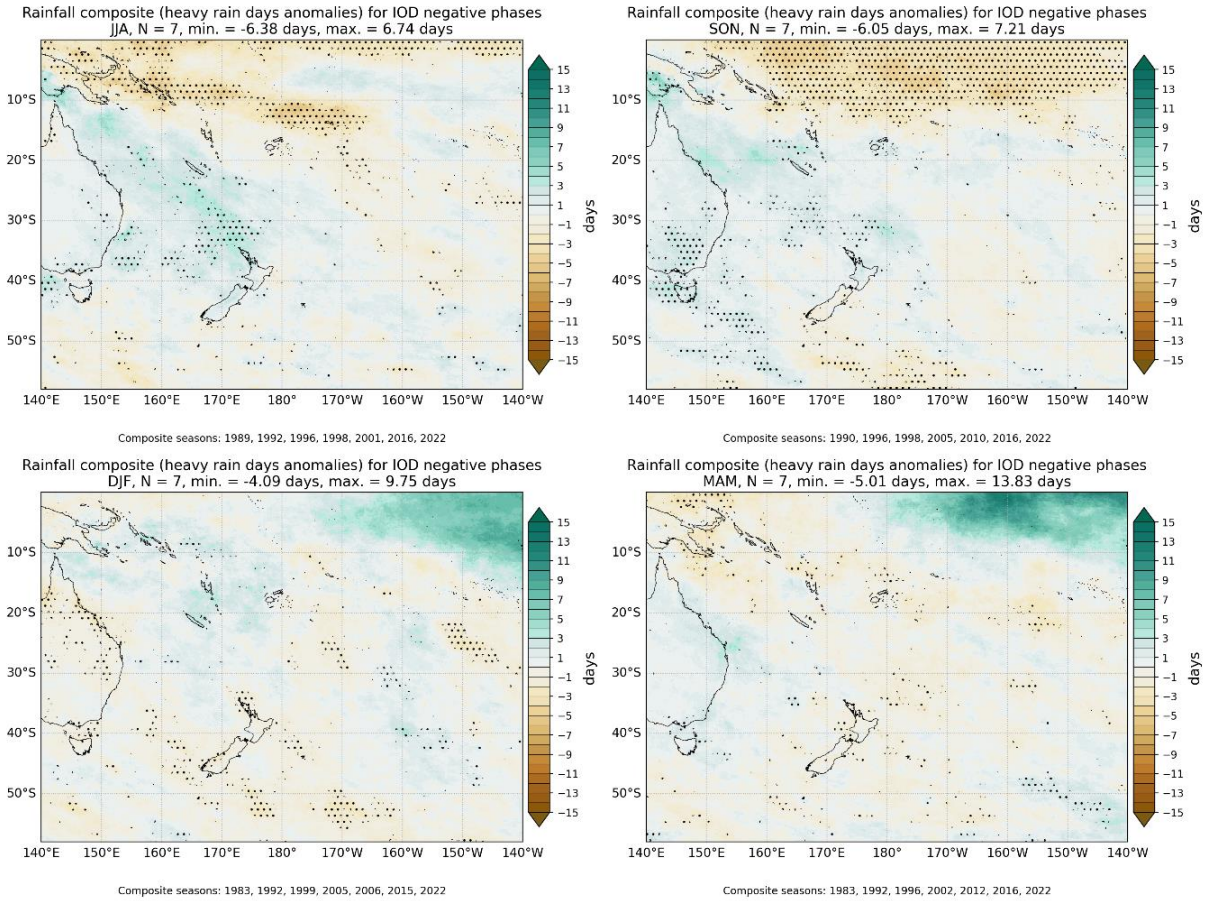

Figure 5-10: Heavy rain day anomalies (MSWEP) during the negative phase of IOD.

5.5 SAM – positive phase

Positive phases of the SAM tend to be associated with fewer than normal heavy rain days during the winter (JJA) for eastern parts of the Greater Wellington region (Figure 5-11). The equatorial Pacific tends to observe fewer heavy rain days in spring (SON) (Figure 5-12).

5.5.1 Operational VCSN

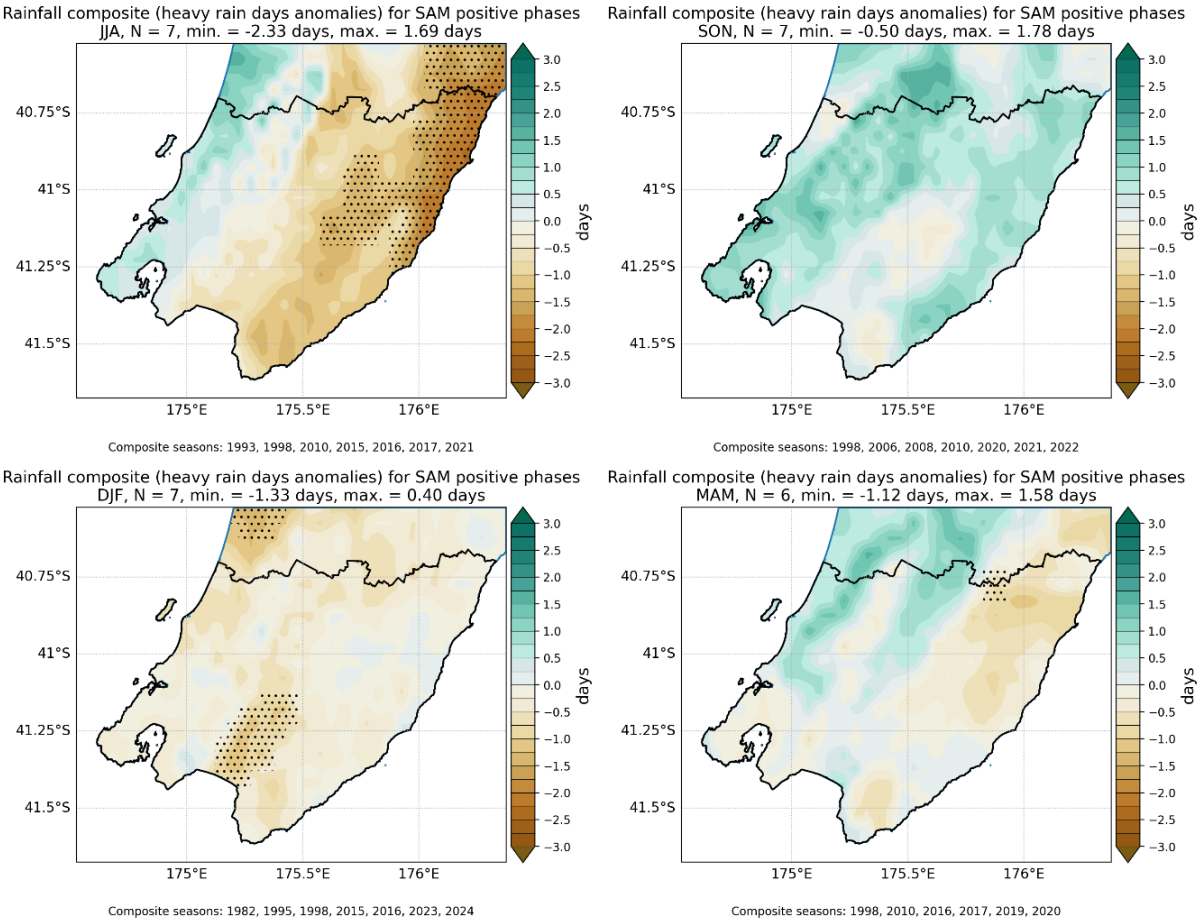

Figure 5-11: Heavy rain day anomalies (operational VCSN) during the positive phase of SAM.

5.5.2 MSWEP

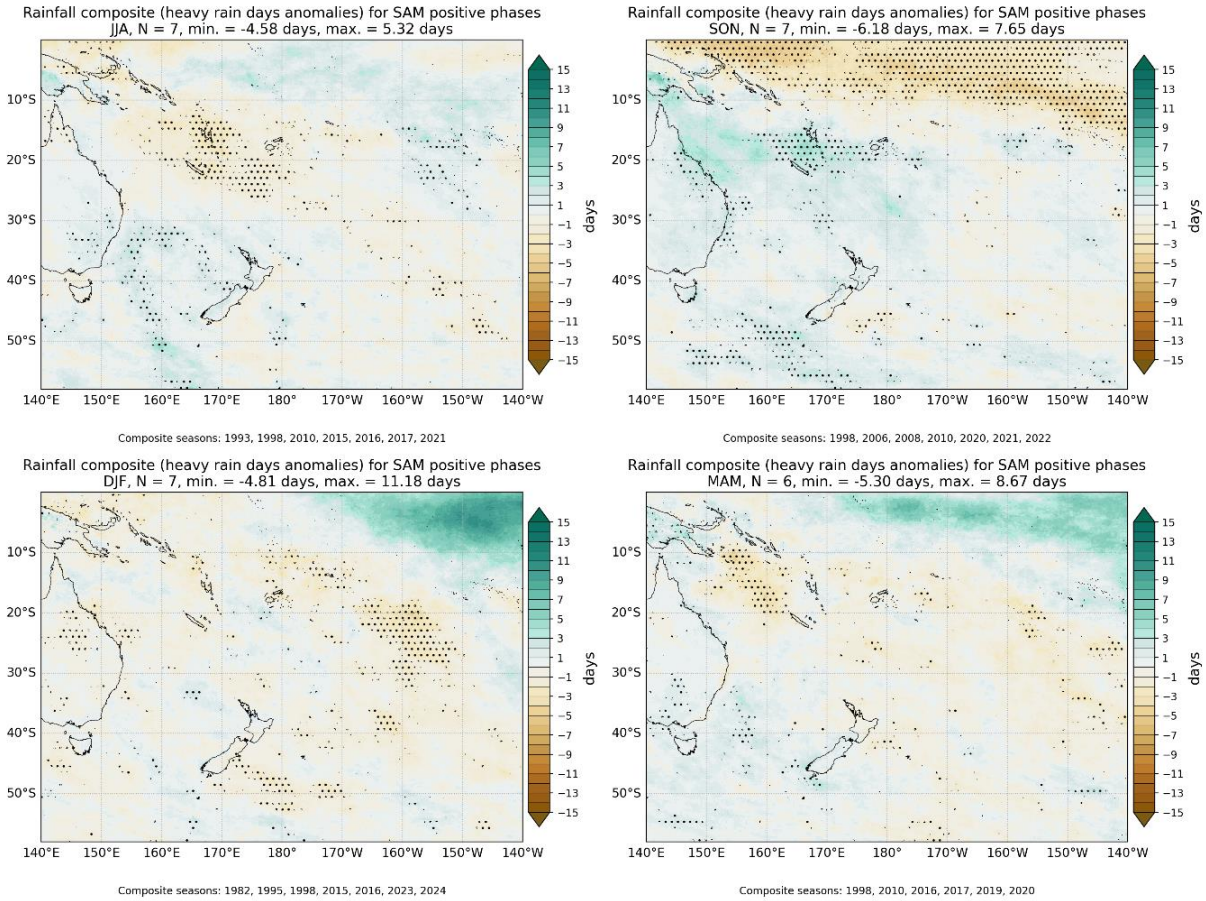

Figure 5-12: Heavy rain day anomalies (MSWEP) during the positive phase of SAM.

5.6 SAM – negative phase

The Greater Wellington region typically observes fewer spring (SON) and summer (DJF) heavy rain days than normal during the negative phase of SAM (Figure 5-13). Fewer heavy rain days are typically observed west of the South Island during the negative phase of SAM, particularly during autumn (MAM) and spring (SON) (Figure 5-14).

5.6.1 Operational VCSN

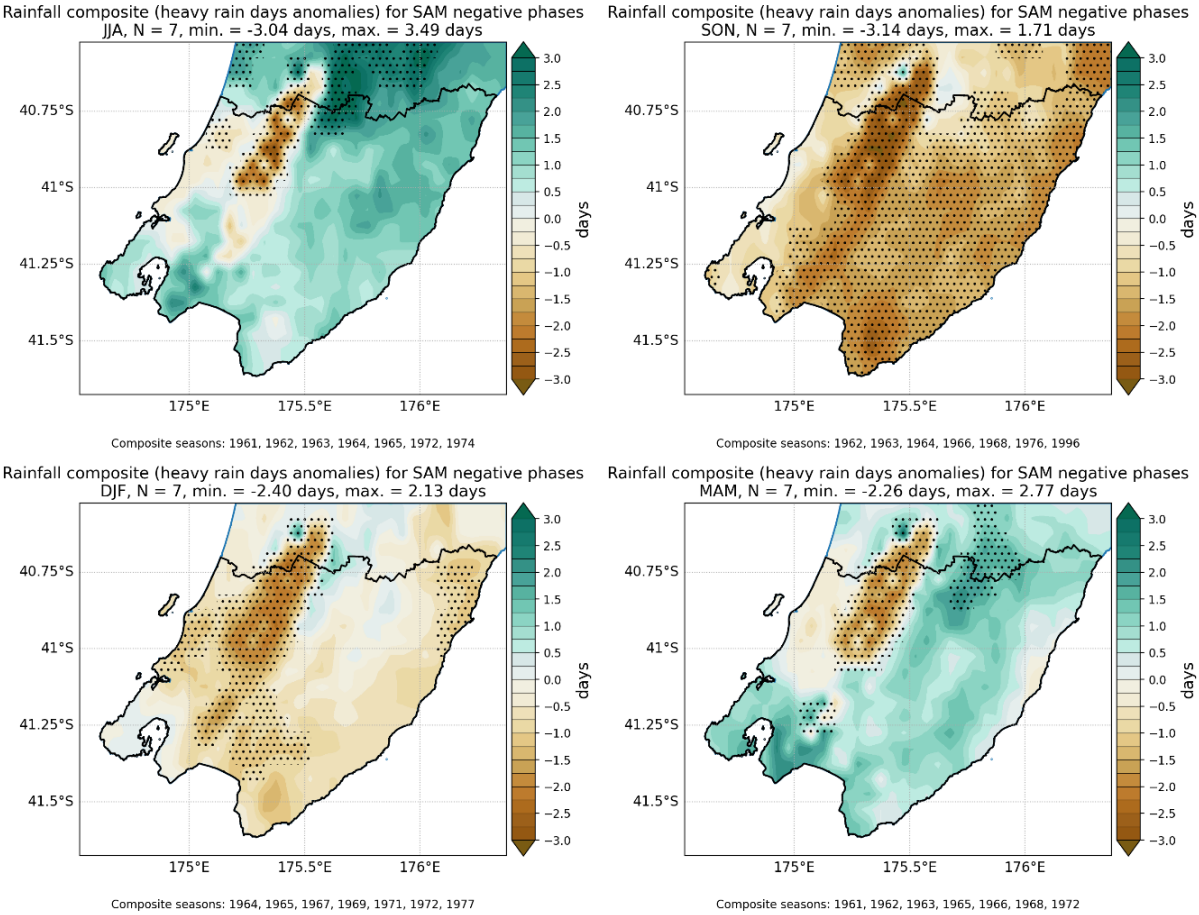

Figure 5-13: Heavy rain day anomalies (operational VCSN) during the negative phase of SAM.

5.6.2 MSWEP

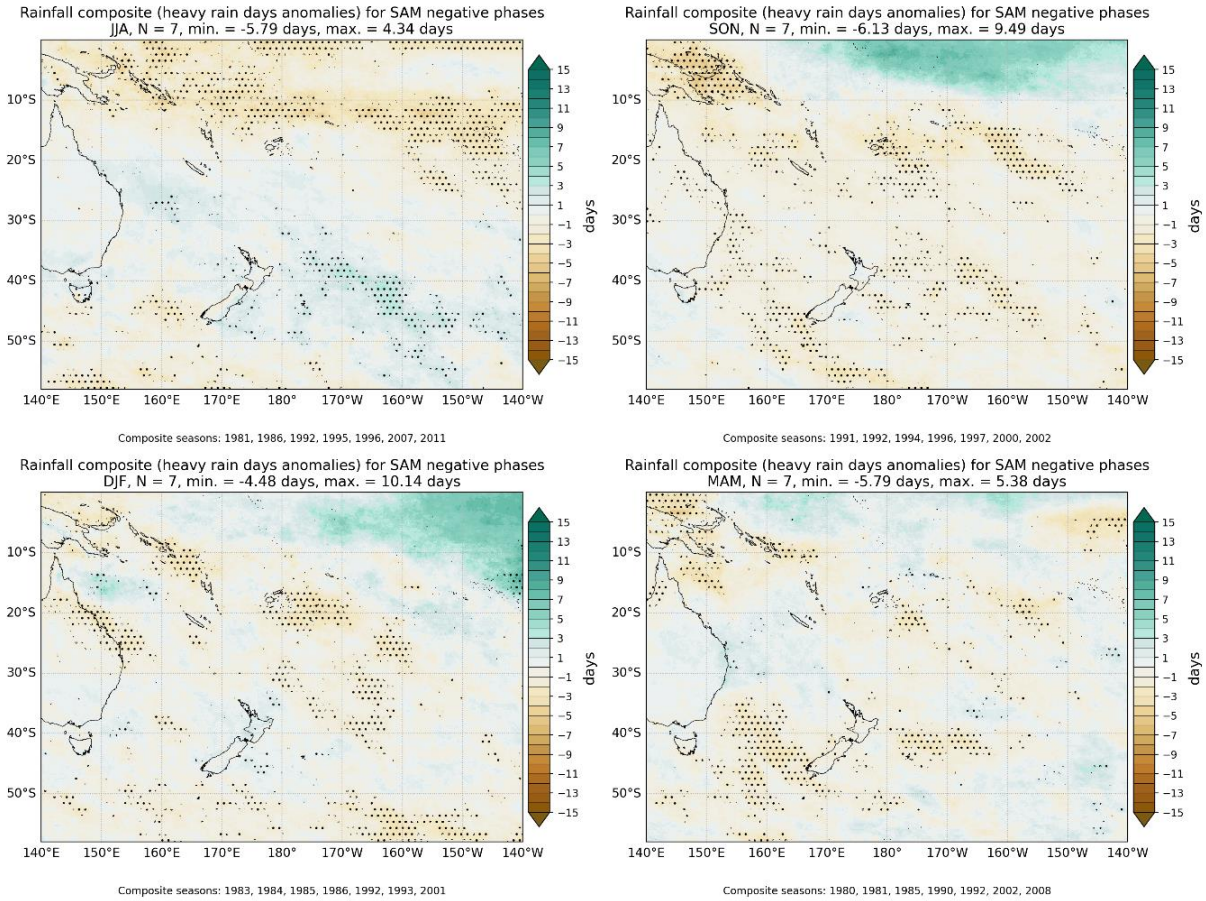

Figure 5-14: Heavy rain day anomalies (MSWEP) during the negative phase of SAM.

5.7 SPSD – positive phase

Positive phases of the SPSD tend to be associated with more summer (DJF) heavy rain days than normal for the Greater Wellington region, except for the Tararua Range (Figure 5-15). Fewer spring (SON) heavy rain days than normal are observed over the Tararua Range. The equatorial Pacific observes fewer heavy rain days than normal throughout the year when the SPSD is positive (Figure 5-16).

5.7.1 Operational VCSN

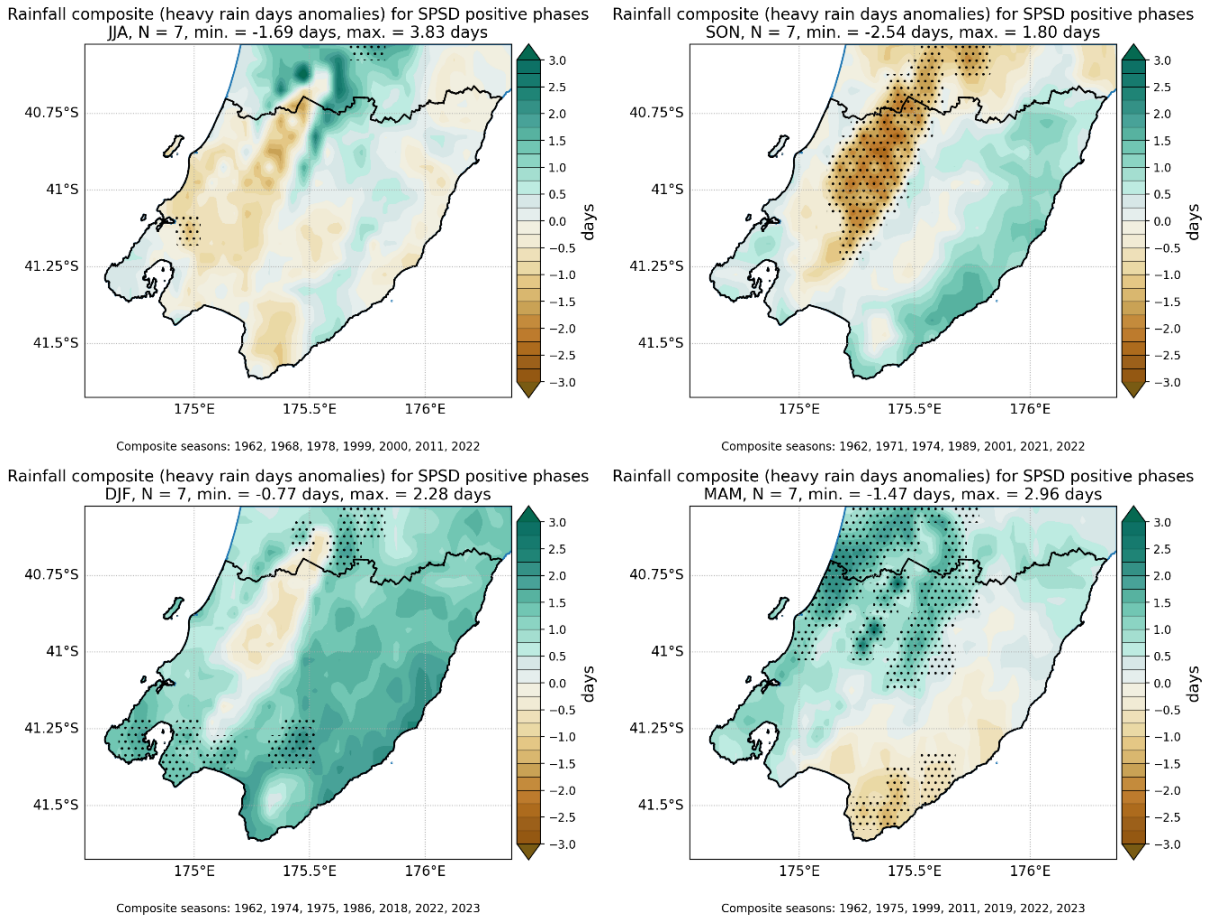

Figure 5-15: Heavy rain day anomalies (operational VCSN) during the positive phase of SPSD.

5.7.2 MSWEP

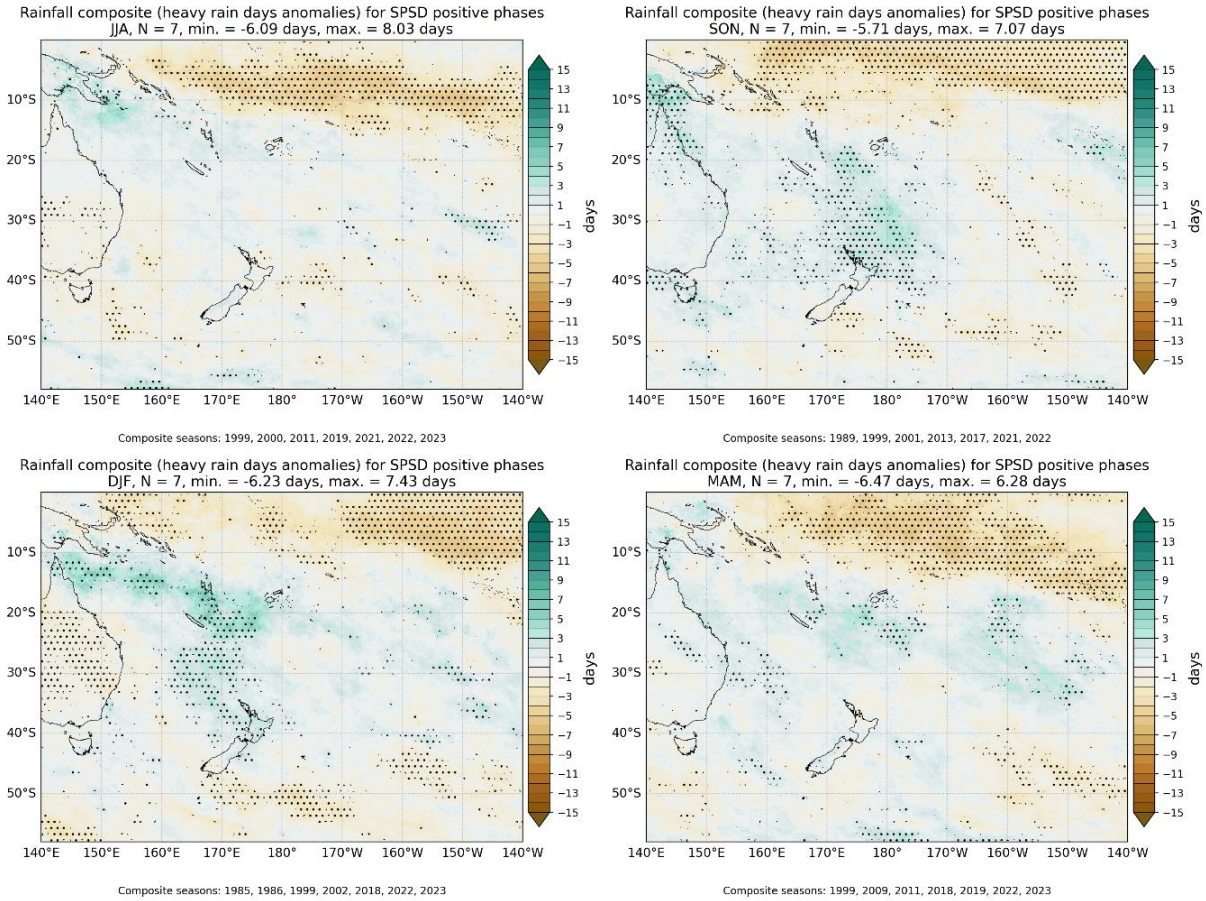

Figure 5-16: Heavy rain day anomalies (MSWEP) during the positive phase of SPSD.

5.8 SPSD – negative phase

Negative phases of the SPSD are associated with fewer winter (JJA) and spring (SON) heavy rain days than normal for the Greater Wellington region (Figure 5-17). Fewer than normal heavy rain days are typically observed about the Pacific Islands during the negative phase of SPSD (Figure 5-18).

5.8.1 Operational VCSN

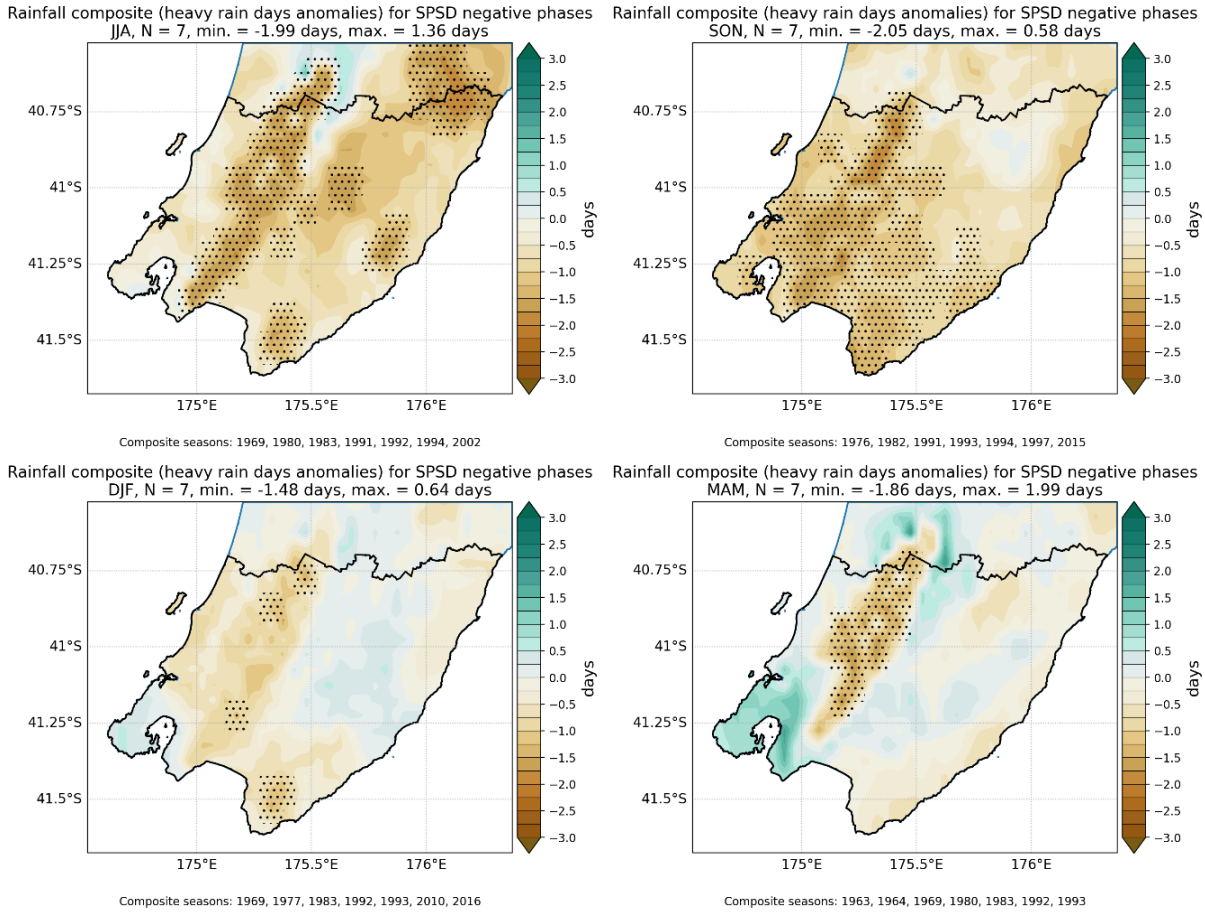

Figure 5-17: Heavy rain day anomalies (operational VCSN) during the negative phase of SPSD.

5.8.2 MSWEP

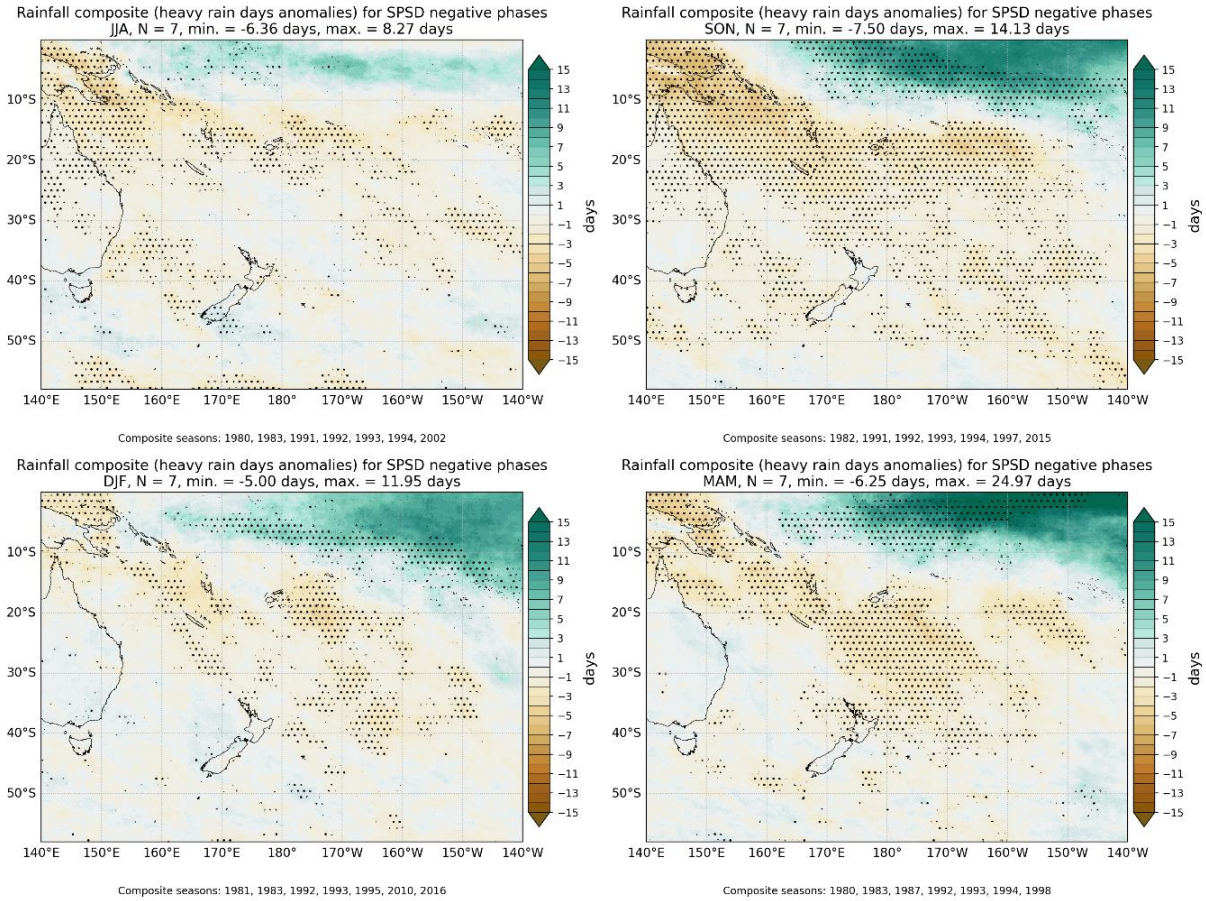

Figure 5-18: Heavy rain day anomalies (MSWEP) during the negative phase of SPSD.

6 Dry days

6.1 ENSO – positive phase (El Niño)

During the positive phases of ENSO, many parts of the region observe more spring (SON) and summer (DJF) dry days (Figure 6-1 and Figure 6-2). This signal is also reflected in the composites anomalies from the MSWEP dataset, with more dry days observed to the north of New Zealand during positive phases of ENSO (Figure 6-3).

6.1.1 Operational VCSN

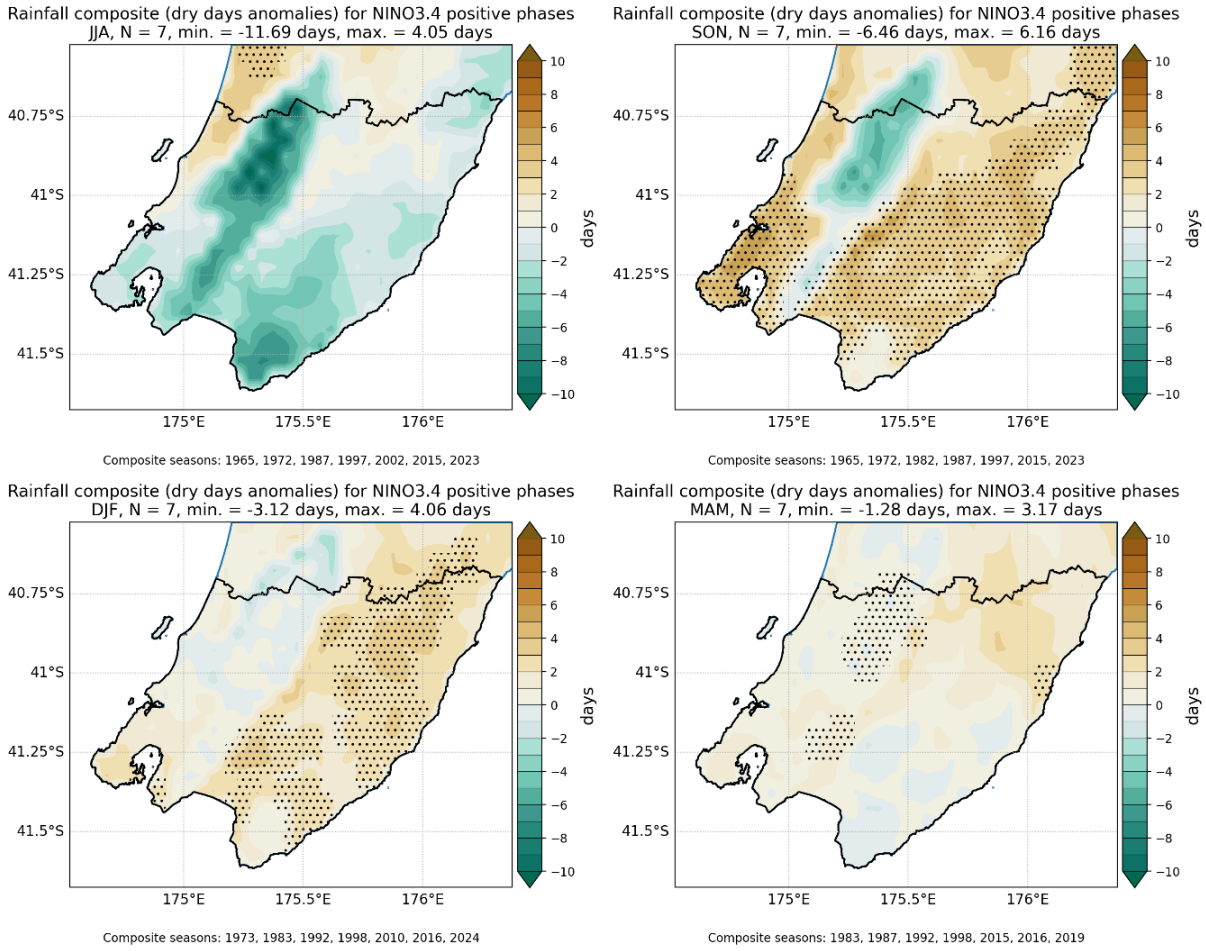

Figure 6-1: Dry day anomalies (operational VCSN) during El Niño. Stippling indicates areas of statistical significance at $p \leq 0.10$. The years indicated under each figure are those of the last month in the season (e.g., DJF 1973 refers to December 1972 – February 1973).

6.1.2 Augmented VCSN

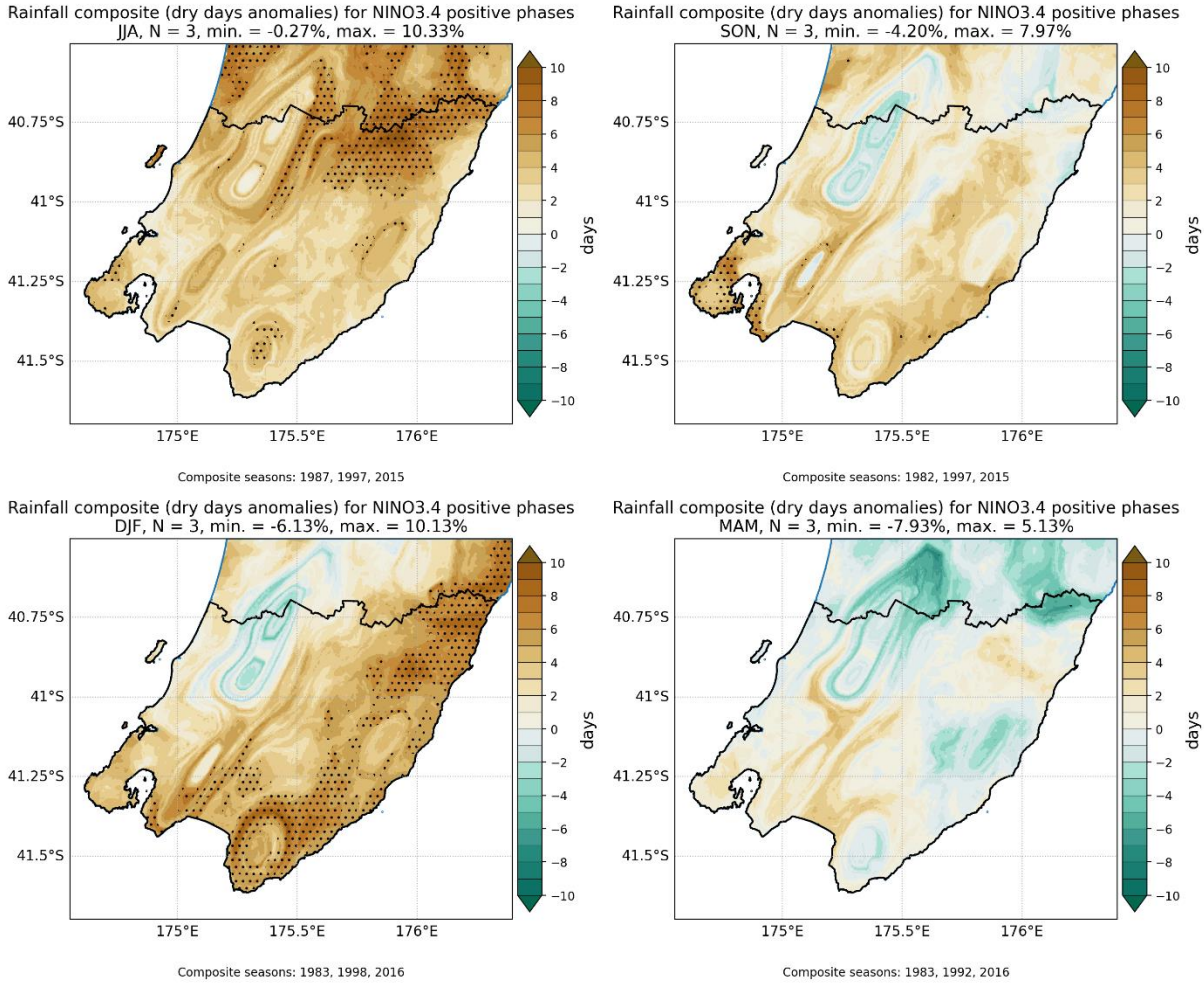

Figure 6-2: Dry day anomalies (augmented VCSN) during El Niño.

6.1.3 MSWEP

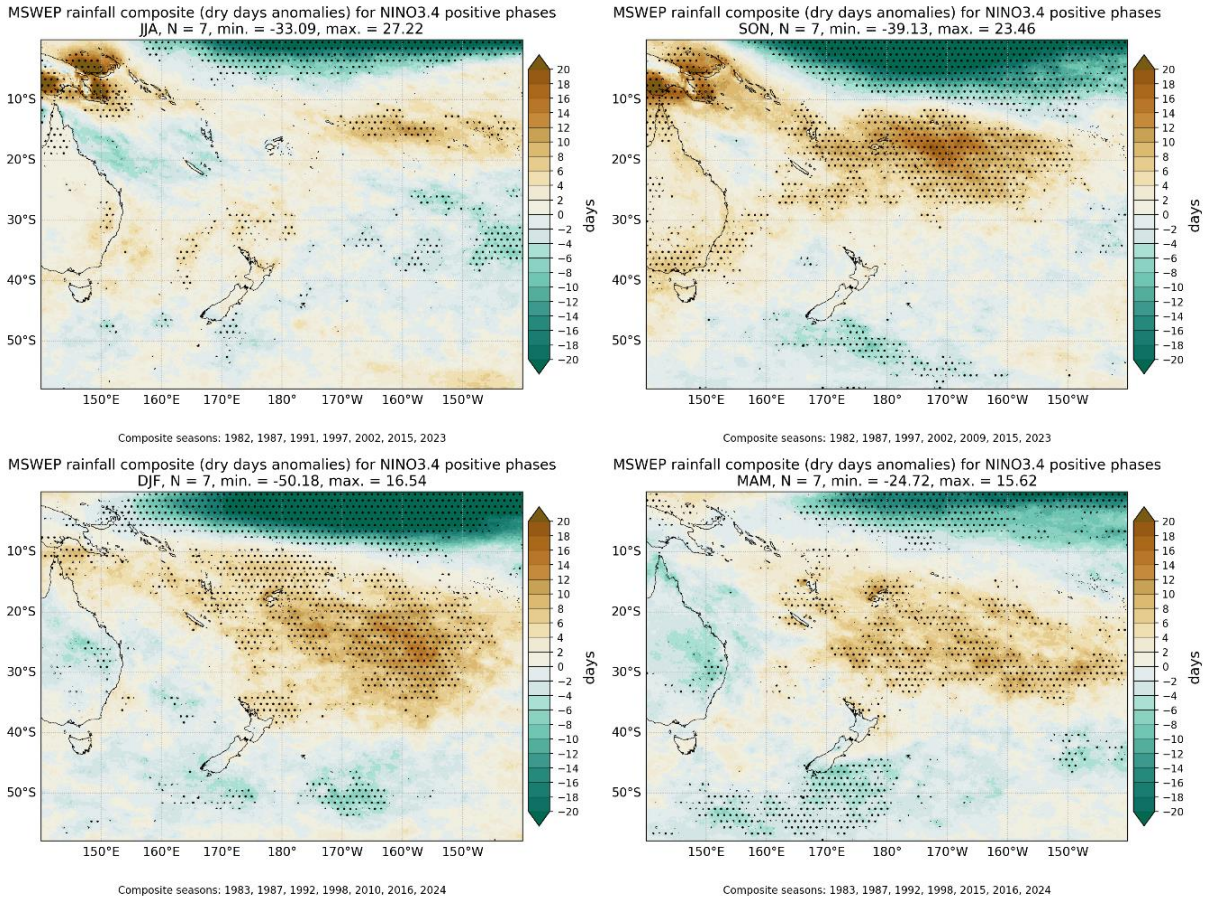

Figure 6-3: Dry day anomalies (MSWEP) during El Niño.

6.2 ENSO – negative phase (La Niña)

La Niña tends to be associated with an increase in summer (DJF) dry days for western parts of the Greater Wellington region (Figure 6-4 and Figure 6-5). Southeastern parts of the region tend to observe a decrease in autumn (MAM) dry days. The Pacific Islands tend to observe fewer than normal dry days during La Niña (Figure 6-6).

6.2.1 Operational VCSN

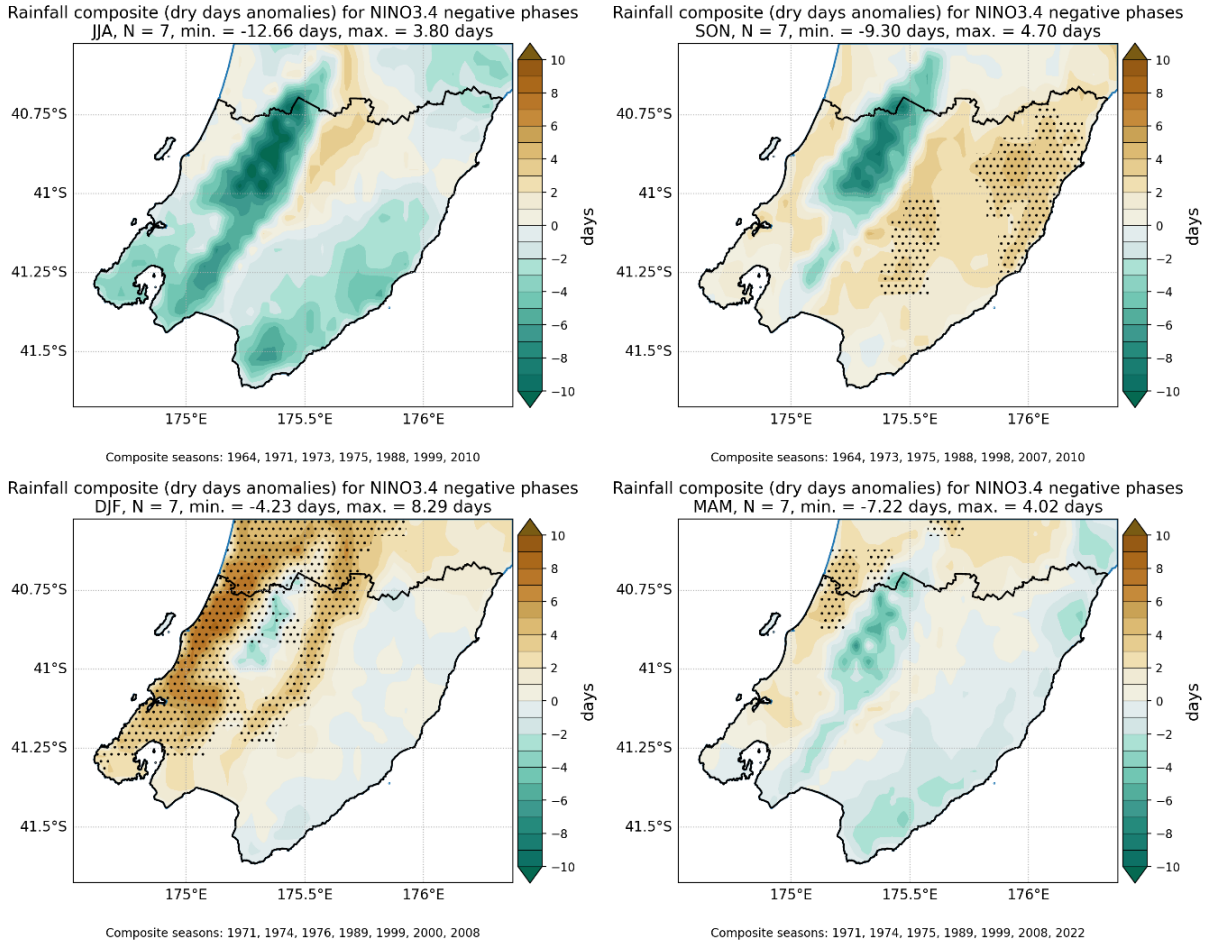

Figure 6-4: Dry day anomalies (operational VCSN) during La Niña.

6.2.2 Augmented VCSN

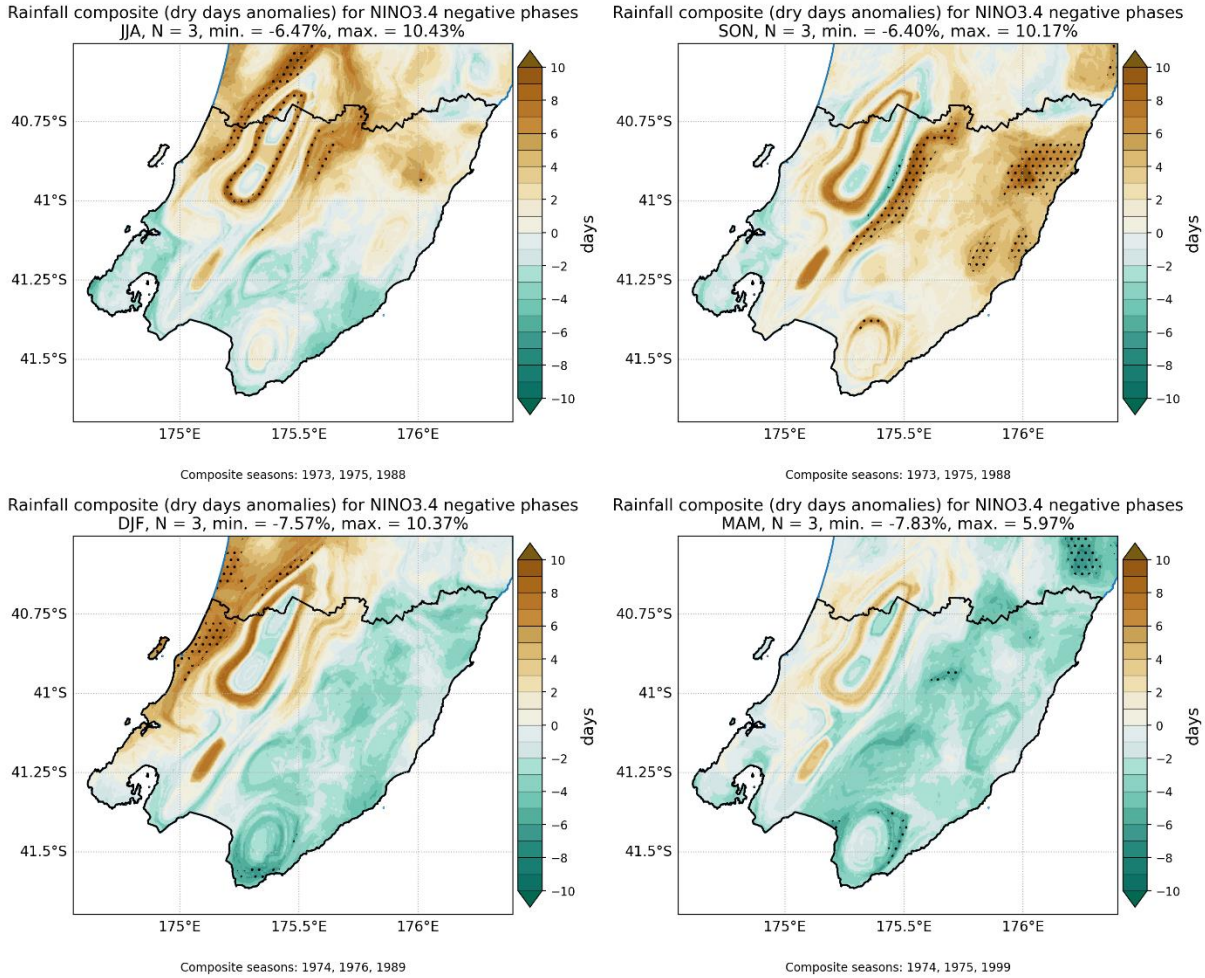

Figure 6-5: Dry day anomalies (augmented VCSN) during La Niña.

6.2.3 MSWEP

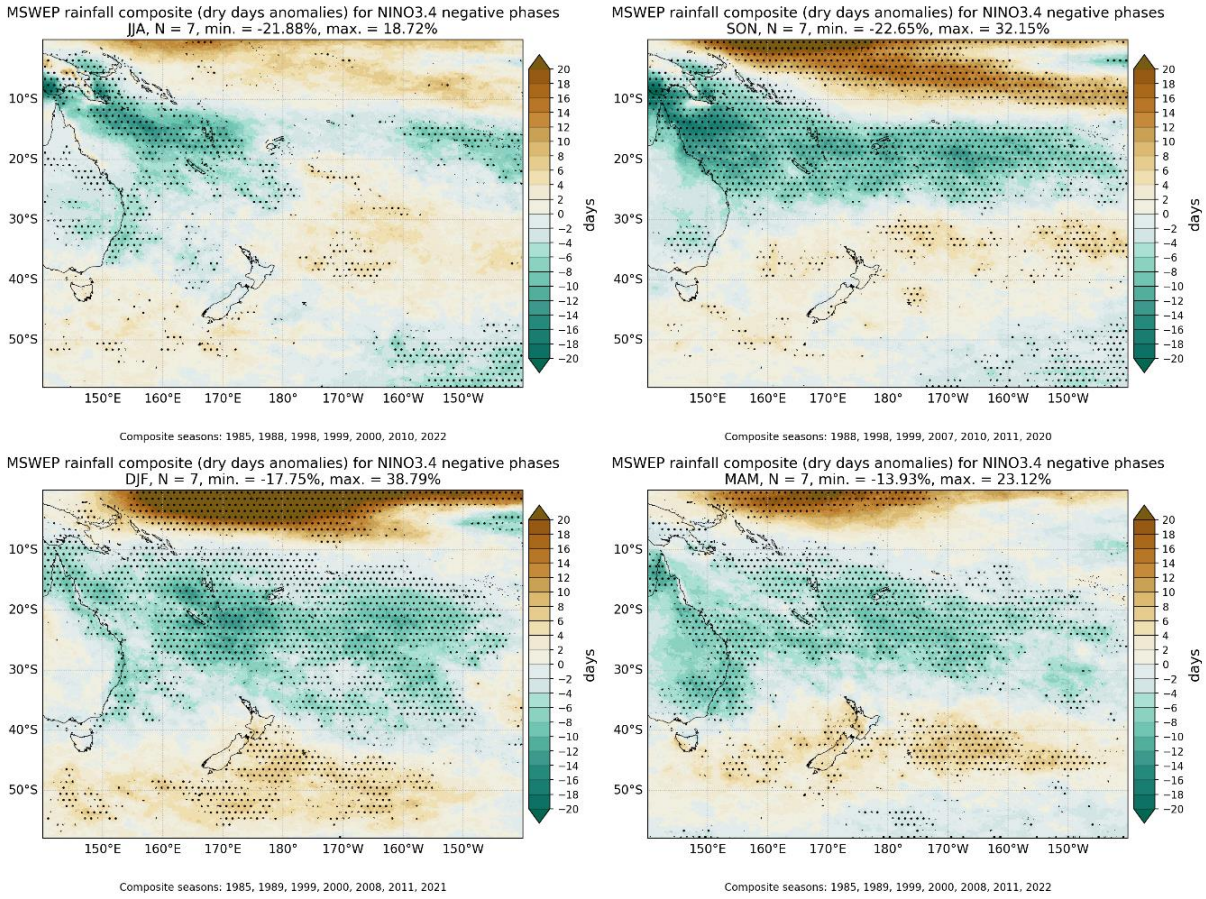

Figure 6-6: Dry day anomalies (MSWEP) during La Niña.

6.3 IOD – positive phase

Positive IOD events tend to be associated with fewer than normal winter (JJA) dry days for most of the region, with more dry days than normal for the Wairarapa during spring (SON) (Figure 6-7). The MSWEP composites highlight an increase in spring (SON) dry days for much of the southwest Pacific and eastern Australia (Figure 6-8).

6.3.1 Operational VCSN

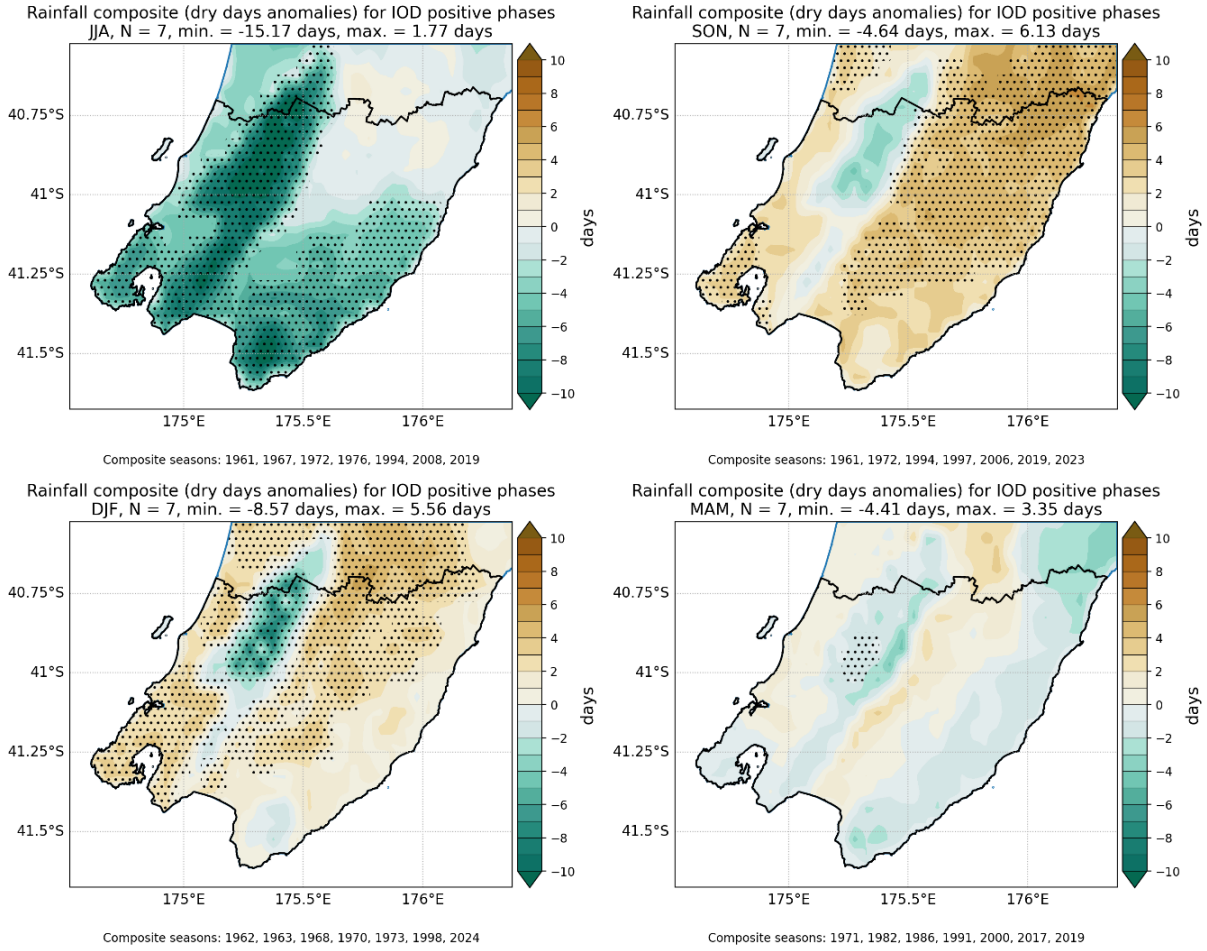

Figure 6-7: Dry day anomalies (operational VCSN) during the positive phase of IOD.

6.3.2 MSWEP

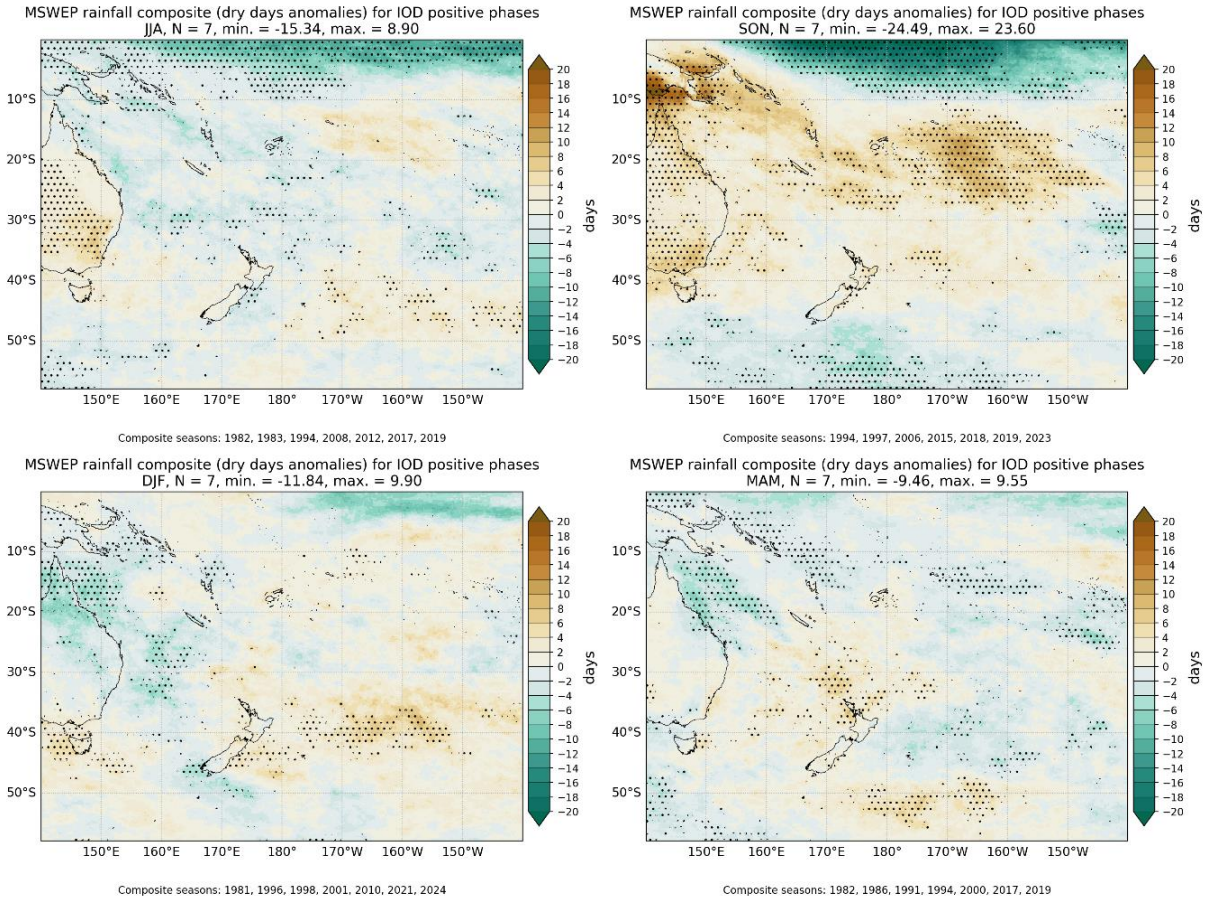

Figure 6-8: Dry day anomalies (MSWEP) during the positive phase of IOD.

6.4 IOD – negative phase

Negative phases of the IOD tend to be associated with decreases in winter (JJA) dry days for the Greater Wellington region (Figure 6-9). The equatorial Pacific tends to observe more dry days in winter (JJA) and spring (SON) (Figure 6-10).

6.4.1 Operational VCSN

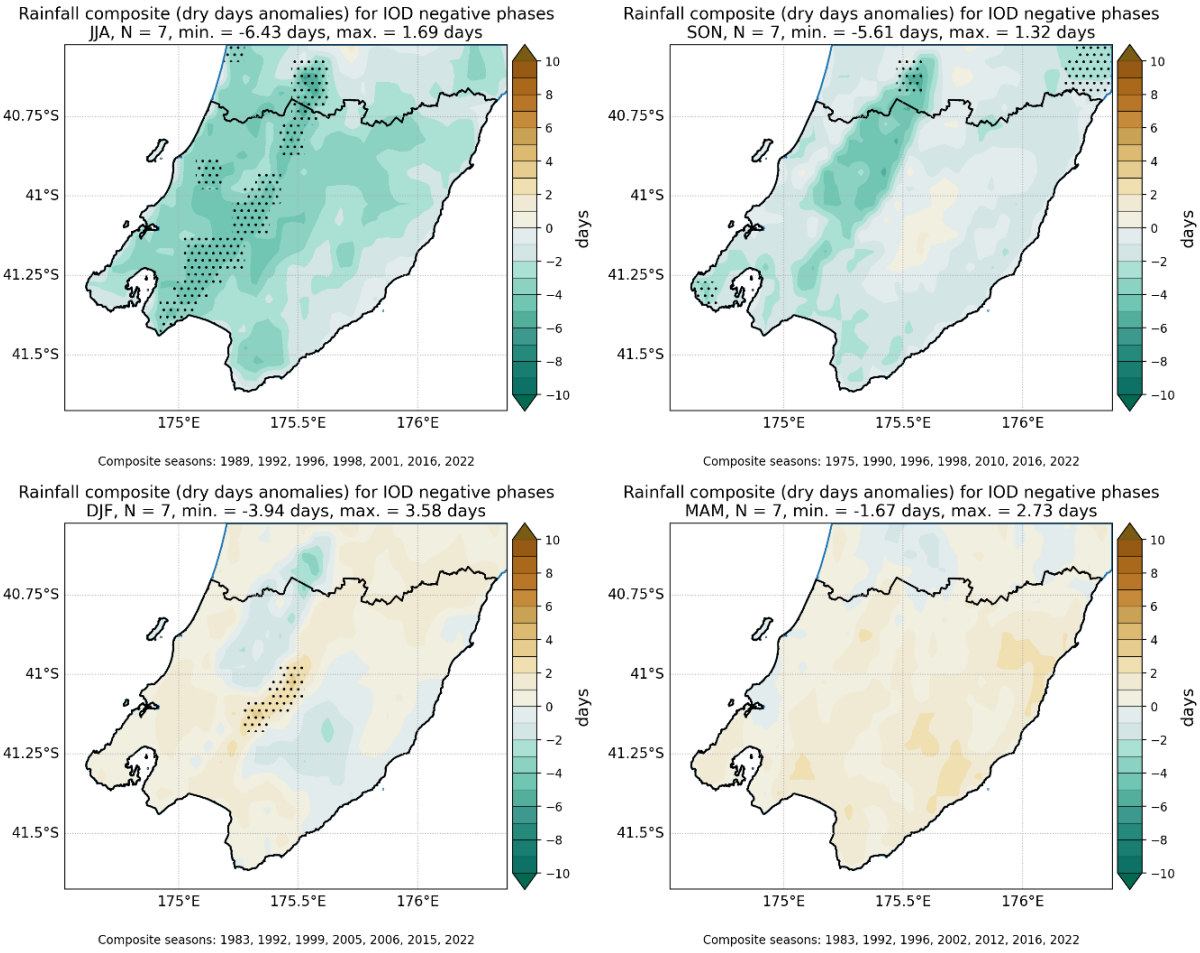

Figure 6-9: Dry day anomalies (operational VCSN) during the negative phase of IOD.

6.4.2 MSWEP

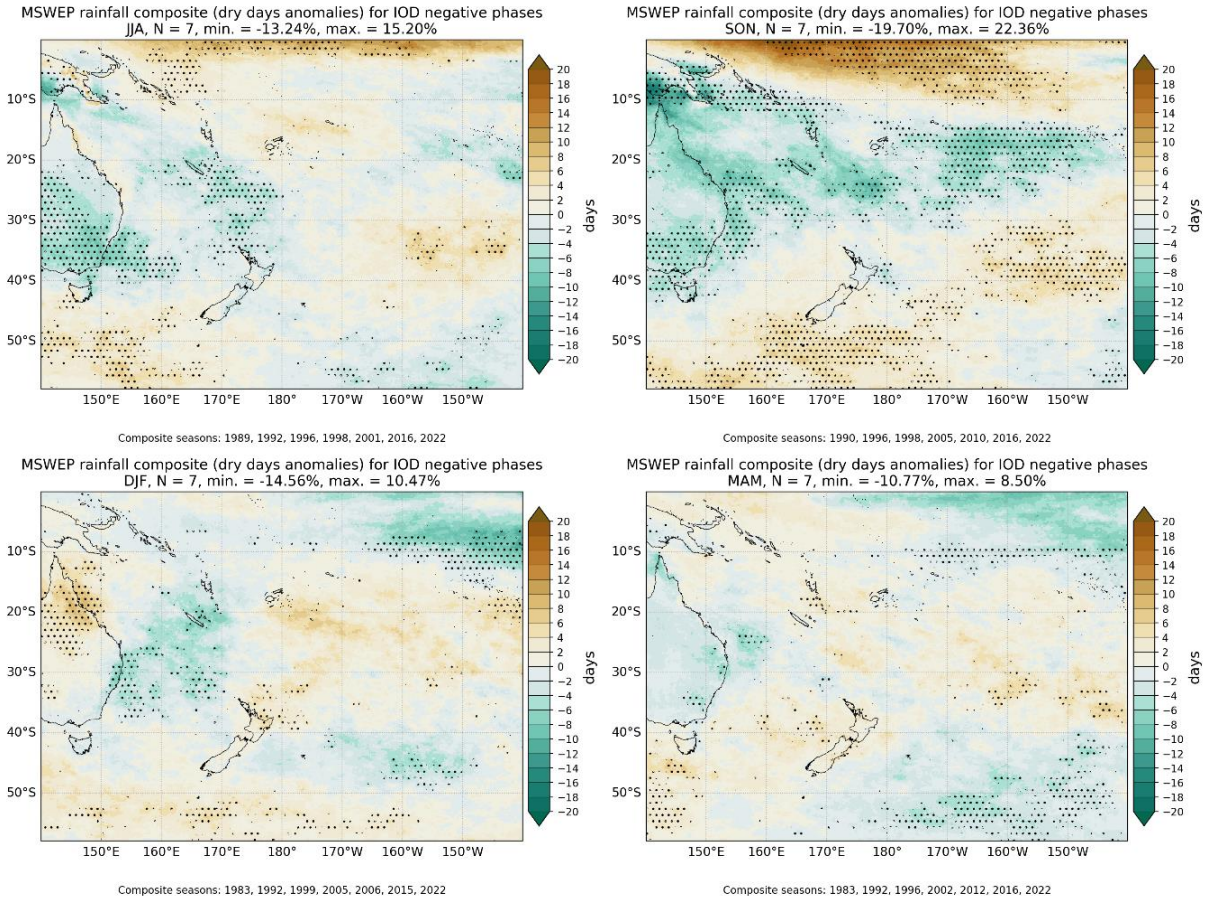

Figure 6-10: Dry day anomalies (MSWEP) during the negative phase of IOD.

6.5 SAM – positive phase

Positive phases of the SAM tend to be associated with more dry days than normal for the Greater Wellington region, particularly during summer (DJF) and autumn (MAM) (Figure 6-11). The Coral Sea tends to observe fewer dry days in spring (SON) (Figure 6-12).

6.5.1 Operational VCSN

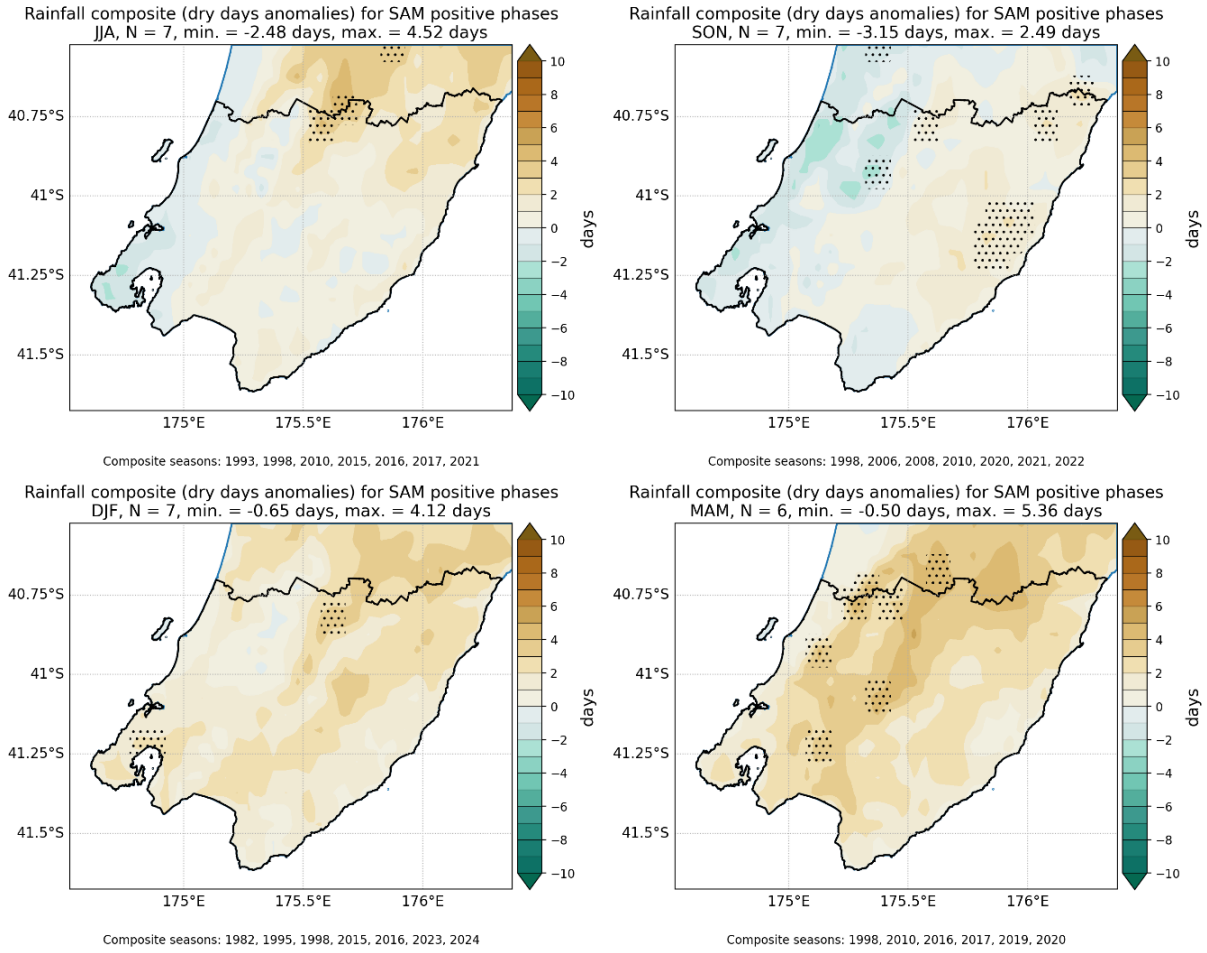

Figure 6-11: Dry day anomalies (operational VCSN) during the positive phase of SAM.

6.5.2 MSWEP

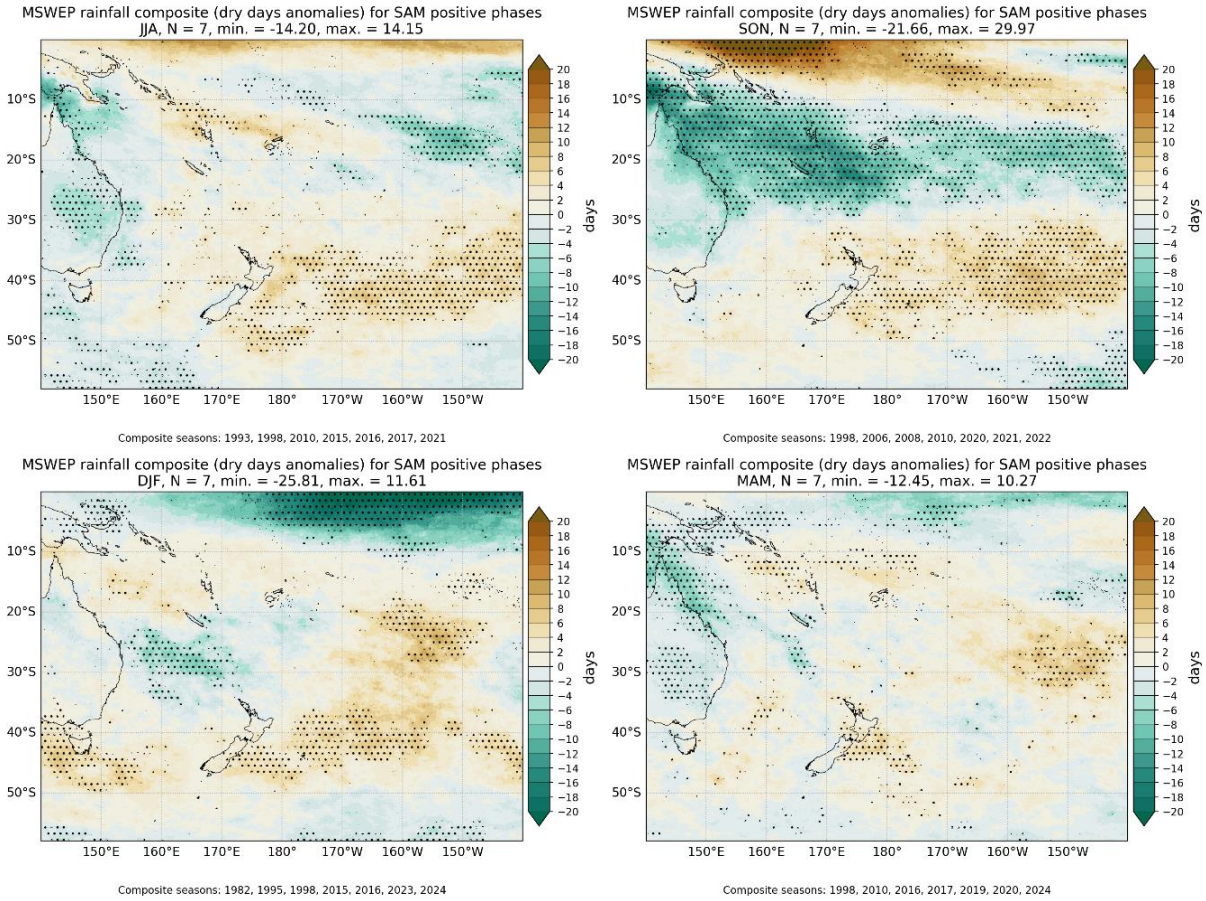

Figure 6-12: Dry day anomalies (MSWEP) during the positive phase of SAM.

6.6 SAM – negative phase

The Greater Wellington region typically observes fewer dry days than normal during the negative phase of SAM (Figure 6-13). Fewer dry days are typically observed in the mid-latitudes over and near New Zealand during the negative phase of SAM, particularly during winter (JJA), spring (SON) and summer (DJF) (Figure 6-14).

6.6.1 Operational VCSN

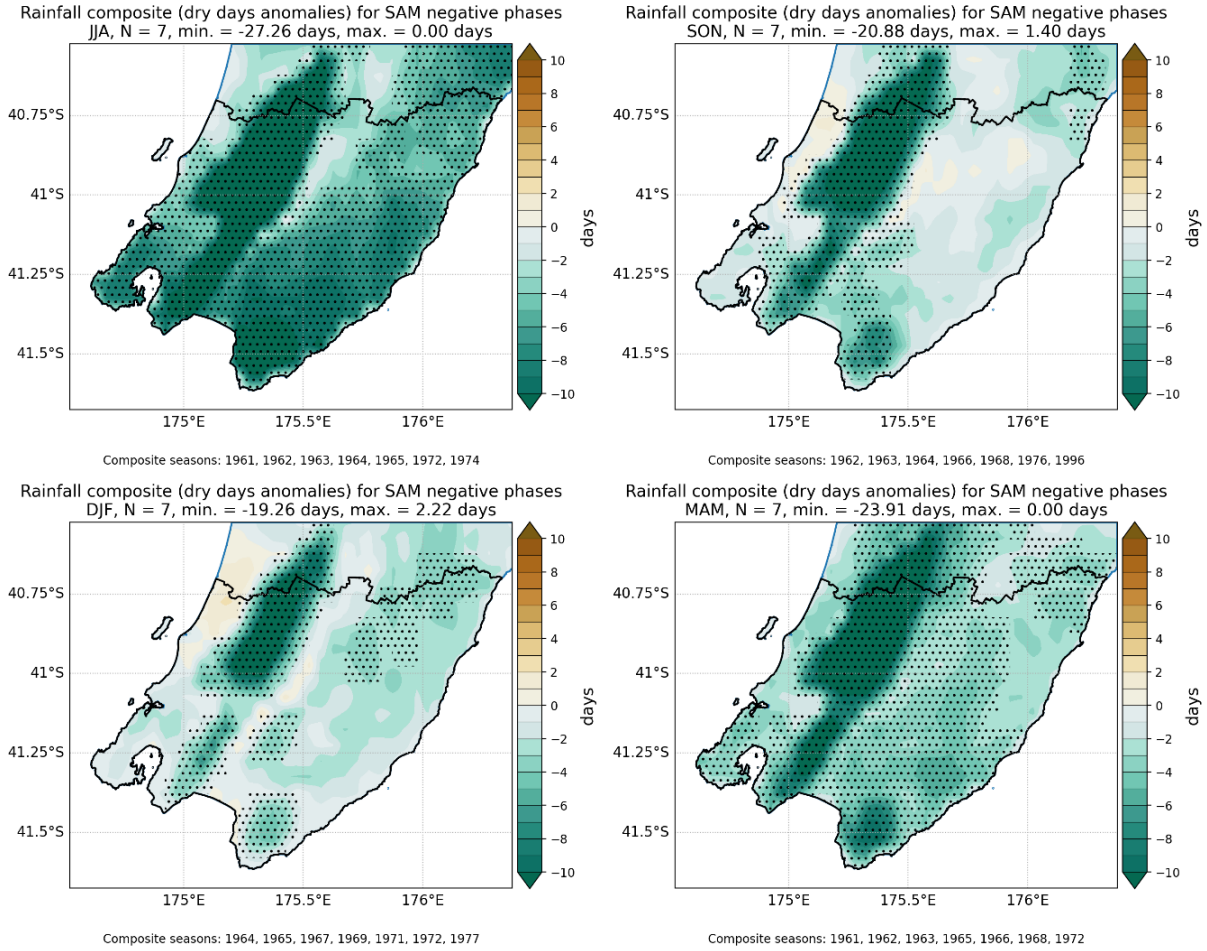

Figure 6-13: Dry day anomalies (operational VCSN) during the negative phase of SAM.

6.6.2 MSWEP

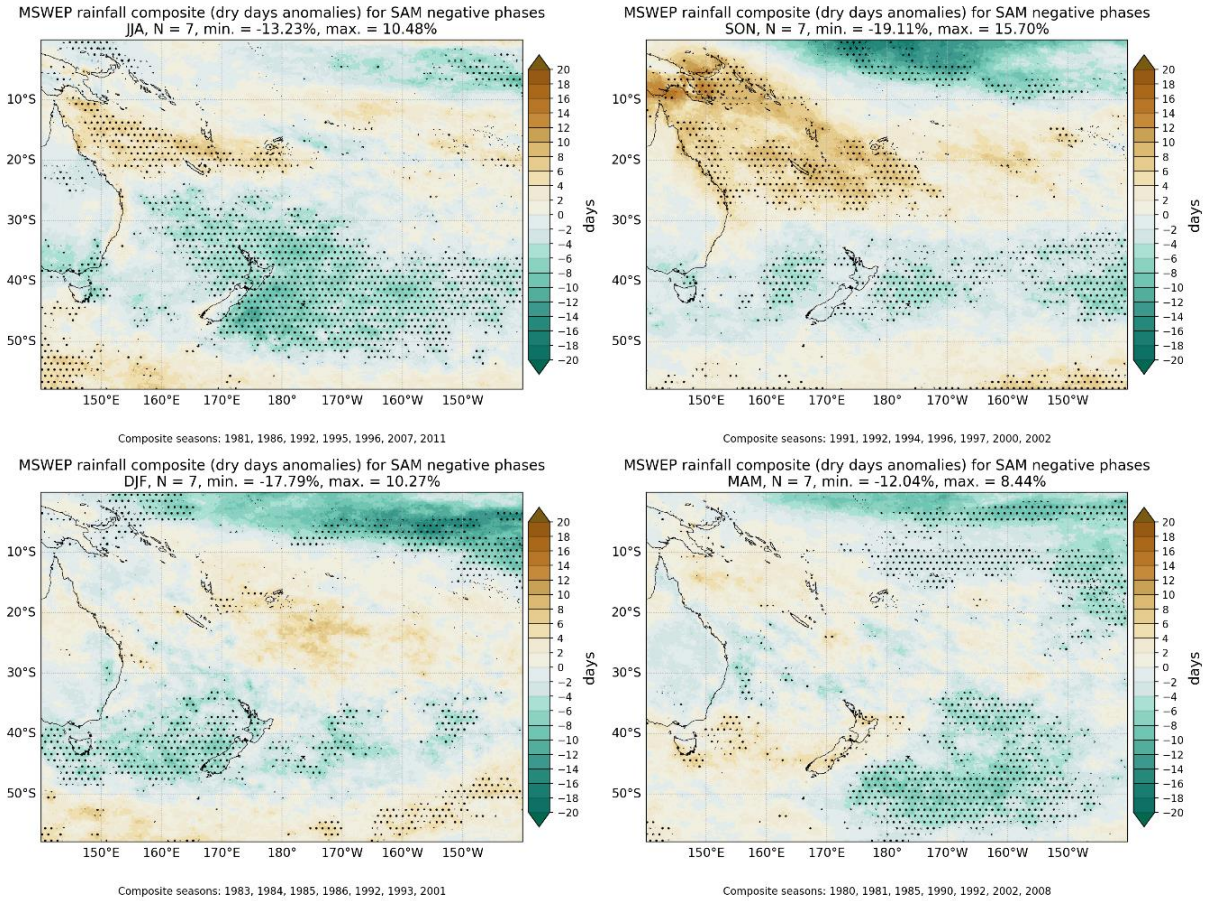

Figure 6-14: Dry day anomalies (MSWEP) during the negative phase of SAM.

6.7 SPSD – positive phase

Positive phases of the SPSD tends to be associated with fewer dry days than normal for the Greater Wellington region, except for western parts of the region during summer (DJF) (Figure 6-15). The equatorial Pacific observes more dry days than normal during autumn (MAM), spring (SON) and summer (DJF) when the SPSD is positive (Figure 6-16).

6.7.1 Operational VCSN

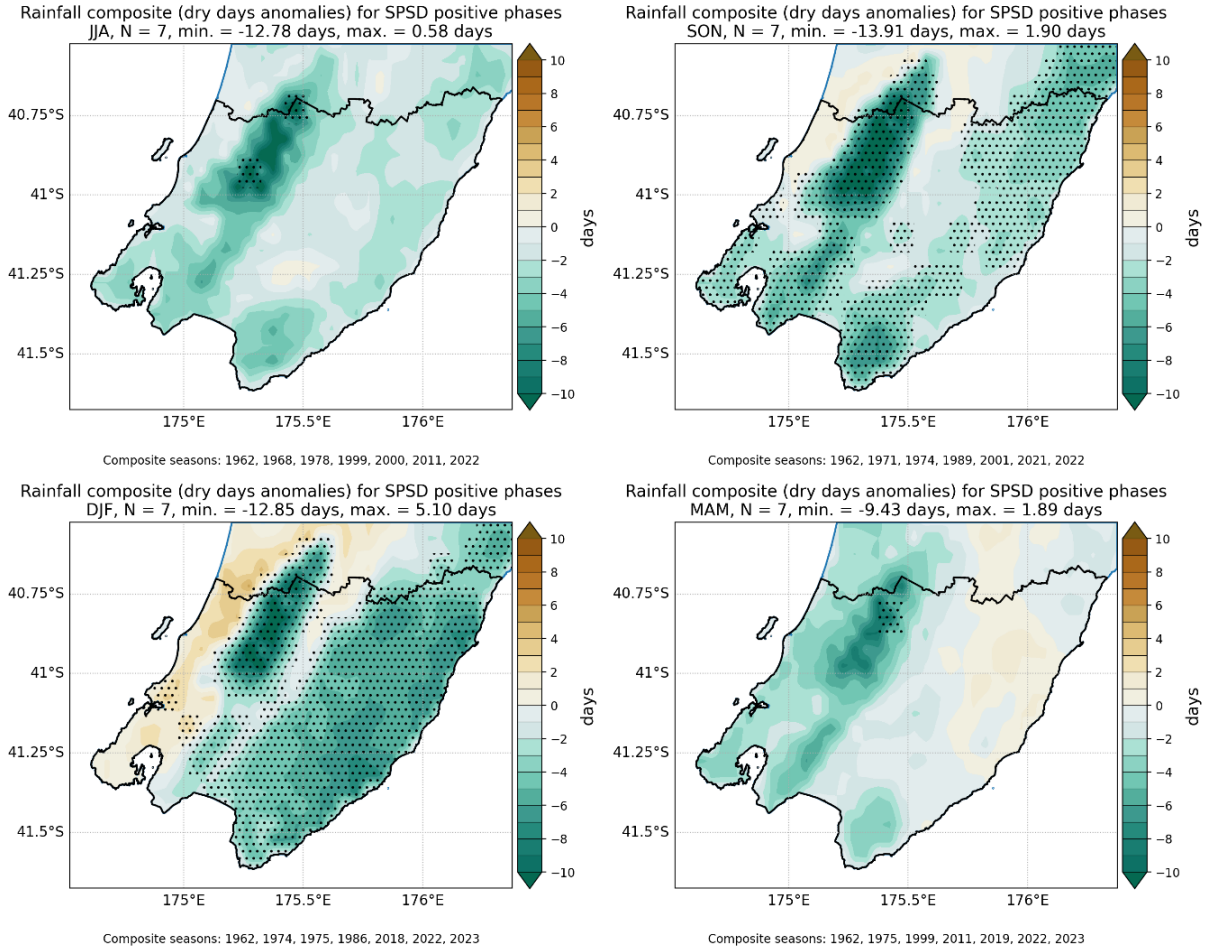

Figure 6-15: Dry day anomalies (operational VCSN) during the positive phase of SPSD.

6.7.2 MSWEP

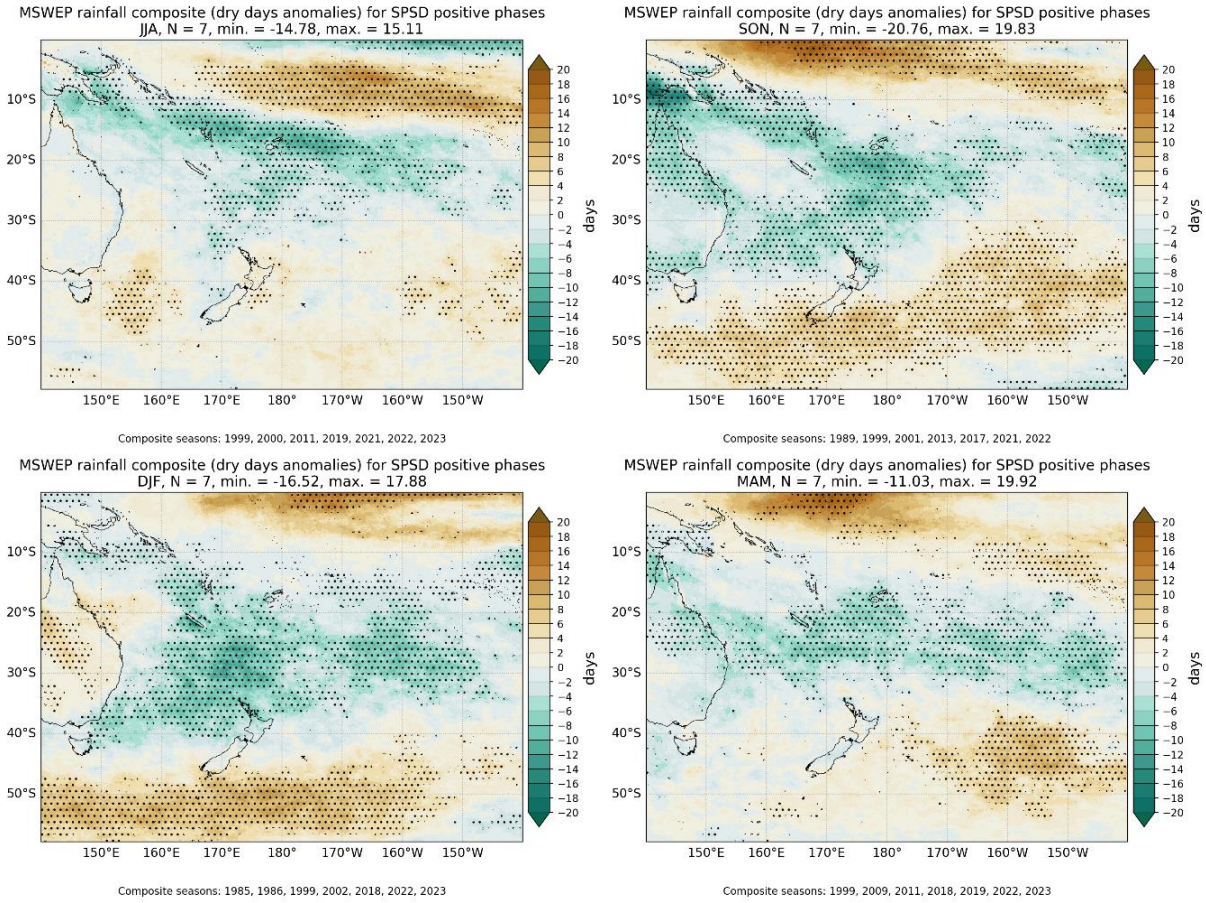

Figure 6-16: Dry day anomalies (MSWEP) during the positive phase of SPSD.

6.8 SPSD – negative phase

Negative phases of the SPSD are associated with fewer winter (JJA) and summer (DJF) dry days than normal for the Greater Wellington region (Figure 6-17). More spring (SON) and summer (DJF) dry days than normal are typically observed about the Pacific Islands and the Coral Sea during the negative phase of SPSD (Figure 6-18).

6.8.1 Operational VCSN

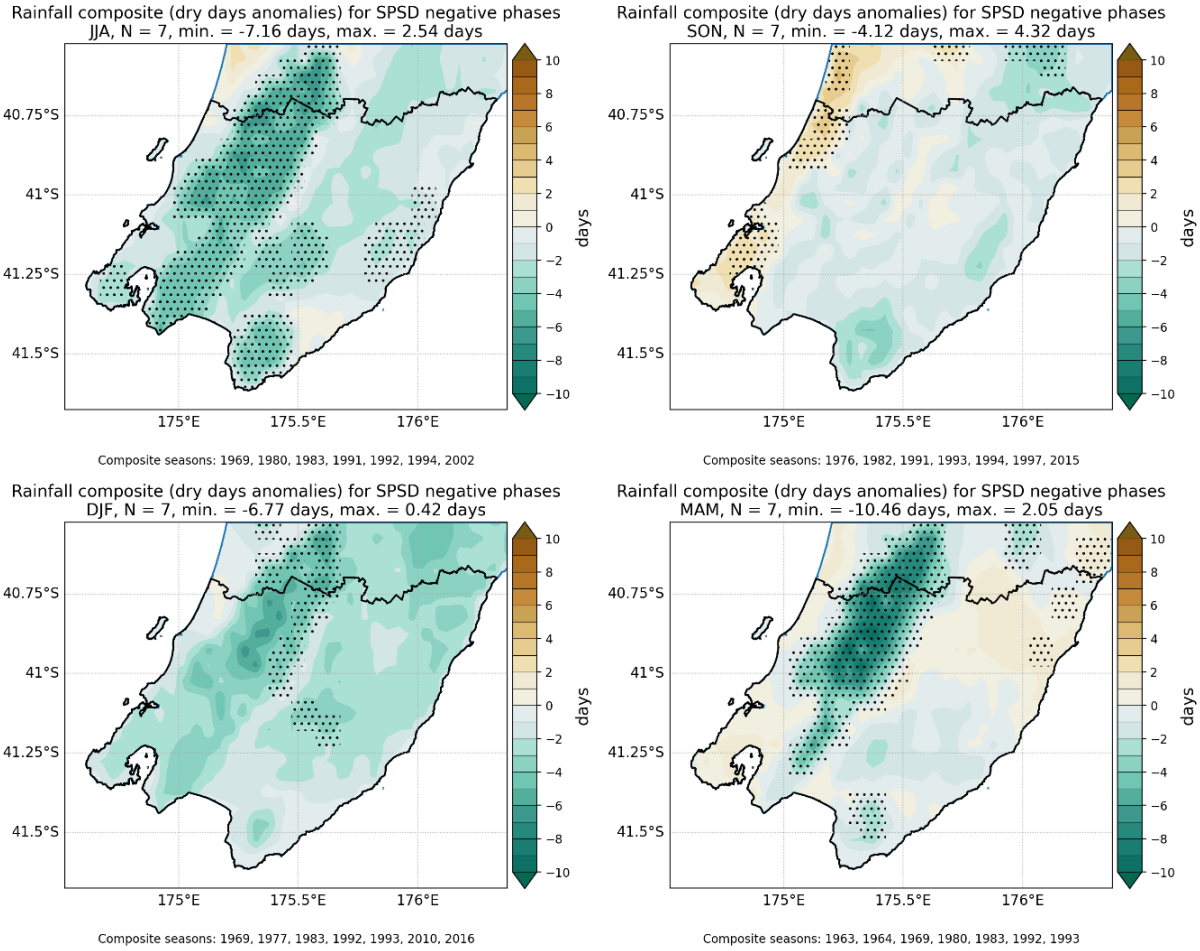

Figure 6-17: Dry day anomalies (operational VCSN) during the negative phase of SPSD.

6.8.2 MSWEP

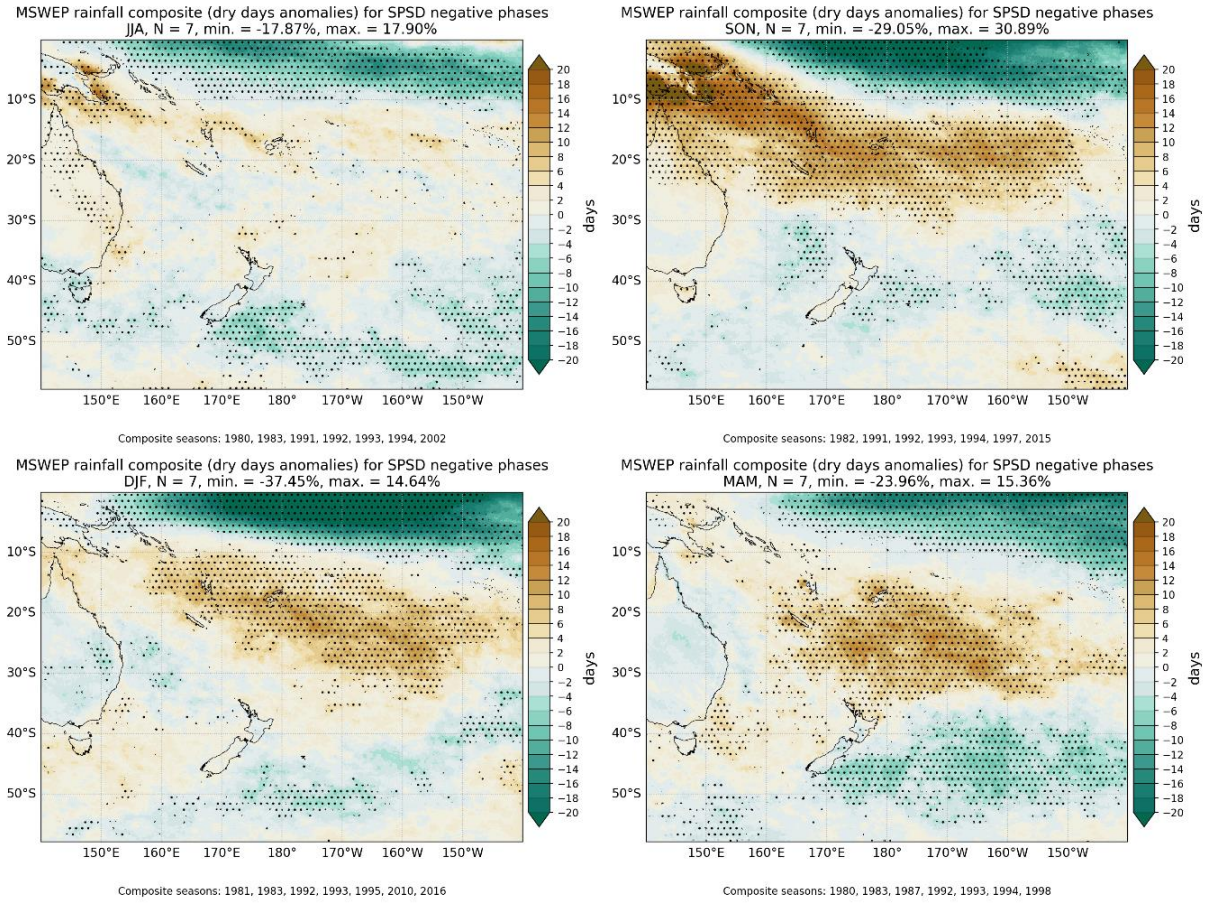

Figure 6-18: Dry day anomalies (MSWEP) during the negative phase of SPSD.

7 Subregional analyses and relationships with large-scale sea surface temperatures

In this section, we take a complementary approach to the analyses presented in Sections 3 to 5: First we define subregional rainfall indices (using only total rainfall for brevity) and then investigate their relationship with large-scale SST anomalies. We undertake these analyses because SSTs are an integral component of the definition of three of the modes investigated, namely ENSO (via the Niño 3.4 region), the IOD (whose index is defined as the difference between the western and eastern tropical ocean SST anomalies) and the SPSD.

Four subregions of Greater Wellington were defined following discussions with Dr. Alex Pezza (Senior Climate Scientist at the GWRC). Figure 7-1 shows the spatial extent of these subregions, and their associated seasonal cycle of total rainfall. Figure 7-2 illustrates the seasonal rainfall anomalies observed across the four subregions for the period 1961-2024.

Figure 7-3 illustrates the seasonal rainfall anomaly correlations between the four Greater Wellington subregions. Region A and B (along and west of the Tararua Range) are very highly correlated, as is the case between region C and D (both east of the Tararua Range).

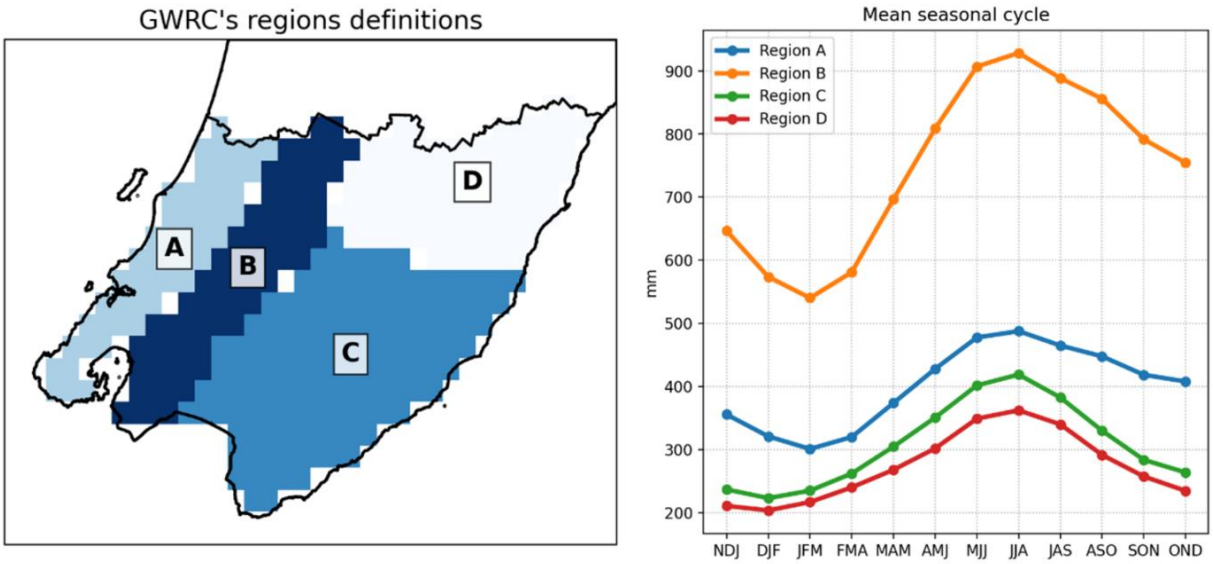

Figure 7-1: Definition of GWRC rainfall regions on the VCSN grid (left) and corresponding mean seasonal cycle (3 month rainfall accumulations).

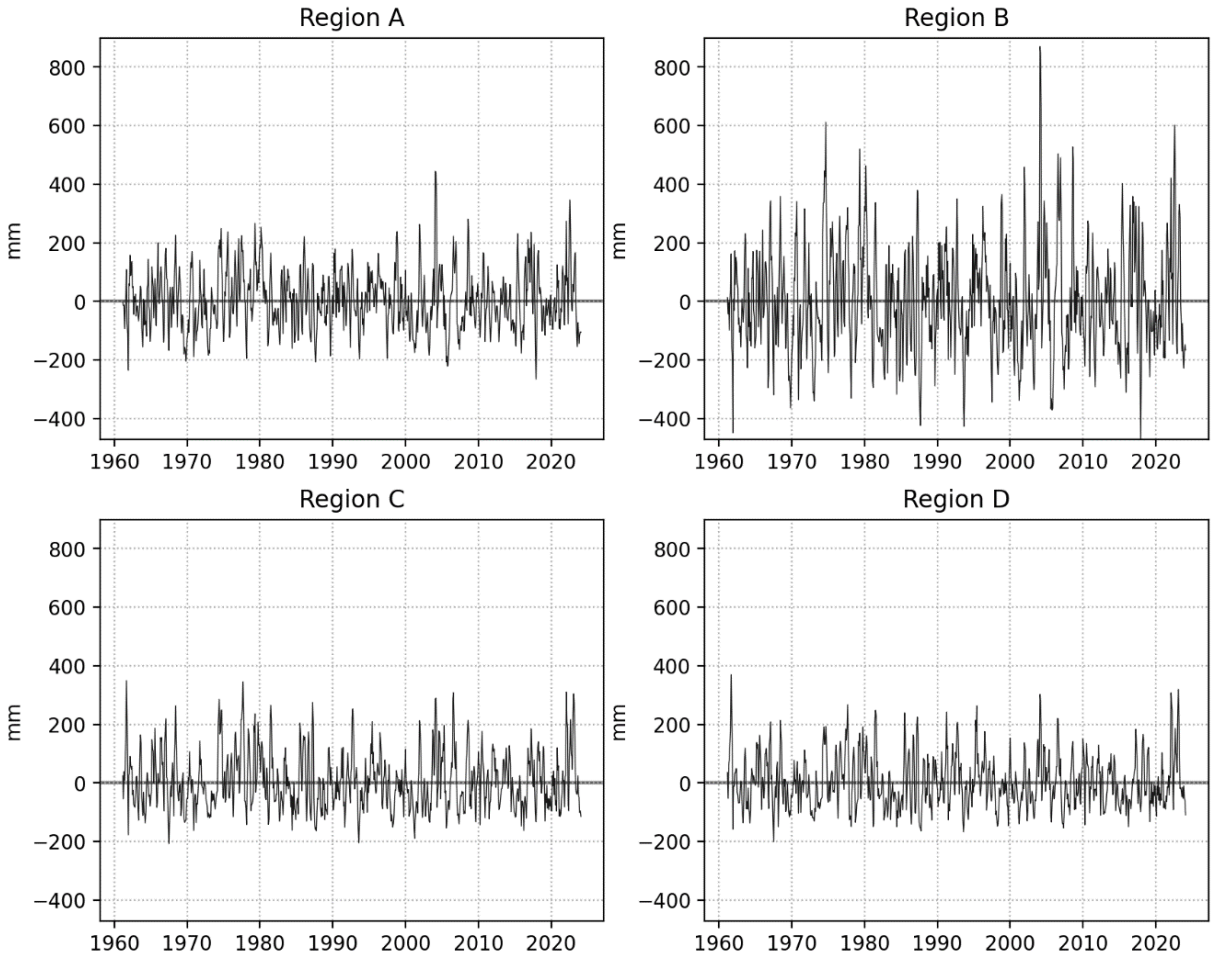

Figure 7-2: Time series of seasonal (3-month sliding windows, i.e., NDJ, DJF, etc.) rainfall anomalies for the four Wellington subregions. Anomalies are relative to the 1991-2020 climatology.

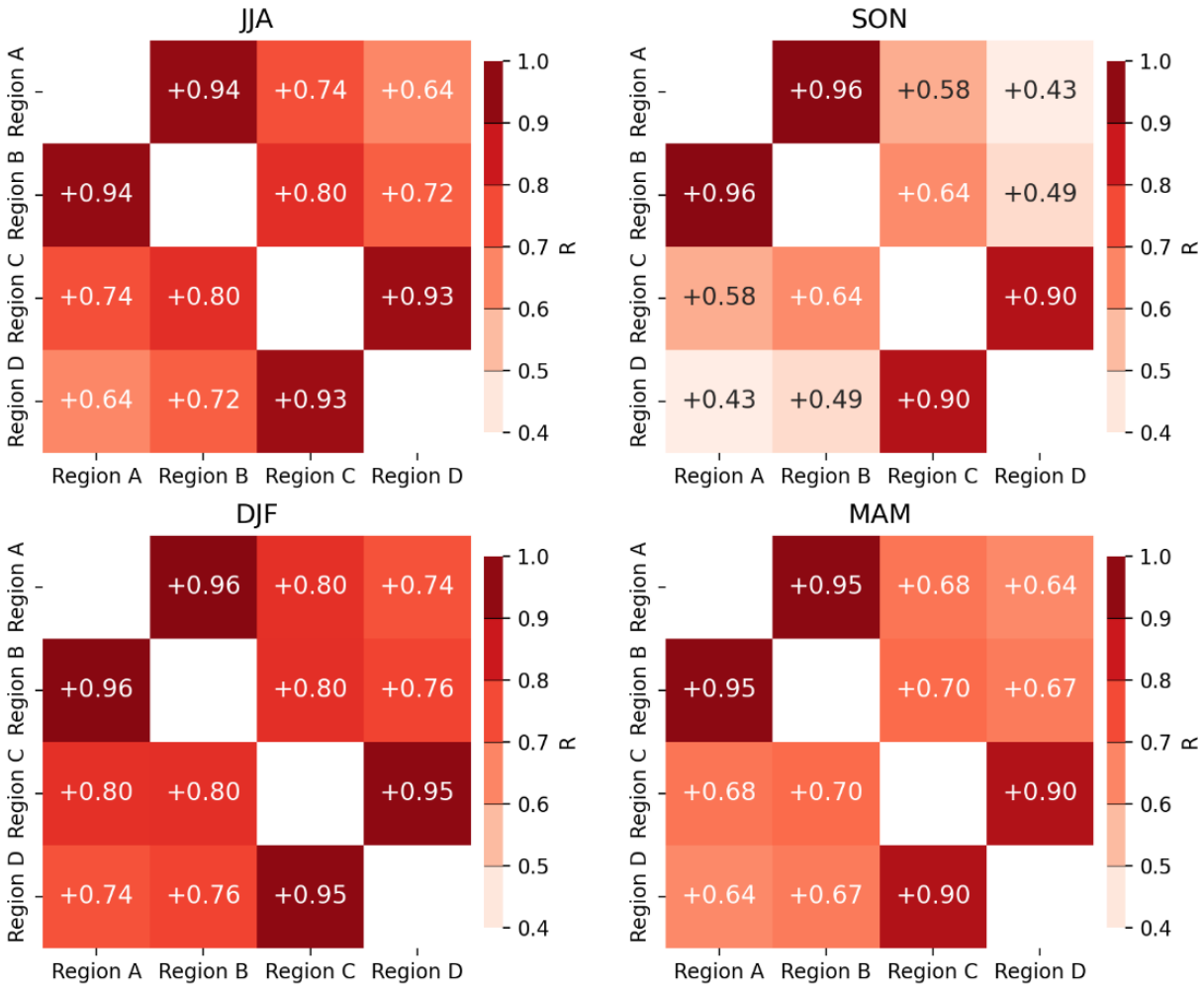

Figure 7-3: Seasonal rainfall anomaly correlations between the four Greater Wellington subregions, over the period 1961-2024.

To better understand the patterns of rainfall variability within the Greater Wellington region, we performed a series of Empirical Orthogonal Function (EOF) Analyses (also referred to in the literature as Principal Component Analysis or PCA). EOF/PCA can decompose a spatio-temporal dataset into a set of spatial patterns (the EOFs) with associated time-series (the Principal Components) and are widely used in climate science to identify coherent modes of variability.

We used the standard (std) EOF analysis, as well as EOF with Varimax and Promax rotations. Varimax is an orthogonal rotation method; it maximizes the sum of the variances of the squared loadings (weights), aiming to achieve a factor structure where each variable loads highly on as few factors as possible. This rotation assumes factors are uncorrelated. Promax is an oblique rotation method that allows factors to be correlated. It starts with an initial Varimax rotation and then raises the loadings to a power (usually 4) to exaggerate the structure before allowing correlations among factors.

The standard EOF analysis suggests that rainfall variability tends to be homogeneous over the whole Greater Wellington region, and it explains a large (76.01%) proportion of the total seasonal rainfall variance (Figure 7-4). However, a small proportion of variance (12.13%) is independent, and characterised by rainfall anomalies of opposite sign either side of the Tararua ranges. In the case of the Promax rotation - which allows the Principal Components to be correlated - we note that the

correlation between the 1st and 2nd PCs is significantly positive (R= +0.51), confirming therefore that a 'dipole' opposing the western and eastern side of the ranges does not constitute a primary major mode of seasonal rainfall variability over the Greater Wellington region.

Figure 7-5 to Figure 7-8 present the seasonal correlations between the regional time series of rainfall anomalies (for subregions A, B, C, and D, respectively), and SST anomalies. As anticipated, the correlations between Wellington's subregional rainfall anomalies and SST anomalies paint a complex picture. As identified earlier in this report (e.g., Sections 3.1 and 3.2) the relationship between ENSO and regional rainfall anomalies is not linear. Accordingly, the correlation between regional rainfall anomalies and SSTs are generally weak and not necessarily consistent.

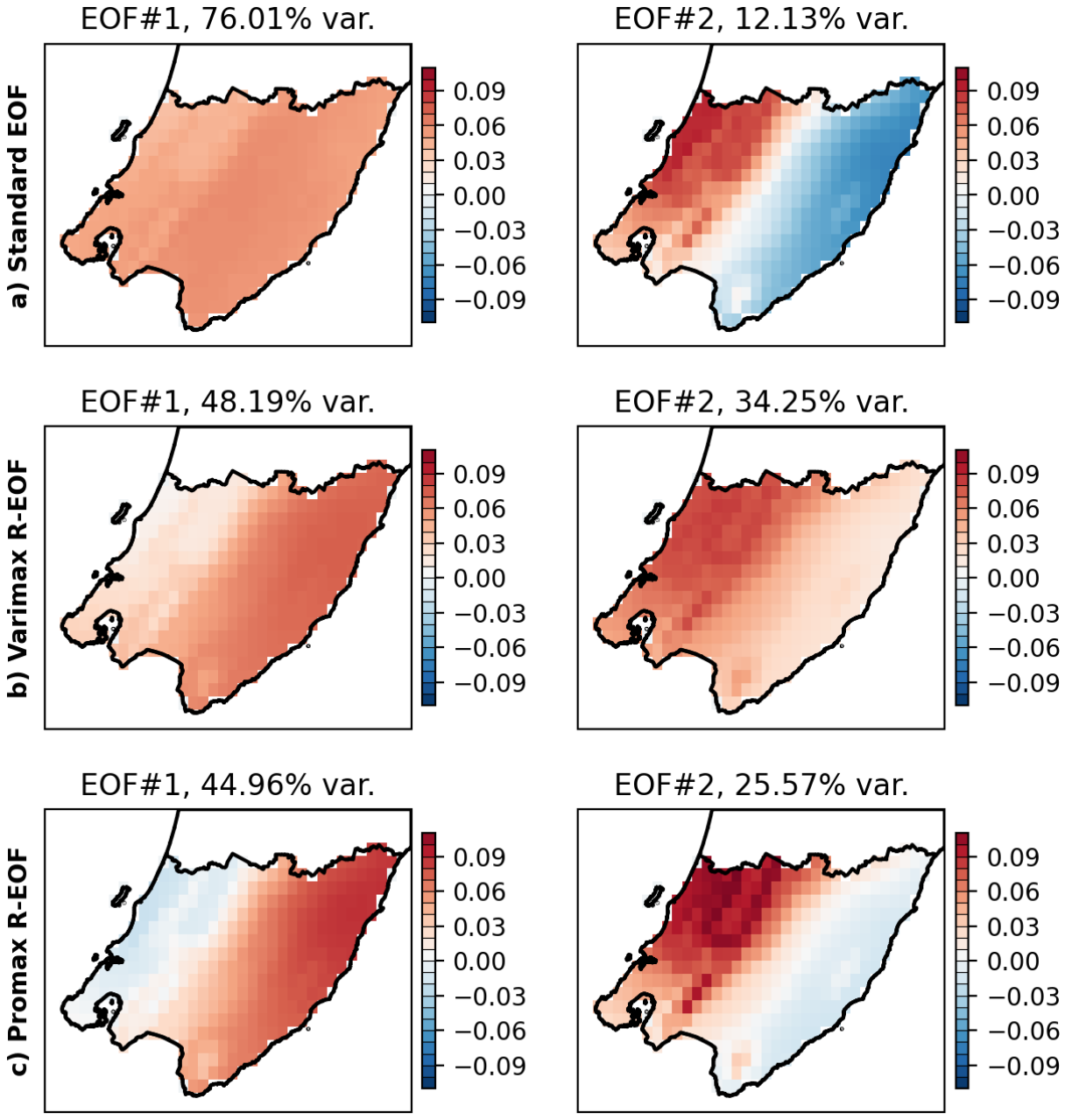

Figure 7-4: First two EOF on rainfall seasonal anomalies (from VCSN) for the period 1961-2024. Standard EOF.

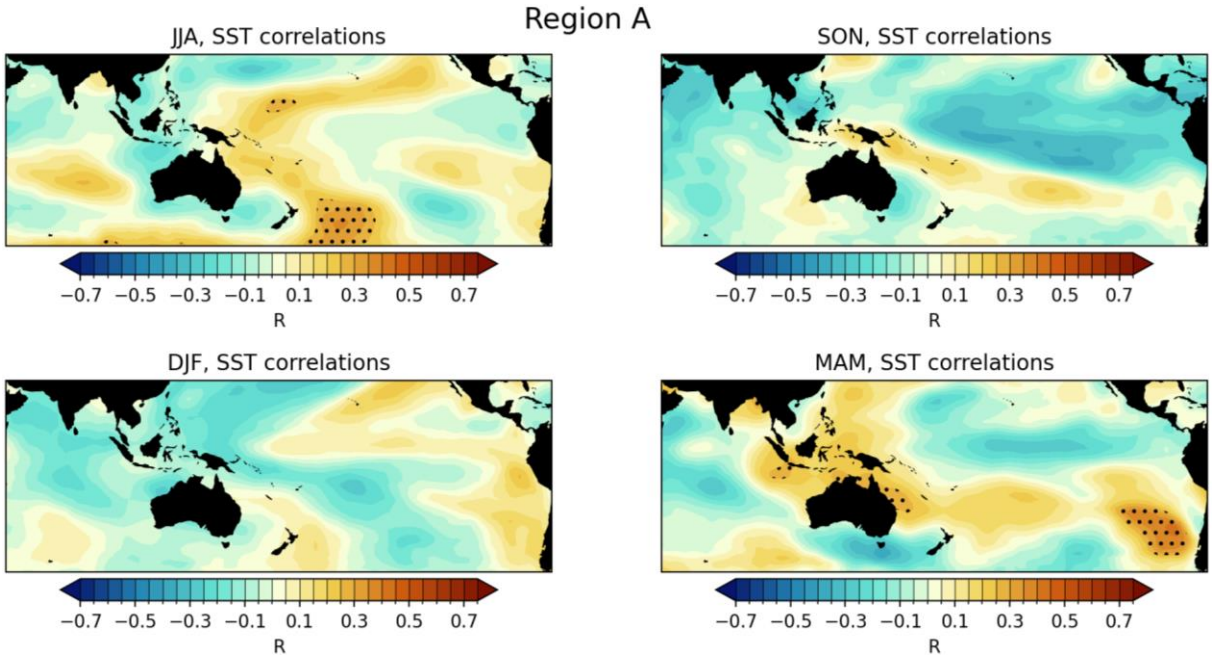

Figure 7-5: Correlation between GWRC Region A seasonal rainfall anomalies and SST anomalies.

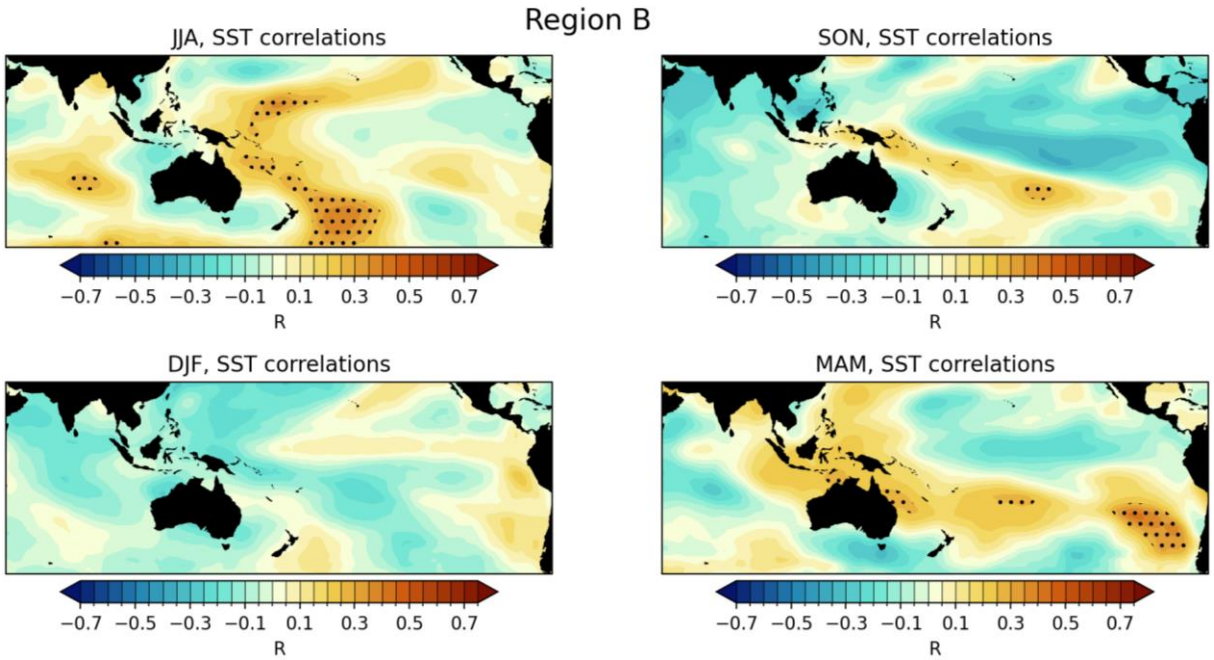

Figure 7-6: Correlation between GWRC Region B seasonal rainfall anomalies and SST anomalies.

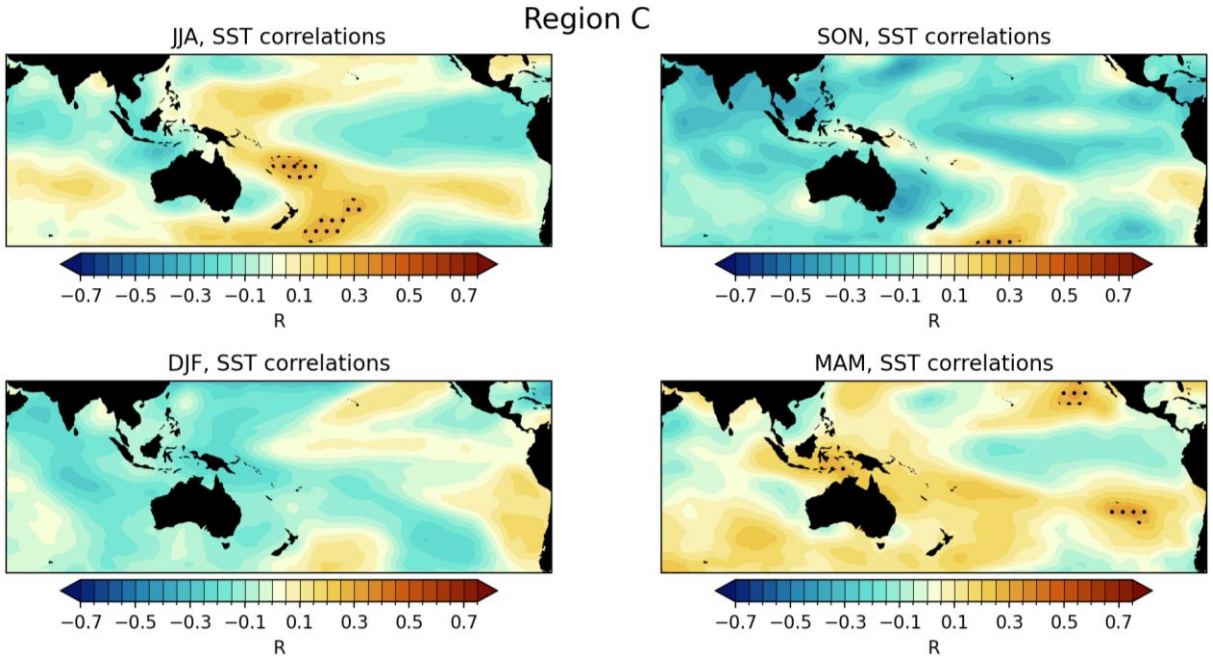

Figure 7-7: Correlation between GWRC Region C seasonal rainfall anomalies and SST anomalies.

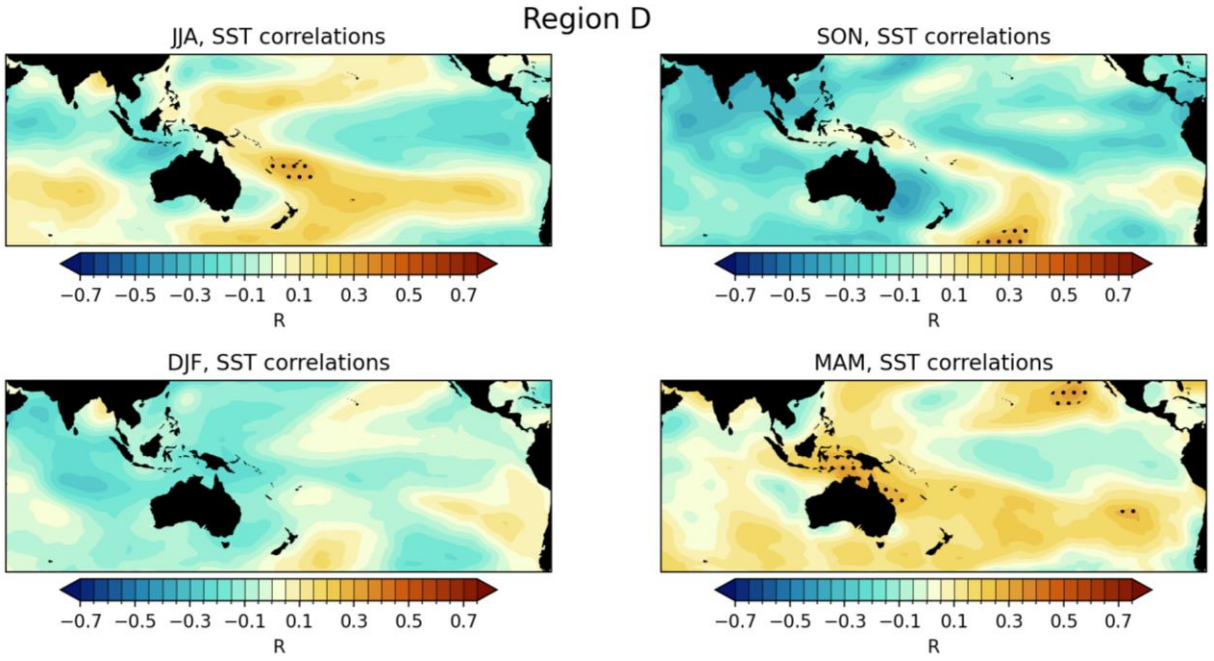

Figure 7-8: Correlation between GWRC Region D seasonal rainfall anomalies and SST anomalies.

8 Summary

Key findings from this report are summarised below:

- Overall, most of the composite analyses show weak signals, and statistical significance is limited in many cases.
- The strongest statistically significant and relatively robust signals observed for the Greater Wellington region include:
  - Reduced spring (SON) rainfall and fewer heavy rain days during positive phases of ENSO (El Niño) across the whole region.
  - Reduced summer (DJF) rainfall for northern parts of the region during positive phases of the IOD.
  - Increased winter (JJA) rainfall and more rain days for many parts of the region during negative phases of SAM.
  - Increased summer (DJF) rainfall for the Wairarapa during positive phases of the SPSD.
- Baseline periods and climatological periods have a large influence on the inclusion/exclusion of seasons/years in the composite samples. The datasets used in this study cover a range of periods (the longest being the 'operational' VCSN, available since 1961 for rainfall, and the shortest being the global MSWEP dataset, available since 1979). These differences and limitations need to be kept in mind when interpreting the results.
- The augmented VCSN dataset (500 m resolution) presents some severe, unrealistic artifacts. Readers are therefore urged to be circumspect when interpreting the data presented in the augmented VCSN maps, particularly for areas about the Tararua Range, Remutaka Range, and the Aorangi Range.

8.1 Recommendations

Based on the results of this report, we make the following recommendations:

- Caveats and limits to interpretation should be clearly understood and communicated alongside any subsequent presentation of these data.
- If findings in this report are intended to be used to complement or provide background information to GWRC's seasonal outlook products;
  - NIWA suggests a discussion takes place towards alternative tailored approaches to improve the relevance – and possibly the accuracy – of tailored seasonal climate outlooks for the Greater Wellington region.
  - Note, due to the complex interactions between the climate modes, rainfall anomalies experienced in any given season are difficult to predict from the sign and amplitude of the climate modes alone.

- Monitoring of climate modes is nevertheless important. NIWA is in the process of consolidating a webpage which presents the status of the climate modes investigated in this report (and additional ones) and which will be regularly updated.
- As the impact of ENSO over the Greater Wellington region is neither strong nor linear, a deeper investigation of what modulates ENSO's impact is warranted. Not one ENSO is the same. ENSO events happen in the context of different background climate states, and the phases and amplitudes of other modes of climate variability; some independent from ENSO, can have constructive or destructive interference with ENSO teleconnections with New Zealand's region. A complicating factor is also related to the impact of the discernible – and climate-change related – trend in Tropical SSTs on the characteristics of ENSO. Recently, the Relation Oceanic Niño Index (RONI) has been proposed to better account for the effect of this recent tropical SST warming trend (van Olderborgh et al., 2021) and NIWA has started to use this index operationally.

9 Glossary of abbreviations and terms

ENSO	El Niño Southern Oscillation
EOF	Empirical Orthogonal Function analysis
ERSST	Extended Reconstructed Sea Surface Temperature
IOD	Indian Ocean Dipole
MSWEP	Multi-Scale Weighted Ensemble Precipitation
NCAR	National Center for Atmospheric Research
NCEP	National Centers for Environmental Prediction
SAM	Southern Annular Mode
SPSD	South Pacific Subtropical Dipole
SST	Sea surface temperature
VCSN	Virtual Climate Station Network

10 References

Beck, H.E., Wood, E.F., Pan, M., Fisher, C.K., Miralles, D.G., Van Dijk, A.I.J.M., McVicar, T.R., Adler, R.F. (2019) MSWEP V2 Global 3-Hourly 0.1° Precipitation: Methodology and Quantitative Assessment. *Bulletin of the American Meteorological Society*, 100, 473–500, https://doi.org/10.1175/BAMS-D-17-0138.1.

Benjamini, Y., Hochberg, Y. (1995) Controlling the False Discovery Rate: A Practical and Powerful Approach to Multiple Testing. *Journal of the Royal Statistical Society: Series B (Methodological),* 57, 289–300, https://doi.org/10.1111/j.2517-6161.1995.tb02031.x

Fauchereau, N., Fedaeff, N., Pearce, P. (2018) Regional climate mode impacts of the Wellington Region. Prepared for Greater Wellington Regional Council. *NIWA Client Report* 2018259AK: 204 pp.

Huang, B., Thorne, P.W., Banzon, V.F., Boyer, T., Chepurin, G., Lawrimore, J.H., Menne, M.J., Smith, T.M., Vose, R.S., Zhang, H.-M. (2017) NOAA Extended Reconstructed Sea Surface Temperature (ERSST), Version 5. NOAA National Centers for Environmental Information. https://doi.org/10.1175/JCLI-D-16-0836.1

Guan, Y., Huang, B., Zhu, J., Hu, Z.-Z., Kinter, J.L. (2014) Interannual variability of the South Pacific Ocean in observations and simulated by the NCEP Climate Forecast System, version 2. *Clim Dyn*, 43, 1141–1157, https://doi.org/10.1007/s00382-014-2148-y.

Kalnay, E., Kanamitsu, M., Kistler, R., Collins, W., Deaven, D., Gandin, L., Iredell, M., Saha, S., White, G., Woollen, J., Zhu, Y., Chelliah, M., Ebisuzaki, W., Higgins, W., Janowiak, J., Mo, K.C., Ropelewski, C., Wang, J., Leetmaa, A., Reynolds, R., Jenne, R., Joseph, D. (1996) The NCEP/NCAR 40-Year Reanalysis Project. Bulletin of the American Meteorological Society, 77, 437–472, https://doi.org/10.1175/1520-0477(1996)077<0437:TNYRP>2.0.CO;2

Macara, G., Noll, B., Meyers, T., Fauchereau, N. (2024) Climate catalogue for the Greater Wellington Region: Seasonal variation of climate, atmospheric and oceanic variables, updated for 1961-2023. Prepared for Greater Wellington Regional Council. *NIWA Client Report* 2024175WN: 129 pp.

NIWA (2024). Virtual Climate Station data and products. Accessed on 9 December 2024 at https://niwa.co.nz/climate-and-weather/virtual-climate-station-data-and-products

Van Oldenborgh, G.J., Hendon, H., Stockdale, T., L'Heureux, M., Coughlan De Perez, E., Singh, R., Van Aalst, M. (2021) Defining El Niño indices in a warming climate. *Environ. Res. Lett.*, 16, 044003, https://doi.org/10.1088/1748-9326/abe9ed.

Vishwanathan, G., McDonald, A., Stone, D.A., Rosier, S., Rana, S., Noble, C. (2023) Mean and extreme precipitation over Aotearoa New Zealand: A comparison across multiple different estimation techniques. *International Journal of Climatology*, 43, 3072–3093, https://doi.org/10.1002/joc.8017

Zhang, L., Han, W., Meehl, G.A., Hu, A., Rosenbloom, N., Shinoda, T., Mcphaden, M.J. (2021) Diverse Impacts of the Indian Ocean Dipole on El Niño–Southern Oscillation. *Journal of Climate,* 34, 9057-9070.

Zheng, J., Wang, F. Atmospheric response to the South Pacific Subtropical Dipole. *Clim Dyn,* 56, 1753–1765 (2021). https://doi.org/10.1007/s00382-020-05559-x